



This is to certify that the

dissertation entitled

A Study of the Interlaminar Stress Continuity Theories

for Composite Laminates

presented by

Chun-Ying Lee

has been accepted towards fulfillment of the requirements for

Ph.D. degree in Mechanics

Major professor

Date May 17, 1991

# LIBRARY Michigan State University

PLACE IN RETURN BOX to remove this checkout from your record. TO AVOID FINES return on or before date due.

	DATE DUE	DATE DUE
<b>8 78</b> 1995		
NAMES 2000)		
<u></u>		

MSU Is An Affirmative Action/Equal Opportunity Institution
c:/c/rc/detectue.pm3-p.;

# A STUDY OF THE INTERLAMINAR STRESS CONTINUITY THEORIES FOR COMPOSITE LAMINATES

Ву

Chun-Ying Lee

#### A DISSERTATION

Submitted to

Michigan State University
in partial fulfillment of the requirements
for the degree of

DOCTOR OF PHILOSOPHY
in
Engineering Mechanics

Department of Metallurgy, Mechanics and Materials Science

#### **ABSTRACT**

# A STUDY OF THE INTERLAMINAR STRESS CONTINUITY THEORIES FOR COMPOSITE LAMINATES

By

#### Chun-Ying Lee

In this study, two stress continuity theories are presented. The first one, named interlaminar stress continuity theory (ISCT), accounts for the variation of transverse displacement through the laminate thickness. The continuity of interlaminar shear stresses and normal stress across the laminate interfaces and traction conditions on laminate surfaces are satisfied exactly. The second, interlaminar shear stress continuity (ISSCT), simplifies ISCT by assuming constant transverse displacement through the thickness. Thus, only the continuity of interlaminar shear stresses and shear traction conditions on laminate surfaces are enforced. The merit of these stress continuity theories is the direct calculation of interlaminar stresses from constitutive equations instead of equilibrium equations. The numerical examples for composite laminates with aspect ratio higher than five in cylindrical bending and bidirectional bending using both theories show excellent accuracy compared with elasticity solutions. ISCT provides significant improvement over ISSCT for composite analysis only when the aspect ratio is lower than five. The comparison among other displacement-based laminate theories and present theories is also performed.

Techniques to reduce the computational effort for these stress continuity theories are proposed in response to the composite analysis of many-layer laminate. The layer re-

duction technique provides a methodology to retain good accuracy while reduces the number of degree-of-freedom in composite analysis using present theories.

The further applications of ISSCT in composite analysis, e.g., vibration, buckling, nonlinear bending, nonlinear vibration, and free-edge stresses are studied. The associated numerical examples show the feasibility and potential of using this new theory in the study of composite laminates.

To Mei-wen

#### **ACKNOWLEDGMENTS**

First, I would like to express my deep gratitude and appreciation to my major advisor, Dr. Dahsin Liu, for his true friendship, constant encouragement, and guidance.

I am also indebted to Dr. Nicholas J. Altiero for his moral support and endeavour to do the best for students.

Thanks also extend to my college friends at MSU for their hearty encouragement during the course of this study. In addition, the sustained discussion and suggestion by Mr. Xianqiang Lu is acknowledged.

Finally, but not the least, I thank the moral support and encouragement of my family that made the difficult time easier to overcome. Especially, a great debt is owed to my wife, Mei-wen, for her understanding and patience during these five years.

## TABLES OF CONTENTS

List of Tables	viii
List of Figures	x
Chapter 1 - Introduction	1
1.1 Motivation	1
1.2 Literature Review	3
1:3 Present Work	6
Chapter 2 - Interlaminar Stress Continuity Theories	8
2.1 Introduction	8
2.2 Interlaminar Stress Continuity Theory (ISCT)	8
2.3 Interlaminar Shear Stress Continuity Theory (ISSCT)	17
2.4 Closed-Form Solution	21
2.5 Finite Element Solution	23
Chapter 3 - Assessments of the Stress Continuity Theories	24
3.1 Introduction	24
3.2 Numerical Examples for Stress Continuity Theories	24
3.2.1 Laminates under Cylindrical Bending	24
3.2.2 Laminates under Bidirectional Bending	33
3.3 Comparison of Different Laminate Theories	49
3.3.1 Number of Degree-of-Freedom	49
3.3.2 Recovery of Transverse Stresses	52
3.3.3 Closed-Form Solutions for Different Laminate Theories	53
3.3.4 Summary	59

Chapter 4 - Techniques for Layer Reduction	67
4.1 Introduction	67
4.2 Fundamental Techniques	67
4.3 Numerical Examples	66
4.3.1 Cylindrical Bending	71
4.3.2 Bidirectional Bending	71
4.4 Discussions	75
Chapter 5 - Applications of ISSCT in Vibration, Buckling, and Nonlinear Analysis.	84
5.1 Introduction	84
5.2 Natural Vibration	84
5.3 Critical Buckling Load	87
5.4 Nonlinear Bending	96
5.4.1 Formulation of Nonlinear Equation	96
5.4.2 Laminates Subjected to Transverse Loadings	100
5.4.3 Laminates Subjected to Inplane Loadings	106
5.5 Large-Amplitude Vibration	109
5.6 Free-Edge Stresses	114
Chapter 6 - Conclusions and Recommendations	119
6.1 Conclusions	119
6.2 Recommendations	120
Appendices	122
Appendix A - [E] and {q} Matrices	122
Appendix B - The Equivalence of ISSCT and HSDT for One-Layer Laminate	126
List of References	128

### LIST OF TABLES

Table 3.1 - Results of a simply-supported [0/90] laminate under cylindrical bending by using ISSCT
Table 3.2 - Results of a simply-supported [0/90/0] laminate under cylindrical bending by using ISSCT
Table 3.3 - Results of a simply-supported [0/90] laminate under cylindrical bending by using ISCT
Table 3.4 - Results of a simply-supported [0/90/0] laminate under cylindrical bending by using ISCT
Table 3.5 - Closed-form solutions of a simply-supported [0/90/90/0] square (a=b) laminate under bidirectional bending by using ISSCT
Table 3.6 - Closed-form solutions of a simply-supported [0/90/0] rectangular (3a=b) laminate under bidirectional bending by using ISSCT
Table 3.7 - Closed-form solutions of a simply-supported [0/90/90/0] square (a=b) laminate under bidirectional bending by using ISCT
Table 3.8 - Closed-form solutions of a simply-supported [0/90/0] rectangular (3a=b) laminate under bidirectional bending by using ISCT
Table 3.9 - Finite element solutions of a simply-supported [0/90/90/0] square (a=b) laminate under bidirectional bending by using ISSCT
Table 3.10 - Comparison of different laminate theories for an n-layer laminate 51
Table 3.11 - Closed-form solutions of a [0/90] laminate under cylindrical bending by using different laminate theories
Table 3.12 - Closed-form solutions of a [0/90/90/0] laminate under cylindrical bending by using different laminate theories
Table 3.13 - Closed-form solutions of a square (a=b) [0/90/90/0] laminate under bidirectional bending by using different laminate theories
Table 3.14 - Closed-form solutions of a rectangular (3a=b) [0/90/0] laminate under bidirectional bending by using different laminate theories

Table 5.1	- Normalized fundamental frequency λ, of a simply-supported [0/90/90/0] square laminate	
Table 5.2	- Normalized first buckling load $\lambda_b$ of a simply-supported [0/90/90/0] square laminate	
Table 5.3	- Normalized first buckling load λ <sub>b</sub> of a simply-supported [0/90] square laminate	
Table 5.4	- Normalized first buckling load $\lambda_b$ of a simply-supported [0/90/0/90/0/90] square laminate	

### LIST OF FIGURES

Figure 2.1 - Coordinate system and displacement variables
Figure 3.1 - Simply-supported composite laminate under cylindrical bending
Figure 3.2 - Normalized transverse displacements at midspan for [0], [0/90], and [0/90/0 laminates with different aspect ratios
Figure 3.3 - Normalized inplane displacement $\bar{u}(0)$ of a simply-supported [0/90] laminate with S=4 under cylindrical bending
Figure 3.4 - Normalized inplane normal stress $\bar{\sigma}_x(l/2)$ of a simply-supported [0/90] laminate with S=4 under cylindrical bending
Figure 3.5 - Normalized transverse shear stress $\bar{\sigma}_{xz}(0)$ of a simply-supported [0/90] laminate with S=4 under cylindrical bending
Figure 3.6 - Normalized transverse normal stress $\bar{\sigma}_{z}(l/2)$ of a simply-supported [0/90 laminate with S=4 under cylindrical bending
Figure 3.7 - Normalized inplane displacement $\bar{u}(0)$ of a simply-supported [0/90/0] laminate with S=4 under cylindrical bending
Figure 3.8 - Normalized inplane normal stress $\bar{\sigma}_x(1/2)$ of a simply-supported [0/90/0] lam inate with S=4 under cylindrical bending
Figure 3.9 - Normalized transverse shear stress $\bar{\sigma}_{xx}(0)$ of a simply-supported [0/90/0 laminate with S=4 under cylindrical bending
Figure 3.10 - Normalized transverse normal stress $\bar{\sigma}_z(l/2)$ of a simply-supported [0/90/0 laminate with S=4 under cylindrical bending
Figure 3.11- Simply-supported composite laminate under bidirectionally sinusoidal load ing
Figure 3.12 - Normalized transverse shear stresses at the edge of a simply-supported [0 90] laminate with S=4 by using different laminate theories. (a) constitutive equations, (b) equilibrium equations
Figure 3.13 - Normalized transverse shear stresses at the edge of a simply-supported [0 90/0] laminate with S=4 by using different laminate theories, (a) constitutive

equations, (b) equilibrium equations57
Figure 3.14 - Normalized midspan deflections $w(l/2,0)$ of a simply-supported [0/90] laminate under cylindrical bending by using different laminate theories 63
Figure 3.15 - Normalized inplane normal stresses $\sigma_x(l/2,h/2)$ of a simply-supported [0/90] laminate under cylindrical bending by using different laminate theories 64
Figure 3.16 - Normalized transverse shear stresses $\sigma_{xx}(0,0)$ of a simply-supported [0/90] laminate under cylindrical bending by using different laminate theories 65
Figure 3.17 -Normalized transverse normal stresses σ <sub>z</sub> ( U2, 0) of a simply-supported [0, 90] laminate under cylindrical bending by using different laminate theories
Figure 4.1 - Cross-sections of original and reduced layups
Figure 4.2 - Normalized midspan deflections of a [0/90/0/90/0]s laminate under cylindrical bending at different aspect ratios from different layer reduction approaches
Figure 4.3 - Normalized inplane normal stress $\bar{\sigma}_x(1/2,\pm h/2)$ of a [0/90/0/90/0]s laminate under cylindrical bending at different aspect ratios from different layer reduction approaches
Figure 4.4 - Normalized transverse shear stress $\bar{\sigma}_{xx}(0,0)$ of a [0/90/0/90/0]s laminate under cylindrical bending at different aspect ratios from different layer reduction approaches
Figure 4.5 - Normalized inplane displacement $\bar{u}$ ( $a/2$ , 0) of a square [0/90/0/90/0]s laminate subjected to bidirectional bending at S=4 from different layer reduction approaches
Figure 4.6 - Normalized inplane displacement $\bar{\nu}(0, b/2)$ of a square [0/90/0/90/0]s laminate subjected to bidirectional bending at S=4 from different layer reduction approaches
Figure 4.7 - Normalized inplane normal stress $\bar{\sigma}_{g}(a/2,b/2)$ of a square [0/90/0/90/0]s laminate subjected to bidirectional bending at S=4 from different layer reduction approaches
Figure 4.8 - Normalized inplane normal stress $\bar{\sigma}_y(a/2,b/2)$ of a square [0/90/0/90/0]s laminate subjected to bidirectional bending at S=4 from different layer reduction approaches
Figure 4.9 - Normalized inplane shear stress $\bar{\sigma}_{xy}(0,0)$ of a square [0/90/0/90/0]s laminate subjected to bidirectional bending at S=4 from different layer reduction approaches
Figure 4.10 - Normalized transverse shear stress $\bar{\sigma}_{-}(0,b/2)$ of a square $[0/90/0/90/0]$ s

	laminate subjected to bidirectional bending at S=4 from different layer reduction approaches
Figure 4.11	- Normalized transverse shear stress $\bar{\sigma}_{yz}(a/2,0)$ of a square $[0/90/0/90/0]$ s laminate subjected to bidirectional bending at S=4 from different layer reduction approaches
Figure 5.1 -	Fundamental frequencies of simply-supported [0],[0/90] and [0/90/0] laminates with different aspect ratios under cylindrical bending
Figure 5.2 -	Pinned-pinned [0/90] laminate with aspect ratio S=225 subjected to uniformly distributed loading: (a) inplane force resultant; (b) midspan deflection 101
Figure 5.3 -	Normalized stresses of a pinned-pinned [0/90] laminate with S=22.5 subjected to uniformly distributed loadings: (a) $\sigma_x$ ( $l/2$ ,- $l/2$ ); (b) $\sigma_{xz}$ ( 0, 0) 103
Figure 5.4 -	Normalized stresses of a pinned-pinned [0/90] laminate with S=22.5 subjected to uniformly distributed loading: (a) $\sigma_x$ ( $l/2$ , $z$ ); (b) $\sigma_{xz}$ (0, $z$ ) 104
Figure 5.5 -	Normalized nonlinear results of [0/90] laminated beam with S=225 subjected to uniformly distributed loading in three different boundary conditions: (a) midspan deflections; (b) inplane force resultants
Figure 5.6 -	The load-deflection curve of a square [0] laminate with all edge clamped and $a/h = 100$ is subjected to uniformly distributed loading
Figure 5.7 -	The load-deflection curve of a simply-supported [0/90] laminate under cylindrical bending with S=225 is subjected to inplane compressive loading 108
Figure 5.8 -	The load-deflection curve of a simply-supported square $[0/90]$ laminate with $a/h = 1000$ is subjected to inplane compressive loading in the x-direction 110
Figure 5.9 -	The amplitude-dependent fundamental frequency of a pinned-pinned [0/90/90/0] laminate with S=100 under cylindrical bending
Figure 5.10	- Normalized amplitude-dependent fundamental frequencies of [0/90/90/0] laminate in three different boundary conditions: (a) S=100; (b) S=10 113
Figure 5.11	- The change of nonlinear fundamental frequency and mode shape of $[0/90/90/0]$ laminate at the vibration amplitude A/r =2.0: (a) fundamental frequency; (b) coherence factor
Figure 5.12	- Mesh layout for [45/-45]s laminate in calculation of free-edge stress 117
Figure 5.13	-Normalized results of a $[45/-45]$ s laminate subjected to uniform inplane loading: (a) the through-the-width in-plane displacement $u$ $(0, y, h/2)$ ; (b) the through-the-width interlaminar shear stress $\sigma_{xx}$ $(0, y, h/4)$

#### CHAPTER 1

#### INTRODUCTION

#### 1.1 Motivation

Fiber-reinforced composite materials have been widely used in both aerospace and automotive industries since 1960 due to their high stiffness-to-weight and high strength-to-weight ratios. Their flexibilities in design and manufacturing are also excellent. However, because of the heterogeneity of the composite materials through the thickness and the anisotropy in the individual layers, the design and analytical techniques developed for conventional materials and structures cannot be used for composite materials. For example, it is more accurate to express the strength of a composite material by a curve of probability of failure instead of a single value; the stress concentration around a cutout in a laminated composite must account for the boundary-layer effect; the low ratio of transverse shear modulus to inplane tensile modulus renders the composite laminates more vulnerable to transverse shear deformation; and the coupling effects among the inplane loading, inplane shear deformation, and out-of-plane deformation make the prediction of composite behavior more complicated. All these unconventional phenomena stimulate new studies on the behavior of composite materials and structures.

The first theory used in the analysis of laminated composites is the classical laminate theory (CLT). It is based on Kirchhoff's deformation assumptions. However, due to the low transverse shear modulus of the composite laminates, CLT seems to overestimate the stiffness of laminated composites due to the neglect of transverse shear deformation. CLT has been there for long time. In recent years, many investigations have been focused on the development of new or refined laminate theories to improve the prediction of the behaviors of laminated composites with various types of geometry and loading conditions

By modifying the assumption of the displacement field of CLT, the first-order shear deformation theory (FSDT) [7] and the high-order shear deformation theories (HSDT) [8-12] take the transverse shear deformation into account and therefore improve the accuracy of composite analysis. Although the properties of the individual layers are considered in these laminate theories, they virtually treat the composite laminates as single-layer structures. Generally, these single-layer approaches give good results in global responses, such as deflection, vibration frequency, critical buckling load, etc. However, as far as the local responses of the composite laminates are concerned, the single-layer approaches usually cannot generate satisfactory results. For example, the transverse stresses and through-the-thickness deformation cannot be obtained from these techniques directly. Unfortunately, these kinds of local information are crucial to the analysis of delamination, debonding, and free-edge effect in composite laminates.

In view of the problems, a laminate theory based on multiple-layer approach is really desired. Among the investigations in this area, the generalized laminated plate theory (GLPT) [5], is the most recent and advanced technique. However, since the displacement field used in the GLPT does not satisfy the interlaminar stress continuity at the composite interfaces, the calculation of transverse stresses needs to resort to stress recovery technique which is usually achieved by using equilibrium equations. During the stress recovery process, the numerical differentiation can worsen the accuracy of the results. This deficiency can be overcome with the introduction of interlaminar stress continuity on the composite interfaces. In addition, the incorporation of interlaminar stress continuity conditions in the displacement field has the potential to increase the accuracy and to decrease the degree-of-freedom of the GLPT. This motivates the studies carried out in this thesis.

#### 1.2 Literature Review

Structures composed of laminated composites are frequently modeled as singlelayer plates by classical laminate theory. However, as the aspect ratio, i.e., the span to thickness ratio, of a structure becomes smaller, the CLT can produce erroneous results [6]. This is due to the neglect of transverse shear deformation which is critically important in materials which have relatively low transverse shear modulus compared to inplane tensile modulus. To account for this deficiency, the idea of Reissner-Mindlin plate theory for isotropic plates was first adopted by Yang, Norris, and Stavsky [7] for composite laminates. However, the determination of shear correction factor for some particular problems is very difficult. This shortcoming of the first-order shear deformation theory was overcome by the so-called higher order shear deformation theories [8-12]. The introduction of a higherorder displacement field made the shear correction factor redundant in the analysis. It also automatically improved the accuracy of transverse shear stress distribution. Although the high-order laminate theories gave better predictions of global responses, such as deflection, vibration frequency, and critical buckling load, they were of single-layer approach and discounted the independence of individual layers. Hence, the transverse stresses could not be obtained satisfactorily from constitutive equations.

By considering the layers in a composite laminate individually, the multiple-layer approaches generally produced more accurate results for both global and local responses. According to the variational theorems employed, the approaches used for multiple-layer laminate theories can be divided into the following four categories.

#### (1) Ambartsumyan's Approach

This method was first proposed by Ambartsumyan for symmetric cross-ply laminates [13], and further generalized by Whitney for symmetric laminates [14]. In this approach, a continuous transverse shear stress field was assumed for composite laminates first. Then, by using constitutive equations and integration through the thickness, a displacement field was obtained. Based on this displacement field and equations of motion

from classical plate theory, the governing differential equations were derived for composite analysis. Since no variational principle was used in this analysis, the displacement field, governing equations, and boundary conditions obtained from this approach were variationally inconsistent. Moreover, the solutions only showed small improvements in the global responses.

#### (2) Hybrid-stress Finite Element Method

Due to the difficulty in satisfying the transverse stress continuity at the composite interfaces by using conventional displacement-based finite element method [15], a so-called hybrid-stress finite element method was developed to overcome this problem by assuming a stress field for finite elements [16,17]. With the assumed stress field, which satisfied the equilibrium equations exactly, and the principle of minimum complementary energy, the formulation of finite element analysis was achieved. Because of the carefully assumed stress field, the stresses resulted from this technique were very accurate when compared with elasticity solutions. However, the shortcoming of this method was the sophistication in determining an appropriate stress field. In addition, as the order of the stress field increased, the derivation became very tedious.

#### (3) Mixed Variational Principle

Another method to satisfy both displacement and transverse stress continuity conditions at the composite interfaces was to assume displacement field and transverse stress field independently. This technique was performed by Murakami and Toledano [18,19] with the use of a mixed variational principle developed by Reissner [20]. Although the inplane response was greatly improved by this technique, the transverse stresses needed to resort to the equilibrium equations for more accurate results.

#### (4) Principle of Virtual Displacement

In this category, all approaches were based on assumed displacement fields. Seide [21] assumed a layer-wise linear displacement field for composite laminates and solved simultaneous equations for individual layers by considering interfacial continuity condi-

tions. DiSciuva developed a shear-deformable rectangular plate element based on a piecewise linear displacement field [22,23]. With this linear displacement field, the transverse shear stresses satisfied the continuity condition at the interfaces of the composite laminate. However, the shear traction boundary conditions at top and bottom surfaces of composite laminates were not assured. Therefore, the transverse stresses could not be calculated directly from constitutive equations. Another approach, proposed by Hinrichsen and Palazotto [24], used a cubic spline functions to describe the displacement field in the thickness direction. However, this C<sup>2</sup> continuous displacement field resulted in a continuous strain field through the thickness, hence overconstrained the composite response. Recently, a socalled generalized laminated plate theory (GLPT) was presented by Reddy [5]. It was further expanded by his colleagues [25,26]. In this theory, a layer-wise representation of inplane displacements resulted in improved inplane response and transverse shear deformation. However, due to the low-order displacement field used, the surface shear traction boundary conditions and the interfacial transverse shear stress continuities could not be satisfied beforehand [25,26]. A sophisticated technique using equilibrium equations for recovering transverse stresses must be enforced in the post-process calculation [26].

Along with all the attempts mentioned above to solve the response of composite laminates, there was little success in using elasticity approach. Pagano [6], and Pagano and Hatfield [27] solved simply-supported cross-ply laminates under cylindrical bending and bidirectional bending, respectively. The exact solution of natural frequencies for laminates under cylindrical bending was presented by Jones for cross-ply layups [28] and off-axis laminae [29]. Kulkarni and Pagano extended this technique for off-axis laminates [30]. The vibration analysis for rectangular laminates by Srinivas, Rao, and Rao [31] was limited to laminates composed of isotropic layers, while the study by Noor was associated with vibration of cross-ply laminates [32] and stability of multi-layered composites [33]. The results from elasticity solutions can serve as examples for assessing the laminate theories.

#### 1.3 Present Studies

Upon the demand for finding both displacements and stresses accurately and efficiently in the composite laminate analysis, it is the intention of this study to develop a displacement-based laminate theory which can calculate the transverse stresses directly from the constitutive equations. Hence, the numerical differentiation during the recovery of transverse stresses, which usually reduces the accuracy of the results, and other deficiency of the recovery technique for some particular problems [34] can be avoided.

In order to calculate the transverse stresses directly from the constitutive equations, the displacement field should conform to the stress field in the laminate. In other words, the continuity of interfacial tractions and the boundary tractions at top and bottom surfaces of composite laminates need to be satisfied exactly when the displacement field is assumed. These requirements can be accomplished by assuming layer-wise cubic displacement functions through the thickness and incorporating the traction boundary conditions in the formulation. With this conformal displacement field, the governing equations and associated boundary conditions can be obtained via the principle of virtual displacement. In this study, an interlaminar stress continuity theory (ISCT) is derived first. Then, by assuming constant transverse displacement through the thickness, which is used in most laminate theories, the derivation can be reduced to interlaminar shear stress continuity theory (ISCT). The formulations of these theories constitute Chapter 2 of this thesis.

In Chapter 3, numerical examples for static bending are used to demonstrate the accuracy of these interlaminar stress continuity theories by comparing them with elasticity solutions. In addition, a comprehensive disscusion regarding the stress continuity theories and other laminate theories is also presented.

Due to the increase of the order of displacement function through the thickness, the number of displacement variables in the interlaminar stress continuity theories increases accordingly. As the number of layers in a composite laminate increases dramatically, the burden of a huge number of degree-of-freedom on the computational effort can easily

jeopardize the feasiblity of these theories. Therefore, a layer reduction technique is proposed in Chapter 4 with a goal to keep the computational effort to minimum while still retain fair accuracy. The demonstration of this technique is carried out for ISSCT only, though similar procedure can be used for ISCT.

Chapter 5 presents the applications of ISSCT for natural vibration, linear buckling load, nonlinear bending, nonlinear vibration, and free-edge stresses of composite laminates. Finally, the conclusions and recommendations for this study are summarized in Chapter 6.

#### CHAPTER 2

#### INTERLAMINAR STRESS CONTINUITY THEORIES

#### 2.1 Introduction

Ever since the use of classical laminate theory (CLT), many studies were devoted to the development of a more accurate theory for composite stress analysis. First was the first-order shear deformation theory (FSDT). It accounted for transverse shear deformation which was ignored in the CLT. However, the difficulty in determining shear correction factor for FSDT rendered it inconvenient to use. By assuming higher order displacement field, the high-order shear deformation theories (HSDT) overcame the problem of shear correction factor. They were also able to give good results for deflection and vibration analysis. Regardless of their advantages, a more refined theory was desired to present more accurate stresses. By modeling the individual layers of a composite laminate separately, the multiple-layer theories gave improvement in predicting both deflection and stress state. Nevertheless, among the developed multiple-layer theories, the continuity of interlaminar stresses was not satisfied. Hence, the correct transverse stresses could only be obtained by means of equilibrium equations. In this respect, two interlaminar stress continuity theories which allow the calculation of transverse stresses directly from the constitutive equations are presented.

#### 2.2 Interlaminar Stress Continuity Theory (ISCT)

In deriving the interlaminar stress continuity theory, the following displacement field is assumed for an n-layer composite laminate:

$$u(x, y, z) = \sum_{i=1}^{n} (U_{i-1}(x, y) \phi_1^{(i)} + \hat{T}_{2i-2}(x, y) \phi_2^{(i)} + U_i(x, y) \phi_3^{(i)} + \hat{T}_{2i-1}(x, y) \phi_4^{(i)})$$

$$v(x, y, z) = \sum_{i=1}^{n} (V_{i-1}(x, y) \phi_1^{(i)} + \hat{S}_{2i-2}(x, y) \phi_2^{(i)} + V_i(x, y) \phi_3^{(i)} + \hat{S}_{2i-1}(x, y) \phi_4^{(i)})$$

$$w(x, y, z) = \sum_{i=1}^{n} (W_{i-1}(x, y) \phi_1^{(i)} + \hat{R}_{2i-2}(x, y) \phi_2^{(i)} + W_i(x, y) \phi_3^{(i)} + \hat{R}_{2i-1}(x, y) \phi_4^{(i)})$$

$$(2.1)$$

where \phi's are so-called Hermite cubic interpolation functions and are defined as follows

$$\phi_{1}^{(i)} = 1 - 3 \left( \frac{z - z_{i-1}}{h_i} \right)^2 + 2 \left( \frac{z - z_{i-1}}{h_i} \right)^3$$

$$\phi_{2}^{(i)} = (z - z_{i-1}) \left( 1 - \frac{z - z_{i-1}}{h_i} \right)^2$$

$$\phi_{3}^{(i)} = 3 \left( \frac{z - z_{i-1}}{h_i} \right)^2 - 2 \left( \frac{z - z_{i-1}}{h_i} \right)^3$$

$$\phi_{4}^{(i)} = (z - z_{i-1}) \left( \left( \frac{z - z_{i-1}}{h_i} \right)^2 - \frac{z - z_{i-1}}{h_i} \right)$$

$$\phi_{1}^{(i)} = \phi_{2}^{(i)} = \phi_{3}^{(i)} = \phi_{4}^{(i)} = 0 \qquad z < z_{i-1} \text{ or } z > z_{i}$$

As depicted in Figure 2.1, (i) represents for the number of layer and  $h_i$  the thickness of the layer.  $U_i$ ,  $V_i$ , and  $W_i$  denote single-valued displacement components at the interface between (i) and (i+1) layers in x, y, and z directions, respectively. Hence, the continuity of displacements across the interface is enforced. In addition,  $\hat{T}_{2i-2}$ ,  $\hat{S}_{2i-2}$ , and  $\hat{R}_{2i-2}$  stand for the first derivatives of u, v, and w with respect to z immediately below the interface, respectively, while  $\hat{T}_{2i-1}$ ,  $\hat{S}_{2i-1}$ , and  $\hat{R}_{2i-1}$  above the interface. Since the continuity of interlaminar tractions must be satisfied at every interface, some of the first derivatives can be eliminated.

In this study, composite laminates are assumed to deform within a linear elastic range. Hence, the following linear strain-displacement relations hold.

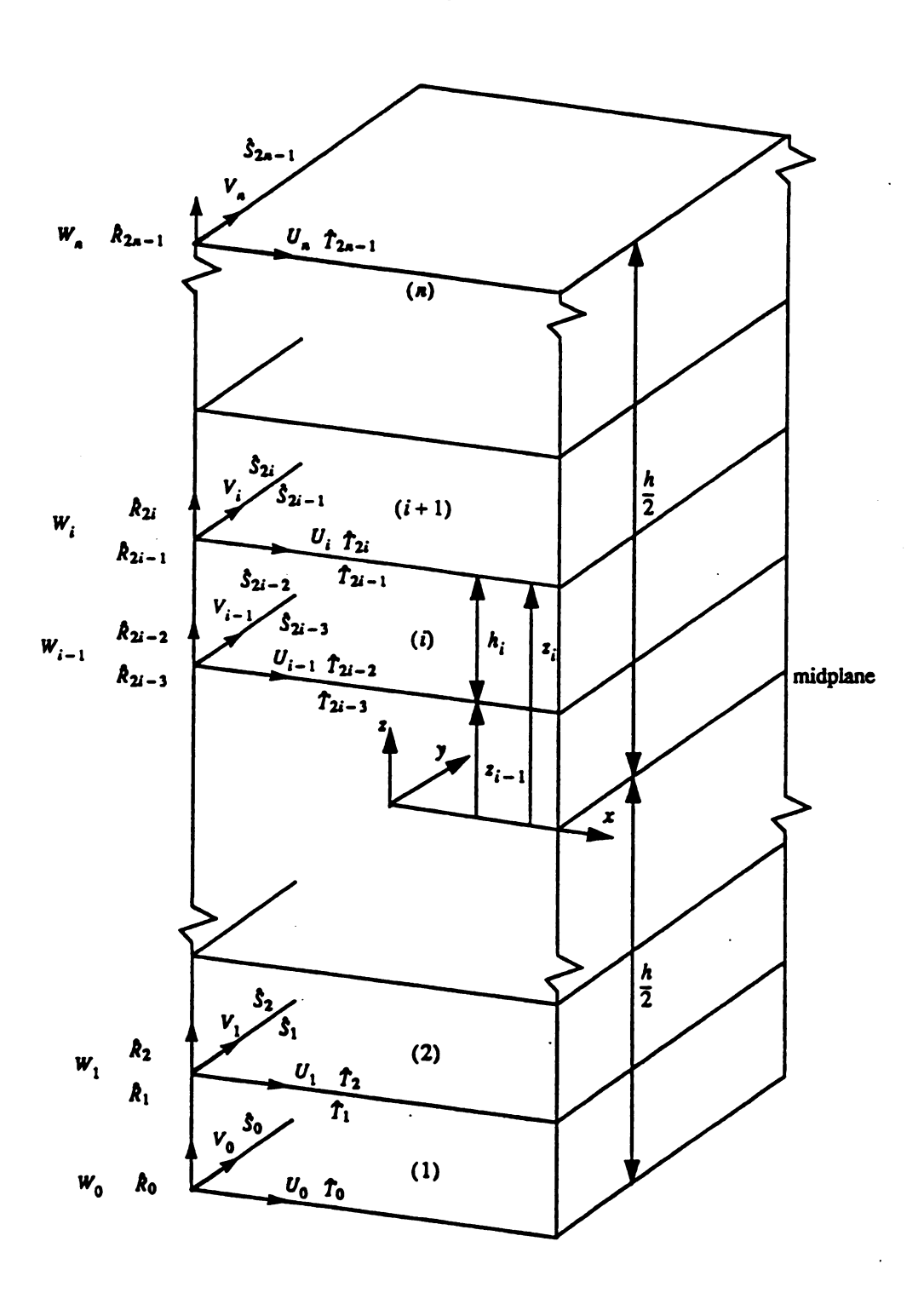


Figure 2.1 Coordinate system and displacement variables.

$$\varepsilon_{x} = \frac{\partial u}{\partial x}, \qquad \varepsilon_{y} = \frac{\partial v}{\partial y}, \qquad \varepsilon_{z} = \frac{\partial w}{\partial z}$$

$$2\varepsilon_{xy} = \frac{\partial u}{\partial y} + \frac{\partial v}{\partial x}, \qquad 2\varepsilon_{yz} = \frac{\partial v}{\partial z} + \frac{\partial w}{\partial y}, \qquad 2\varepsilon_{xz} = \frac{\partial u}{\partial z} + \frac{\partial w}{\partial x}$$
(2.3)

With these strain components, the stresses in each layer can be calculated from the following constitutive equations for orthotropic materials,

$$\begin{cases}
\sigma_{x} \\
\sigma_{y} \\
\sigma_{z} \\
\sigma_{xy}
\end{cases}^{(i)} = 
\begin{bmatrix}
Q_{11} Q_{12} Q_{13} Q_{16} \\
Q_{12} Q_{22} Q_{23} Q_{26} \\
Q_{13} Q_{23} Q_{33} Q_{36} \\
Q_{16} Q_{26} Q_{36} Q_{66}
\end{bmatrix}^{(i)} 
\begin{cases}
\varepsilon_{x} \\
\varepsilon_{y} \\
\varepsilon_{z} \\
2\varepsilon_{xy}
\end{cases}^{(i)}$$
(2.4a)

where the definitions of Q's can be found in Reference [35]. By substituting the displacement field into the transverse shear strains in the strain-diaplacement relations and then the constitutive equations, the continuity condition for the transverse shear stresses at the i-interface can be employed, i.e.,

$$\left\{ \begin{array}{l} \sigma_{yz} \\ \sigma_{xz} \end{array} \right\}_{z=z_{i}}^{(i)} = \left\{ \begin{array}{l} \sigma_{yz} \\ \sigma_{xz} \end{array} \right\}_{z=z_{i}}^{(i+1)} \qquad i=1,2,3,...,n-1$$
(2.5)

These equations can help to eliminate some variables. In fact, the following correlations between the first derivatives can be established,

$$\left\{\begin{array}{c} \hat{S}_{2i-1} \\ \hat{T}_{2i-1} \end{array}\right\} = \left[A\right]^{(i)} \left\{\begin{array}{c} \hat{S}_{2i} \\ \hat{T}_{2i} \end{array}\right\} + \left[B\right]^{(i)} \left\{\begin{array}{c} \frac{\partial W_i}{\partial y} \\ \frac{\partial W_i}{\partial x} \end{array}\right\}$$
(2.6)

where

$$\begin{bmatrix} A \end{bmatrix}^{(i)} = \begin{bmatrix} A_{11} & A_{12} \\ A_{21} & A_{22} \end{bmatrix}^{(i)} = \begin{bmatrix} Q_{44}^{(i)} & Q_{45}^{(i)} \\ Q_{45}^{(i)} & Q_{55}^{(i)} \end{bmatrix}^{-1} \begin{bmatrix} Q_{44}^{(i+1)} & Q_{45}^{(i+1)} \\ Q_{45}^{(i+1)} & Q_{55}^{(i+1)} \end{bmatrix}$$
(2.7a)

$$\begin{bmatrix} B \end{bmatrix}^{(i)} = \begin{bmatrix} B_{11} & B_{12} \\ B_{21} & B_{22} \end{bmatrix}^{(i)} = \begin{bmatrix} A_{11} & A_{12} \\ A_{21} & A_{22} \end{bmatrix}^{(i)} - \begin{bmatrix} 1 & 0 \\ 0 & 1 \end{bmatrix} \qquad i = 1,2,3,...,n-1 \qquad (2.7b)$$

Similarly, the continuity condition of the transverse normal stress at the *i*-interface, i.e.,

$$\sigma_z^{(i)}\Big|_{z=z_i} = \sigma_z^{(i+1)}\Big|_{z=z_i} \qquad i=1,2,3,...,n-1$$
 (2.8)

can also be satisfied by requiring

$$\hat{R}_{2i-1} = C_1^{(i)} \frac{\partial U_i}{\partial x} + C_2^{(i)} \frac{\partial U_i}{\partial y} + C_2^{(i)} \frac{\partial V_i}{\partial x} + C_3^{(i)} \frac{\partial V_i}{\partial y} + C_4^{(i)} \hat{R}_{2i}$$
 (2.9)

in which

$$C_1^{(i)} = \frac{Q_{13}^{(i+1)} - Q_{13}^{(i)}}{Q_{33}^{(i)}}$$
 (2.10a)

$$C_2^{(i)} = \frac{Q_{36}^{(i+1)} - Q_{36}^{(i)}}{Q_{33}^{(i)}}$$
 (2.10b)

$$C_3^{(i)} = \frac{Q_{23}^{(i+1)} - Q_{23}^{(i)}}{Q_{33}^{(i)}}$$
 (2.10c)

$$C_4^{(i)} = \frac{Q_{33}^{(i+1)}}{Q_{33}^{(i)}} \tag{2.10d}$$

From Equations (2.6) and (2.9), it is clear that the first derivatives of u, v, and w with respect to z right below the interface are related to those right above the interface and some other dispacement components. By letting

$$\begin{bmatrix} A^{(n)} \end{bmatrix} = \begin{bmatrix} 1 & 0 \\ 0 & 1 \end{bmatrix} \quad \text{and} \quad \begin{bmatrix} B^{(n)} \end{bmatrix} = \begin{bmatrix} 0 & 0 \\ 0 & 0 \end{bmatrix}$$
 (2.11a)

$$C_1^{(n)} = C_2^{(n)} = C_3^{(n)} = 0;$$
  $C_4^{(n)} = 1$  (2.11b)

and changing the notations

$$\hat{T}_{2i} = T_i$$
;  $\hat{S}_{2i} = S_i$ ;  $\hat{R}_{2i} = R_i$   $i = 0,1,2,3,...,n-1$   
 $\hat{T}_{2n-1} = T_n$ ;  $\hat{S}_{2n-1} = S_n$ ;  $\hat{R}_{2n-1} = R_n$  (2.12)

the displacement field can be rewritten as follows,

$$u = \sum_{i=1}^{n} (U_{i-1} \phi_{1}^{(i)} + T_{i-1} \phi_{2}^{(i)} + U_{i} \phi_{3}^{(i)} + B_{22}^{(i)} \phi_{4}^{(i)} \frac{\partial W_{i}}{\partial x} + B_{21}^{(i)} \phi_{4}^{(i)} \frac{\partial W_{i}}{\partial y} + A_{22}^{(i)} \phi_{4}^{(i)} T_{i} + A_{21}^{(i)} \phi_{4}^{(i)} S_{i})$$

$$v = \sum_{i=1}^{n} (V_{i-1} \phi_{1}^{(i)} + S_{i-1} \phi_{2}^{(i)} + V_{i} \phi_{3}^{(i)} + B_{12}^{(i)} \phi_{4}^{(i)} \frac{\partial W_{i}}{\partial x} + B_{11}^{(i)} \phi_{4}^{(i)} \frac{\partial W_{i}}{\partial y} + A_{12}^{(i)} \phi_{4}^{(i)} T_{i} + A_{11}^{(i)} \phi_{4}^{(i)} S_{i})$$

$$w = \sum_{i=1}^{n} (W_{i-1} \phi_{1}^{(i)} + R_{i-1} \phi_{2}^{(i)} + W_{i} \phi_{3}^{(i)} + C_{1}^{(i)} \phi_{4}^{(i)} \frac{\partial U_{i}}{\partial x} + C_{2}^{(i)} \phi_{4}^{(i)} (\frac{\partial U_{i}}{\partial y} + \frac{\partial V_{i}}{\partial x}) + C_{3}^{(i)} \phi_{4}^{(i)} \frac{\partial V_{i}}{\partial y} + C_{4}^{(i)} \phi_{4}^{(i)} R_{i})$$

$$(2.13)$$

It should be noted that the interlaminar stress continuity conditions reduce the total number of displacement variables from 9n+3 of Equation (2.1) to 6n+6 of Equation (2.13). In this study, for simplicity, a bidirectional laminate with dimensions of  $a \times b$  subjected to a distributed lateral load q(x, y) on the top surface of the laminate is presented. The shear tractions on both top and bottom surfaces and the normal traction on the bottom surface are all equal to zero. Hence, with the principle of virtual displacement, the following variational equation can be written for the composite laminate considered herein,

$$0 = \int_{0}^{a} \int_{0}^{b} \left\{ \int_{-\frac{h}{2}}^{\frac{h}{2}} \left\{ \begin{array}{c} \sigma_{x} \\ \sigma_{y} \\ \sigma_{z} \\ \sigma_{xy} \end{array} \right\}^{T} \left\{ \begin{array}{c} \delta \varepsilon_{x} \\ \delta \varepsilon_{y} \\ \delta \varepsilon_{z} \\ \delta (2\varepsilon_{xy}) \end{array} \right\} + \left\{ \begin{array}{c} \sigma_{yz} \\ \sigma_{xz} \end{array} \right\}^{T} \left\{ \begin{array}{c} \delta (2\varepsilon_{yz}) \\ \delta (2\varepsilon_{xz}) \end{array} \right\} dz - q \delta W_{x} dy dx \quad (2.14)$$

By using the linear strain-displacement relation, Equation (2.3) can be expressed

as

$$\left\{ \begin{array}{l}
2\varepsilon_{yz} \\
2\varepsilon_{xz}
\end{array} \right\}^{(i)} = [N_s^{(i)}] \{\hat{X}_s^{(i)}\}$$
(2.15b)

where the matrices are defined as follows,

$$[N_{a}^{(i)}] = \begin{bmatrix} \phi_{1} \\ \phi_{1} \\ \phi_{1} \end{bmatrix} \begin{bmatrix} \phi_{2} \\ \phi_{2} \end{bmatrix} \begin{bmatrix} \phi_{2} \\ \phi_{2} \end{bmatrix} \begin{bmatrix} \phi_{2} \\ \phi_{2} \end{bmatrix} \begin{bmatrix} \phi_{3} \\ C_{1} \phi'_{4} \end{bmatrix} \begin{bmatrix} C_{2} \phi'_{4} \\ \phi_{3} \end{bmatrix} \begin{bmatrix} C_{2} \phi'_{4} \\ \phi_{3} \end{bmatrix} \begin{bmatrix} C_{3} \phi'_{4} \\ \phi'_{3} \end{bmatrix} \begin{bmatrix} C_{3} \phi'_{4} \\ B_{12} \phi_{4} \\ + B_{22} \phi_{4} \end{bmatrix} \begin{bmatrix} A_{22} \phi_{4} \\ A_{12} \phi_{4} \end{bmatrix} \begin{bmatrix} A_{21} \phi_{4} \\ A_{12} \phi_{4} \end{bmatrix} \begin{bmatrix} A_{21} \phi_{4} \\ A_{11} \phi_{4} \end{bmatrix} \begin{bmatrix} C_{4} \phi'_{4} \end{bmatrix} \begin{bmatrix} C_{4} \phi'_{4} \end{bmatrix} \begin{bmatrix} C_{2} \phi_{4} \\ C_{2} \phi_{4} \end{bmatrix} \begin{bmatrix} C_{3} \phi_{4} \end{bmatrix} \begin{bmatrix} C_{4} \phi'_{3} \\ C_{2} \phi_{4} \end{bmatrix} \begin{bmatrix} C_{4} \phi_{4} \\ C_{2} \phi_{4} \end{bmatrix} \begin{bmatrix} C_{4} \phi_{4} \\ C_{4} \phi'_{4} \end{bmatrix} \begin{bmatrix} C_{4} \phi_{4} \\ C_{$$

$$\{\hat{X}_{n}^{(i)}\}^{T} = \begin{bmatrix} \frac{\partial U_{i-1}}{\partial x}, \frac{\partial U_{i-1}}{\partial y}, \frac{\partial V_{i-1}}{\partial x}, \frac{\partial V_{i-1}}{\partial y}, w_{i-1}, \frac{\partial^{2} w_{i-1}}{\partial x^{2}}, \frac{\partial^{2} w_{i-1}}{\partial x^{2}}, \frac{\partial^{2} w_{i-1}}{\partial y^{2}}, \frac{\partial^{2} w_{i-1}}{\partial x}, \frac{\partial T_{i-1}}{\partial y}, \frac{\partial S_{i-1}}{\partial y}, \frac{\partial S_$$

$$\frac{\partial U_i}{\partial x} \frac{\partial U_i}{\partial y} \frac{\partial V_i}{\partial x} \frac{\partial V_i}{\partial y} \frac{\partial^2 W_i}{\partial y} \frac{\partial^2 W_i}{\partial x^2} \frac{\partial^2 W_i}{\partial x \partial y} \frac{\partial^2 W_i}{\partial y^2} \frac{\partial T_i}{\partial x} \frac{\partial T_i}{\partial y} \frac{\partial S_i}{\partial x} \frac{\partial S_i}{\partial y} \frac{\partial S_i}{\partial x} \frac{\partial S_i}{\partial y} \frac{\partial S_i}{\partial x} \frac{\partial S_i}{\partial y}$$
(2.17a)

$$\{\hat{X}_{s}^{(i)}\}^{T} = \left[U_{i-1}, \frac{\partial^{2}U_{i-1}}{\partial x^{2}}, \frac{\partial^{2}U_{i-1}}{\partial x \partial y}, \frac{\partial^{2}U_{i-1}}{\partial y^{2}}, V_{i-1}, \frac{\partial^{2}V_{i-1}}{\partial x^{2}}, \frac{\partial^{2}V_{i-1}}{\partial x \partial y}, \frac{\partial^{2}V_{i-1}}{\partial y^{2}}, \frac{\partial^{2}V_{i-1}}{\partial x}, \frac{\partial W_{i-1}}{\partial x}, \frac{\partial W_{i-1}}{\partial y}, T_{i-1}, S_{i-1}, \frac{\partial^{2}V_{i-1}}{\partial x^{2}}, \frac{\partial^{2}V_{i-1}}{\partial x^{2}}$$

$$\frac{\partial R_{i-1}}{\partial x}, \frac{\partial R_{i-1}}{\partial y}, U_{i'}, \frac{\partial^{2}U_{i}}{\partial x^{2}}, \frac{\partial^{2}U_{i}}{\partial x \partial y}, \frac{\partial^{2}U_{i}}{\partial y^{2}}, V_{i'}, \frac{\partial^{2}V_{i}}{\partial x^{2}}, \frac{\partial^{2}V_{i}}{\partial x \partial y}, \frac{\partial^{2}V_{i}}{\partial y^{2}}, \frac{\partial^{2}V_{i}}{\partial x}, \frac{\partial W_{i}}{\partial y}, \frac{\partial W_{i}}{\partial y}, T_{i'}, S_{i'}, \frac{\partial R_{i}}{\partial x}, \frac{\partial R_{i}}{\partial y} \right] (2.17b)$$

It should be noted that (') depicts the differentiation with respect to z. Substituting the above expressions into Equation (2.15) and using Equation (2.4), the principle of virtual displacement becomes

$$0 = \int_0^a \int_0^b (\{\delta \hat{X}_n\}^T [S\hat{K}_n] \{\hat{X}_n\} + \{\delta \hat{X}_s\}^T [S\hat{K}_s] \{\hat{X}_s\} - q\delta W_n) \, dy dx \qquad (2.18)$$

In the above equation, the following notations, which represent for the assembled matrices through the thickness, are used.

$$\{\hat{X}_n\} = \sum_{i=1}^n \{\hat{X}_n^{(i)}\}$$
 (2.19a)

$$\{\hat{X}_s\} = \sum_{i=1}^n \{\hat{X}_s^{(i)}\}$$
 (2.19b)

$$[\hat{S}\hat{K}_{n}] = \sum_{i=1}^{n} \int_{z_{i-1}}^{z_{i}} [N_{n}^{(i)}]^{T} \begin{bmatrix} Q_{11} Q_{12} Q_{13} Q_{16} \\ Q_{12} Q_{22} Q_{23} Q_{26} \\ Q_{13} Q_{23} Q_{33} Q_{36} \\ Q_{16} Q_{26} Q_{36} Q_{66} \end{bmatrix}^{(i)} [N_{n}^{(i)}] dz$$
 (2.20a)

$$[S\hat{K}_{s}] = \sum_{i=1}^{n} \int_{z_{i-1}}^{z_{i}} [N_{s}^{(i)}]^{T} \begin{bmatrix} Q_{44} & Q_{45} \\ Q_{45} & Q_{55} \end{bmatrix}^{(i)} [N_{s}^{(i)}] dz$$
 (2.20b)

It is not difficult to see that  $\{\hat{X}_n\}$  has dimensions of  $(13n+13)\times 1$  while  $\{\hat{X}_s\}$   $(14n+14)\times 1$ . Since the laminate surface traction conditions should be satisfied in the assumed displacement field, the number of displacement variables can be further reduced. First, the vanished shear tractions on the surfaces give rise to

$$\left\{ \begin{array}{c} \sigma_{yz} \\ \sigma_{xz} \end{array} \right\}^{(1)} \bigg|_{z=z_0} = \left[ \begin{array}{c} Q_{44}^{(1)} & Q_{45}^{(1)} \\ Q_{45}^{(1)} & Q_{55}^{(1)} \end{array} \right] \left\{ \begin{array}{c} S_0 + \frac{\partial W_0}{\partial y} \\ T_0 + \frac{\partial W_0}{\partial x} \end{array} \right\} = \left\{ \begin{array}{c} 0 \\ 0 \end{array} \right\} \tag{2.21a}$$

$$\left. \left\{ \begin{array}{c} \sigma_{yz} \\ \sigma_{xz} \end{array} \right\}^{(n)} \right|_{z=z_n} = \left[ \begin{array}{c} \mathcal{Q}_{44}^{(n)} & \mathcal{Q}_{45}^{(n)} \\ \mathcal{Q}_{45}^{(n)} & \mathcal{Q}_{55}^{(n)} \end{array} \right] \left\{ \begin{array}{c} S_n + \frac{\partial W_n}{\partial y} \\ T_n + \frac{\partial W_n}{\partial x} \end{array} \right\} = \left\{ \begin{array}{c} 0 \\ 0 \end{array} \right\} \tag{2.21b}$$

Because the matrices of shear moduli are nonsingular, the following equations can be concluded.

$$S_0 = -\frac{\partial W_0}{\partial y}$$
;  $S_n = -\frac{\partial W_n}{\partial y}$  (2.22a)

$$T_0 = -\frac{\partial W_0}{\partial x}$$
 ;  $T_n = -\frac{\partial W_n}{\partial x}$  (2.22b)

Similarly, the conditions to satisfy the applied normal tractions on laminate surfaces,

$$\sigma_z\Big|_{z=-\frac{h}{2}}=0$$
 ;  $\sigma_z\Big|_{z=\frac{h}{2}}=q(x,y)$ 

can be achieved with the following two equations,

$$R_0 = -\frac{Q_{13}^{(1)} \partial U_0}{Q_{33}^{(1)} \partial x} - \frac{Q_{23}^{(1)} \partial V_0}{Q_{33}^{(1)} \partial y} - \frac{Q_{36}^{(1)}}{Q_{33}^{(1)}} (\frac{\partial U_0}{\partial y} + \frac{\partial V_0}{\partial x})$$
(2.23a)

$$R_{n} = -\frac{Q_{13}^{(n)}}{Q_{33}^{(n)}} \frac{\partial U_{n}}{\partial x} - \frac{Q_{23}^{(n)}}{Q_{33}^{(n)}} \frac{\partial V_{n}}{\partial y} - \frac{Q_{36}^{(n)}}{Q_{33}^{(n)}} (\frac{\partial U_{n}}{\partial y} + \frac{\partial V_{n}}{\partial x}) + \frac{q}{Q_{33}^{(n)}}$$
(2.23b)

By incorporating Equations (2.22a,b) and (2.23a,b) in Equations (2.17a,b), the assembled matrices  $\{\hat{X}_n\}$  and  $\{\hat{X}_s\}$  can be associated with the reduced ones,  $\{\hat{X}_n\}$  and  $\{\hat{X}_s\}$ , i.e.,

$$\{\hat{X}_n\} = [E_n] \{\tilde{X}_n\} + \{q_n\}$$
 (2.24a)

$$\{\hat{X}_s\} = [E_s] \{\tilde{X}_s\} + \{q_s\}$$
 (2.24b)

where  $[E_n]$  and  $[E_s]$  are constraint matrices with dimensions of  $(13n+13) \times (13n+3)$  and  $(14n+14) \times (14n+6)$ , respectively, while  $\{q_n\}$  and  $\{q_s\}$  are associated column matrices related to the distributed loading q(x,y). Details of these matrices are listed in Appendix A. It can also be concluded that the total number of independent displacement variables required for the reduced displacement field is 6n. Since both  $\{q_n\}$  and  $\{q_s\}$  are known quantities, the variation of these two column matrices will vanish. Therefore, the substitution of Equation (2.24) into Equation (2.18) yields

$$0 = \int_0^a \int_0^b (\{\delta \tilde{X}_n\}^T ([S\tilde{K}_n] \{\tilde{X}_n\} + [E_n] [S\hat{K}_n] \{q_n\}) + \{\delta \tilde{X}_s\}^T ([S\tilde{K}_s] \{\tilde{X}_s\} + [E_s] [S\hat{K}_s] \{q_s\}) - q\delta W_n) dy dx$$
(2.25)

where

$$[S\tilde{K}_n] = [E_n]^T [S\hat{K}_n] [E_n]$$
 (2.26a)

$$[S\tilde{K}_s] = [E_s]^T [S\hat{K}_s] [E_s]$$
 (2.26b)

#### 2.3 Interlaminar Shear Stress Continuity Theory (ISSCT)

In the foregoing formulation for ISCT, the variation of transverse displacement w in the thickness direction has been taken into account. For very thick composite laminates,

as it will be seen later, this consideration provides a more accurate modeling for composite deformation and stress analysis. However, the high degree-of-freedom results from this assumption becomes a major concern for analysis efficiency. Moreover, as the aspect ratio of a composite laminate increases, the assumption of uniform transverse displacement through the thickness becomes more practical. Hence, there is a need to have a simpler theory for composite lamainate analysis. An interlaminar shear stress continuity theory is then proposed.

Following the notations used in the previous derivation, the displacement field for the interlaminar shear stress continuity theory can be written as

$$u(x, y, z) = \sum_{i=1}^{n} (U_{i-1}(x, y) \phi_{1}^{(i)} + \hat{T}_{2i-2}(x, y) \phi_{2}^{(i)} + U_{i}(x, y) \phi_{3}^{(i)} + \hat{T}_{2i-1}(x, y) \phi_{4}^{(i)})$$

$$v(x, y, z) = \sum_{i=1}^{n} (V_{i-1}(x, y) \phi_{1}^{(i)} + \hat{S}_{2i-2}(x, y) \phi_{2}^{(i)} + V_{i}(x, y) \phi_{3}^{(i)} + \hat{S}_{2i-1}(x, y) \phi_{4}^{(i)}) \qquad (2.27)$$

$$w(x, y, z) = w_{0}(x, y)$$

It should be noted that by assuming constant w over the thickness, the normal strain in the z direction vanishes. Hence the effect of transverse normal stress is neglected in this theory. In other words, the continuity condition of transverse normal stress, Equation (2.8), is automatically satisfied. Again, the number of the first derivatives in Equation (2.27) can be reduced by employing the continuity conditions of transverse shear stresses at the composite interfaces, i.e., Equation (2.5). With the same notations used in Equation (2.12), the reduced displacement field becomes

$$u = \sum_{i=1}^{n} \left( U_{i-1} \phi_{1}^{(i)} + T_{i-1} \phi_{2}^{(i)} + U_{i} \phi_{3}^{(i)} + A_{22}^{(i)} \phi_{4}^{(i)} T_{i} + A_{21}^{(i)} \phi_{4}^{(i)} S_{i} + B_{22}^{(i)} \phi_{4}^{(i)} \frac{\partial w_{0}}{\partial x} + B_{21}^{(i)} \phi_{4}^{(i)} \frac{\partial w_{0}}{\partial y} \right)$$

$$v = \sum_{i=1}^{n} \left( V_{i-1} \phi_{1}^{(i)} + S_{i-1} \phi_{2}^{(i)} + V_{i} \phi_{3}^{(i)} + A_{12}^{(i)} \phi_{4}^{(i)} T_{i} + A_{11}^{(i)} \phi_{4}^{(i)} S_{i} + B_{12}^{(i)} \phi_{4}^{(i)} \frac{\partial w_{0}}{\partial x} + B_{11}^{(i)} \phi_{4}^{(i)} \frac{\partial w_{0}}{\partial y} \right)$$

$$w = w_{0}(x, y)$$

$$(2.28)$$

The principle of virtual displacement for the laminate with the same geometry and loading condition as used in the formulation of ISCT can be obtained from Equation (2.14) by simply dropping the virtual displacement term corresponding to the transverse normal strain, the principle then becomes as follows,

$$0 = \int_{0}^{a} \int_{0}^{b} \left( \int_{-\frac{h}{2}}^{\frac{h}{2}} \left( \left\{ \begin{array}{c} \sigma_{x} \\ \sigma_{y} \\ \sigma_{xy} \end{array} \right\}^{T} \left\{ \begin{array}{c} \delta \varepsilon_{x} \\ \delta \varepsilon_{y} \\ \delta \left( 2\varepsilon_{xy} \right) \end{array} \right\} + \left\{ \begin{array}{c} \sigma_{yz} \\ \sigma_{xz} \end{array} \right\}^{T} \left\{ \begin{array}{c} \delta \left( 2\varepsilon_{yz} \right) \\ \delta \left( 2\varepsilon_{xz} \right) \end{array} \right\} \right) dz - q \delta w_{0} dy dx \quad (2.29)$$

Using Equations (2.3) and (2.28), the strains can be substituted by the displacement variables shown below,

$$\left\{ \begin{array}{l} 2\varepsilon_{yz} \\ 2\varepsilon_{zz} \end{array} \right\}^{(i)} = \left[ N_z^{(i)} \right] \left\{ \dot{X}_z^{(i)} \right\} \tag{2.30b}$$

where the following matrix definitions are used,

$$[N_{A}^{(i)}] = \begin{bmatrix} \phi_{1} \\ \phi_{1} \\ \phi_{1} \end{bmatrix} \phi_{1} \begin{vmatrix} \phi_{2} \\ \phi_{2} \end{vmatrix} \phi_{2} \begin{vmatrix} \phi_{2} \\ \phi_{2} \end{vmatrix} \phi_{3} \begin{vmatrix} \phi_{3} \\ \phi_{3} \end{vmatrix} \phi_{3} \begin{vmatrix} A_{22}\phi_{4} \\ A_{12}\phi_{4} \end{vmatrix} A_{12}\phi_{4} \begin{vmatrix} A_{21}\phi_{4} \\ A_{22}\phi_{4} \end{vmatrix} A_{11}\phi_{4} \begin{vmatrix} A_{11}\phi_{4} \\ A_{21}\phi_{4} \end{vmatrix}$$

$$= \begin{bmatrix} B_{22}\phi_{4} \\ B_{12}\phi_{4} \\ B_{12}\phi_{4} \end{vmatrix} \begin{bmatrix} B_{21}\phi_{4} \\ B_{12}\phi_{4} \\ B_{21}\phi_{4} \end{bmatrix} B_{11}\phi_{4}$$

$$= \begin{bmatrix} B_{22}\phi_{4} \\ B_{12}\phi_{4} \\ B_{11}\phi_{4} + B_{22}\phi_{4} \end{vmatrix} \begin{bmatrix} B_{11}\phi_{4} \\ B_{21}\phi_{4} \\ B_{21}\phi_{4} \end{bmatrix} (2.31a)$$

$$[N_{s}^{(i)}] = \begin{bmatrix} \phi'_{1} & \phi'_{2} & \phi'_{3} & \phi'_{3} & A_{12}\phi'_{4} & A_{11}\phi'_{4} & B_{12}\phi'_{4} & 1 + B_{22}\phi'_{4} \\ \phi'_{1} & \phi'_{2} & \phi'_{3} & \phi'_{3} & A_{22}\phi'_{4} & A_{21}\phi'_{4} & 1 + B_{22}\phi'_{4} & B_{21}\phi'_{4} \end{bmatrix}$$
(2.31b)

$$\begin{cases}
\hat{X}_{n}^{(i)}
\end{cases}^{T} = \begin{bmatrix}
\frac{\partial U_{i-1}}{\partial x}, \frac{\partial U_{i-1}}{\partial y}, \frac{\partial V_{i-1}}{\partial x}, \frac{\partial V_{i-1}}{\partial y}, \frac{\partial T_{i-1}}{\partial x}, \frac{\partial T_{i-1}}{\partial y}, \frac{\partial S_{i-1}}{\partial x}, \frac{\partial S_{i-1}}{\partial y}, \frac{\partial U_{i}}{\partial x}, \frac{\partial V_{i}}{\partial y}, \frac{\partial V_{i}}{\partial x}, \frac{\partial V_{i}}{\partial y}$$

$$\frac{\partial T_{i}}{\partial x}, \frac{\partial T_{i}}{\partial y}, \frac{\partial S_{i}}{\partial x}, \frac{\partial S_{i}}{\partial y}, \frac{\partial S_{i}}{\partial x^{2}}, \frac{\partial S_{i-1}}{\partial y}, \frac{\partial S_{i-1}}{\partial x}, \frac{\partial U_{i}}{\partial y}, \frac{\partial V_{i}}{\partial x}, \frac{\partial V_{i}}{\partial y}$$

$$\frac{\partial T_{i}}{\partial x}, \frac{\partial T_{i}}{\partial y}, \frac{\partial S_{i}}{\partial x}, \frac{\partial S_{i}}{\partial y}, \frac{\partial S_{i}}{\partial x^{2}}, \frac{\partial S_{i-1}}{\partial y}, \frac{\partial U_{i}}{\partial x}, \frac{\partial V_{i}}{\partial y}, \frac{\partial V_{i}}{\partial x}, \frac{\partial V_{i}}{\partial y}$$
(2.32a)

$$\{\hat{X}_{s}^{(i)}\}^{T} = \left[U_{i-1}, V_{i-1}, T_{i-1}, S_{i-1}, U_{p} V_{p} T_{p} S_{p} \frac{\partial w_{0}}{\partial x}, \frac{\partial w_{0}}{\partial y}\right]$$
(2.32b)

It should be mentioned that although the same matrix notations as those of ISCT are used, the contents of these matrices are different. This also applies to the upcoming derivations. Plug these expressions into Equation (2.29) and utilize the constitutive equations of Equation (2.4), after integration over the thickness, a similar equation as obtained in ISCT can be achieved.

$$0 = \int_{0}^{a} \int_{0}^{b} (\{\delta \hat{X}_{n}\}^{T} [S\hat{K}_{n}] \{\hat{X}_{n}\} + \{\delta \hat{X}_{s}\}^{T} [S\hat{K}_{s}] \{\hat{X}_{s}\} - q\delta w_{0}) dy dx \qquad (2.33)$$

In the above equation, all the matrices denote the corresponding assembled ones over the thickness, i.e.,

$$\{\hat{X}_n\} = \sum_{i=1}^n \{\hat{X}_n^{(i)}\} \quad ; \quad \{\hat{X}_s\} = \sum_{i=1}^n \{\hat{X}_s^{(i)}\}$$
 (2.34)

$$[S\hat{K}_n] = \sum_{i=1}^{n} \int_{z_{i-1}}^{z_i} [N_n^{(i)}]^T \begin{bmatrix} Q_{11} \ Q_{12} \ Q_{22} \ Q_{26} \\ Q_{16} \ Q_{26} \ Q_{66} \end{bmatrix}^{(i)} [N_n^{(i)}] dz$$
 (2.35a)

$$[S\hat{K}_{s}] = \sum_{i=1}^{n} \int_{z_{i-1}}^{z_{i}} [N_{s}^{(i)}]^{T} \begin{bmatrix} Q_{44} & Q_{45} \\ Q_{45} & Q_{55} \end{bmatrix}^{(i)} [N_{s}^{(i)}] dz$$
 (2.35b)

The matrices associated with the inplane strains have a dimension of (8n+11) while those with transverse shear strains (4n+6). Moreover, the shear traction-free conditions on both top and bottom surfaces of the composite laminate enforce the displacement

variables to be further reduced. This similar manipulation as performed in the derivation of ISCT results in the following relations.

$$S_0 = S_n = -\frac{\partial w_0}{\partial y} \qquad ; \qquad T_0 = T_n = -\frac{\partial w_0}{\partial x}$$
 (2.36)

These equations can be employed to eliminate the dependent displacement variables in  $\{\hat{X}_n\}$  and  $\{\hat{X}_s\}$  by introducing constraint matrices  $[E_n]$  and  $[E_s]$ , i.e.,

$$\{\hat{X}_n\} = [E_n] \{\tilde{X}_n\} \tag{2.37a}$$

$$\{\hat{X}_z\} = [E_z] \{\tilde{X}_z\} \tag{2.37b}$$

where  $\{\bar{X}_n\}$  and  $\{\bar{X}_s\}$  are the reduced matrices with dimensions of (8n+3) and (4n+2), respectively. The complete expressions of  $[E_n]$  and  $[E_s]$  can also be found in Appendix A. With these reduced displacement matrices, the equation for the principle of virtual displacement becomes

$$0 = \int_0^a \int_0^b (\{\delta \bar{X}_n\}^T [S\bar{K}_n] \{\bar{X}_n\} + \{\delta \bar{X}_z\}^T [S\bar{K}_z] \{\bar{X}_z\} - q\delta w_0) \, dy dx \qquad (2.38)$$

where

$$[S\tilde{K}_n] = [E_n]^T [S\hat{K}_n] [E_n]$$
 (2.39a)

$$[S\tilde{K}_s] = [E_s]^T [S\hat{K}_s] [E_s]$$
 (2.39b)

#### 2.4 Closed-Form Solution

The governing equations and associated boundary conditions for ISCT and ISSCT can be obtained by substituting the displacement fields, Equations (2.13) and (2.28), into the corresponding principle of virtual displacement, i.e., Equations (2.14) and (2.29), respectively, with the use of Gaussian theorem. Since the purpose of this study is to discuss and compare the results from different theories, these equations are not described here. In-

stead, the techniques for solving the closed-form solution and finite element analysis are presented. Since the solution phases for both ISCT and ISSCT are similar, only ISCT is discussed.

For a laminate with all edges simply-supported and subjected to bidirectionally sinusoidal loading,

$$q(x,y) = \sum_{k,l=1}^{\infty} \bar{q}^{kl} \sin \frac{k\pi x}{a} \sin \frac{l\pi y}{b}$$
 (2.40)

there exists a closed-form solution. By assuming the following displacement functions,

$$U_{i} = \sum_{k,l=1}^{\infty} \overline{U}_{i}^{kl} \cos \frac{k\pi x}{a} \sin \frac{l\pi y}{b} \qquad T_{j} = \sum_{k,l=1}^{\infty} \overline{T}_{j}^{kl} \cos \frac{k\pi x}{a} \sin \frac{l\pi y}{b}$$

$$V_{i} = \sum_{k,l=1}^{\infty} \overline{V}_{i}^{kl} \sin \frac{k\pi x}{a} \cos \frac{l\pi y}{b} \qquad S_{j} = \sum_{k,l=1}^{\infty} \overline{S}_{j}^{kl} \sin \frac{k\pi x}{a} \cos \frac{l\pi y}{b} \qquad i=0,1,2,...,n \\ j=1,2,3,...,n-1$$

$$W_{i} = \sum_{k,l=1}^{\infty} \overline{W}_{i}^{kl} \sin \frac{k\pi x}{a} \sin \frac{l\pi y}{b} \qquad R_{j} = \sum_{k,l=1}^{\infty} \overline{R}_{j}^{kl} \sin \frac{k\pi x}{a} \sin \frac{l\pi y}{b}$$

$$(2.41)$$

the boundary conditions on the edges will be satisfied automatically. In the above equations, the displacement variables with "-" on top of them represent for the corresponding displacement amplitudes. Substitute these displacement functions into Equation (2.25) and carry out the integration over the x-y plane, the governing equation for the unknown displacement amplitudes can be obtained,

$$[D^{kl}] \{ \overline{X}^{kl} \} = \{ F^{kl} \}$$
  $k, l = 1, 2, 3, ..... \infty$  (2.42)

In Equation (2.42),  $[D^{kl}]$  is a coefficient matrix with dimensions of  $6n \times 6n$ ,  $\{\overline{X}^{kl}\}$  is a  $6n \times 1$  column matrix and contains all the unknown displacement amplitudes, and  $\{F^{kl}\}$  a  $6n \times 1$  column matrix associated with the external loading q(x, y).

### 2.5 Finite Element Solution

For loading types other than sinusoidal distribution and boundary conditions other than simple support, a closed-form solution becomes impossible. Hence, finite element solution should be pursued. In finite element formulation, a set of shape function for an element on x-y plane is introduced,

$$\begin{aligned}
\{\tilde{X}_n\} &= \{\psi_n\} \{X\} \\
\{\tilde{X}_x\} &= \{\psi_n\} \{X\}
\end{aligned} (2.43)$$

where  $\{X\}$  is the nodal column matrix and  $\{\psi\}$ 's are the matrices consisting of the shape functions and their derivatives. Plugging Equation (2.43) into Equation (2.25) and performing the integrations, the principle of virtual displacement results in the following finite element equation

$$[K] \{X\} = \{F\}$$
 (2.44)

in which [K] is the stiffness matrix and  $\{F\}$  is the external loading vector, i.e.,

$$[K] = \int_0^a \int_0^b ([\psi_n]^T [S\bar{K}_n] [\psi_n] + [\psi_n]^T [S\bar{K}_s] [\psi_s]) \, dy dx \qquad (2.45a)$$

$$\{F\} = -\int_0^a \int_0^b ([\psi_n]^T [E_n]^T [S\hat{K}_n] \{q_1\} + [\psi_s]^T [E_s]^T [S\hat{K}_s] \{q_2\}) \, dy dx$$

$$+ \int_0^a \int_0^b \{\varphi\} \, q \, dy \, dx$$
 (2.45b)

In the above equation  $\{\phi\}$  is the interpolation function associated with  $W_n$  only.

### CHAPTER 3

# ASSESSMENTS OF THE STRESS CONTINUITY THEORIES

### 3.1 Introduction

The stress continuity theories presented in the previous chapter provide a direct way to calculate the interlaminar stresses from constitutive equations. In this chapter, several examples which have exact elasticity solutions are used to demonstrate the accuracy and feasibility of these theories. In addition, since the solutions from other laminate theories such as HSDT and GLPT are also available, it is the objective of this chapter to compare the advantage and disadvantage of the different theories.

### 3.2 Numerical Examples for Stress Continuity Theories

## 3.2.1 Laminates under Cylindrical Bending

For a composite laminate which consists of cross-ply layups and is under cylindrical bending along x-axis, as shown in Figure 3.1, the displacement field becomes independent of y-direction. Consequently, the laminate analysis can be reduced to a two-dimensional problem and is easy to be done. In fact, Pagano [6] has presented an elasticity solution for this problem. His investigation has long been considered as a standard study to assess the accuracy of laminate theories. Therefore, a similar routine is performed here.

The material properties used in this study are exactly the same as those used in [6], i.e.,

$$E_1 = 25 \times 10^6 psi; E_2 = E_3 = 1 \times 10^6 psi; G_{12} = G_{13} = 0.5 \times 10^6 psi; G_{23} = 0.2 \times 10^6 psi$$
  
 $v_{12} = v_{13} = v_{23} = 0.25.$ 

The results are presented with the following normalizations.

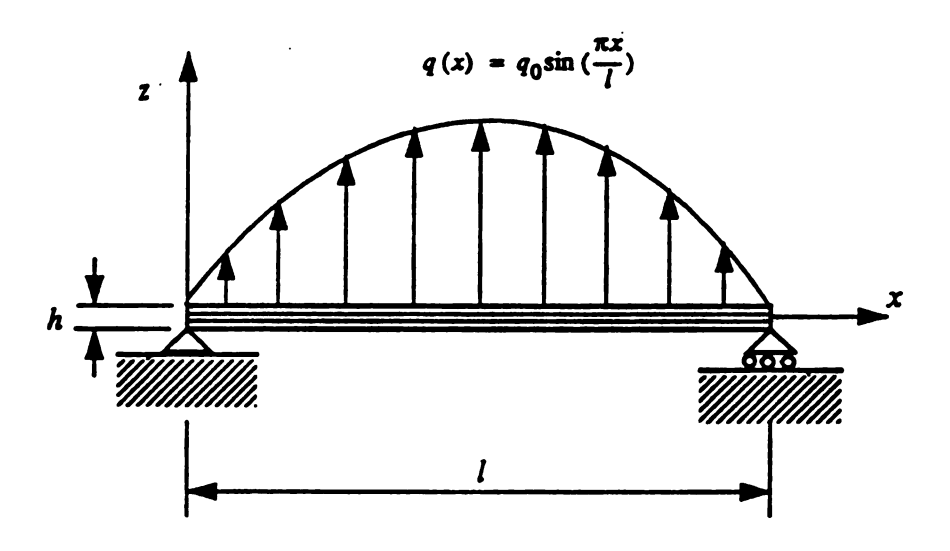


Figure 3.1 Simply-supported composite laminate under cylindrical bending.

$$\overline{w} = \frac{100E_T h^3 w}{q_0 l^4}; \overline{u} = \frac{E_T u}{h q_0}; \overline{\sigma}_z = \frac{\sigma_z}{q_0}; \overline{\sigma}_{zz} = \frac{\sigma_{zz}}{q_0}; \overline{\sigma}_z = \frac{\sigma_z}{q_0}$$

The assessments of the interlaminar stress continuity theories are presented in the following sections.

#### 1. Assessment of ISSCT

The investigation starts from ISSCT. Tables 3.1 and 3.2 present both closed-form solutions and finite element results for asymmetric [0/90] and symmetric [0/90/0] laminates, respectively. The normalized midspan deflection and transverse shear stress are of major interest. In the finite element analysis, Hermite cubic interpolation functions are used for through-the-thickness assembly while both cubic and linear interpolation functions are used for inplane assembly. Hence, in an n-layer composite laminate, the number of degree-of-freedom for one element is 8n+4 when using cubic functions while 4n+4 when using linear functions. As shown in Tables 3.1 and 3.2, only the four-layer ones are presented with both cubic and linear interpolation functions for comparison. It is clear that the cubic interpolation has faster convergence than the linear one even when they have the same number of degrees-of-freedom. This conclusion becomes more distinct as the aspect ratio of the composite laminates increases. Nevertheless, all the finite element results converge to the closed-form solutions as the number of elements increases.

There is no surprise that the transverse displacement converges faster than the transverse shear stress. This is because that ISSCT is a displacement-based approach. Furthermore, the number of layers used in the analysis does not seem to have significant effect on the results, especially when the laminates have large aspect ratios, say S=20 and S=40. It should also be noted that due to the assumption of constant transverse displacement through the thickness, both the transverse displacement and the transverse shear stress show high deviations from the exact solutions when S=4. As the aspect ratio of the

Table 3.1 Results of a simply-supported [0/90] laminate under cylindrical bending by using ISSCT.

			Inter-			FEM				
	Aspect ratio	No. of layers	polation function		No	of eleme	ents		Closed- form	Exact
			Iuicuon	2	4	6	10	20		
	S=4	2 4 4 6	Cubic Cubic Linear Cubic	4.7977 4.7983 4.1088 4.7983	4.7808 4.7818 4.6748 4.7848	4.7790 4.7801 4.7311 4.7802	4.7786 4.7796 4.7647 4.7798	4.7786 4.7796 4.7760 4.7797	4.7785 4.7797 4.7797 4.7797	4.6950
$\overline{w}(\frac{l}{2},0)$	S=20	2 4 4 6	Cubic Cubic Linear Cubic	2.7122 2.7122 2.1405 2.7122	2.7078 2.7077 2.5718 2.7077	2.7071 2.7071 2.6490 2.7071	2.7069 2.7069 2.6878 2.7069	2.7069 2.7069 2.7030 2.7069	2.7069 2.7069 2.7069 2.7069	2.7027
	S=40	2 4 4 6	Cubic Cubic Linear Cubic	2.6430 2.6430 2.0778 2.6430	2.6414 2.6414 2.5051 2.6414	2.6410 2.6410 2.5814 2.6410	2.6409 2.6409 2.6201 2.6409	2.6409 2.6409 2.6362 2.6409	2.6408 2.6407 2.6407 2.6408	2.6398
	S=4	2 4 4 6	Cubic Cubic Linear Cubic	0.8995 0.9395 1.0698 0.9352	0.8555 0.8763 1.0710 0.8735	0.8534 0.8714 0.9549 0.8680	0.8531 0.8704 0.9010 0.8666	0.8530 0.8703 0.8716 0.8664	0.8530 0.8703 0.8703 0.8664	0.9135
ਰੌ <sub>x2</sub> (0, 0)	S=20	2 4 4 6	Cubic Cubic Linear Cubic	6.1093 6.1055 4.8953 6.0885	4.2095 4.2548 5.3319 4.2532	3.9985 4.0224 5.3973 4.0221	3.9416 3.9503 5.2201 3.9499	3.9344 3.9380 4.6595 3.9373	3.9340 3.9372 3.9372 3.9365	3.9460
	S <del>=4</del> 0	2 4 4 6	Cubic Cubic Linear Cubic	13.933 13.996 9.7482 13.979	8.8000 8.8347 10.716 8.8314	8.1848 8.2165 11.007 8.2156	7.8414 7.9213 11.031 7.9213	7.9038 7.8457 10.451 7.8450	7.8374 7.8395 7.8395 7.8405	7.8436

Table 3.2 Results of a simply-supported [0/90/0] laminate under cylindrical bending by using ISSCT.

			Inter-			FEM				
	Aspect ratio	No. of layers	polation function		No.	of eleme	nts		Closed- form	Exact
		Ŭ		2	4	6	10	20		
	S=4	4 4 6	Cubic Linear Cubic	2.9217 2.6596 2.9217	2.9110 2.8687 2.9110	2.9099 2.8965 2.9100	2.9096 2.9062 2.9098	2.9096 2.9089 2.9097	2.9096 2.9096 2.9097	2.8868
$\overline{w}(\frac{l}{2},0)$	S=20	4 4 6	Cubic Linear Cubic	0.6197 0.5039 0.6197	0.6179 0.5909 0.6178	0.6177 0.6063 0.6176	0.6176 0.6140 0.6176	0.6176 0.6170 0.6176	0.6176 0.6176 0.6176	0.6172
	S=40	4 4 6	Cubic Linear Cubic	0.5381 0.4264 0.5381	0.5370 0.5103 0.5370	0.5368 0.5252 0.5368	0.5368 0.5328 0.5368	0.5368 0.5359 0.5368	0.5368 0.5368 0.5368	0.5367
	S=4	4 4 6	Cubic Linear Cubic	1.4545 1.6571 1.4655	1.4265 1.5449 1.4351	1.4252 1.4917 1.4328	1.4251 1.4523 1.4322	1.4250 1.4323 1.4321	1.4251 1.4251 1.4321	1.4318
σ <sub>xz</sub> (0, 0)	S=20	4 4 6	Cubic Linear Cubic	9.7495 10.446 9.7613	8.8230 9.7329 8.8279	8.7608 9.5946 8.7639	8.7471 9.4110 8.7495	8.7452 9.0906 8.7474	8.7451 8.7451 8.7472	8.7490
	S <del>=4</del> 0	4 4 6	Cubic Linear Cubic	23.462 21.103 23.479	18.218 19.662 18.228	17.757 19.463 17.761	17.654 19.293 17.656	17.640 18.906 17.642	17.639 17.639 17.641	17.634

laminates increase, good agreements between the ISSCT and the exact analysis are obtained. In addition, it is concluded that the results of the symmetric layup, [0/90/0], show better accuracy than those of the asymmetric layup, [0/90].

### 2. Assessment of ISCT

The same examples are investigated by using ISCT and the results are given in Tables 3.3 and 3.4. Comparing the closed-form solutions of ISCT with the exact solutions, it is clear that both the transverse displacement and stresses converge as the number of layer increases. However, the number of elements affects the solutions in a different manner. This result can be viewed from the finite element aspect ratio which is defined as the ratio of the element length to the element thickness. For composite laminates with high aspect ratios, it requires more elements to keep the finite element aspect ratio close to one. On the contrary, for composite laminates with low aspect ratios, it requires fewer elements. Accordingly, there is no advantage to use too many elements for composite laminate with small aspect ratio. It then is understandable that the convergences of the transverse displacement and transverse shear stress are not monotonic for the cases under investigation. In addition, for symmetric laminates, [0/90/0], the interlaminar normal stress converges to the exact solution very well. However, for asymmetric laminate, [0/90], this stress converges from lower values at S=4, while from higher values at S=20 and S=40.

## 3. Effect of Aspect Ratio

In order to verify the feasibility of using the new theories for both thin and thick composite laminates, the normalized deflections at the midplane and midspan are presented in Figure 3.2. It is in a logarithmic scale with the aspect ratios ranging from four to 200 for all three laminates, [0], [0/90], and [0/90/0]. The results show that both stress continuity theories agree with the exact solutions perfectly through the entire span of aspect ratio. Hence, they can be used for deflection analysis for both thin and thick composite laminates.

Table 3.3 Results of a simply-supported [0/90] laminate under cylindrical bending by using ISCT.

					FEM				
	Aspect ratio	No. of layers		No	. of eleme	ents		Closed- form	Exact
		,	2	4	6	10	20		
	6.4	2	4.7266	4.7281	4.7352	4.7402	4.7349	4.6918 -4.6950	4.6950
	S=4	4 - 6	4.7144 4.7139	4.7002 4.6984	4.7000 4.6974	4.7014 4.6979	4.7033 4.6989	4.6952	4.0930
$\overline{w}(\frac{l}{2},0)$		2	2.7080	2.7037	2.7030	2.7029	2.7030	2.7027	2.7027
$w(\overline{2},0)$	S=20	4 6	2.7079 2.7079	2.7036 2.7036	2.7029 2.7029	2.7028 2.7028	2.7027 2.7027	2.7027 2.7027	2.7027
	C 40	2 4	2.6418	2.6403	2.6400	2.6399	2.6398	2.6398	2.6398
	S <del>=4</del> 0	6	2.6418 2.6418	2.6403 2.6403	2.6400 2.6400	2.6398 2.6398	2.6398 2.6398	2.6397 2.6399	2.0376
	6.4	2	0.9806	0.9936	1.0446	1.1218	1.1189	0.9055	0.9135
	S <del>=4</del>	4 6	0.9907 0.9854	0.9349 0.9259	0.9428 0.9238	0.9781 0.9352	1.0563 0.9742	0.9212 0.9174	0.9133
	0.00	2 4	6.1426	4.2638	4.0780	4.1143	4.3936	3.9451	3.9460
$\bar{\sigma}_{xz}(0,0)$	S=20	6	6.2074 6.1872	4.2775 4.2742	4.0376 4.0349	3.9688 3.9631	3.9878 3.9563	3.9479 3.9472	3.9400
	0.40	2	14.371	8.9330	8.2559	8.0049	8.1679	7.8431	7.8436
	S=40	4 6	14.384 14.356	8.9371 8.9305	8.2500 8.2470	7.9340 7.9306	7.8665 7.8561	7.8437 7.8448	7.0430
	S 4	2	0.6192	0.7629	0.8346	0.8531	0.8533	0.8468	0.7860
	S <del>=4</del>	4 6	0.7041 0.7436	0.7468 0.7609	0.7789 0.7781	0.7944 0.7880	0.7956 0.7890	0.7947 0.7887	0.7800
- 1	0.00	2	1.0821	0.8203	0.8525	0.8874	0.8889	0.8875	0.8180
$\bar{\sigma}_{z}(\frac{l}{2},0)$	S=20	4 6	1.2045 1.2507	0.8547 0.8768	0.8294 0.8345	0.8320 0.8249	0.8282 0.8216	0.8273 0.8208	0.0100
		2	3.2649	1.4036	1.0634	0.9326	0.8955	0.8891	0.8193
	S <del>=4</del> 0	4 6	3.4873 3.5518	1.4349 1.4559	1.0403 1.0453	0.8764 0.8710	0.8345 0.8278	0.8285 0.8220	0.0173

Table 3.4 Results of a simply-supported [0/90/0] laminate under cylindrical bending by using ISCT.

					FEM				
	Aspect ratio	No. of layers		No.	of eleme	ents		Closed- form	Exact
			2	4	6	10	20		
	S=4	4 6	2.9025 2.8992	2.8982 2.8887	2.9011 2.8879	2.9052 2.8878	2.9078 2.8880	2.8868 2.8872	2.8868
$\overline{w}(\frac{l}{2},0)$	S=20	4 6	0.6194 0.6194	0.6176 0.6175	0.6174 0.6173	0.6173 0.6173	0.6173 0.6173	0.6173 0.6173	0.6172
	S=40	4 6	0.5380 0.5380	0.5369 0.5369	0.5368 0.5367	0.5367 0.5367	0.5367 0.5367	0.5367 0.5367	0.5367
	S=4	4 6	1.4548 1.4643	1.4653 1.4337	1.5136 1.4318	1.6001 1.4341	1.6534 1.4396	1.4244 1.4314	1.4318
$\bar{\sigma}_{xz}(0,0)$	S=20	4 6	9.7509 9.7613	8.8301 8.8297	8.7740 8.7661	8.7811 8.7514	8.8976 8.7440	8.7462 8.7480	8.7490
	S=40	4	23.471 23.485	18.224 18.228	17.767 17.763	17.673 17.660	17.706 17.645	17.640 17.641	17.643
	S=4	4 6	0.5000 0.5000	0.4993 0.4987	0.4976 0.4987	0.4985 0.4987	0.4985 0.4987	0.4985 0.4987	0.4988
$\bar{\sigma}_z(\frac{l}{2},0)$	S=20	4 6	0.5018 0.5018	0.5002 0.5000	0.5002 0.5000	0.5001 0.5001	0.5001 0.5001	0.5001 0.5001	0.5001
	S <del>=4</del> 0	4 6	0.5018 0.5018	0.4997 0.4997	0.4999 0.4999	0.5000 0.5000	0.5000 0.5000	0.5000 0.5000	0.5000

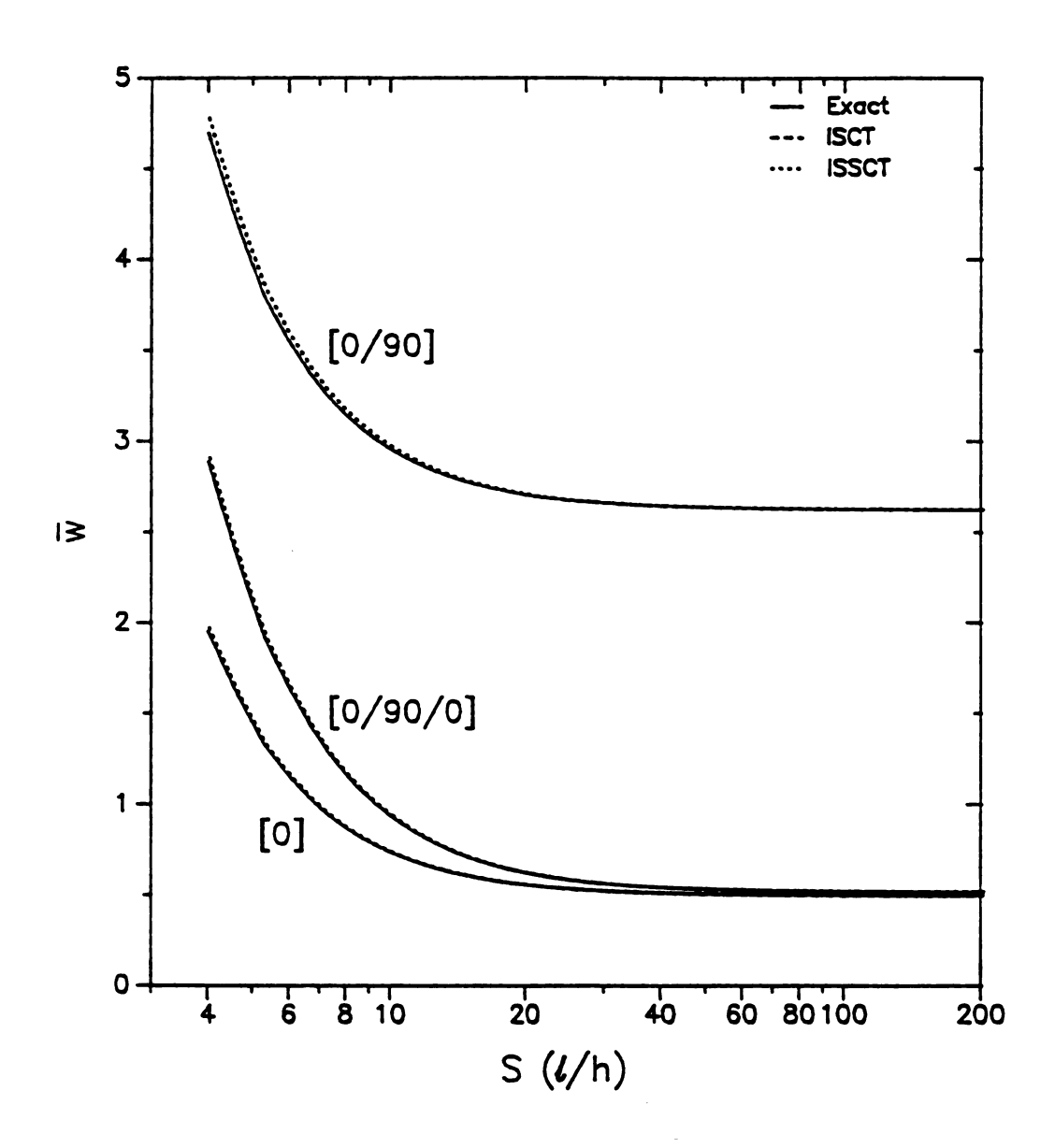


Figure 3.2 Normalized transverse displacements at midspan for [0], [0/90], and [0/90/0] laminates with different aspect ratios.

### 4. Through-The-Thickness Distribution

Aside from the results calculated at the particular points as discussed in the previous tables, another way to assess the results obtained from the new theories is to compare them with exact solutions through the thickness. The closed-form solutions for [0/90] and [0/90/0] laminates with S=4 using four-layer analysis are presented in Figures 3.3 to 3.10. In Figures 3.6 and 3.10, the results of transverse normal stress  $\sigma_z$  of ISSCT are recovered from equilibrium equations. Details of the stress recovery technique will be discussed in Section 3.3.2. From these figures, it is concluded that both ISSCT and ISCT agree with the elasticity analysis very well. In most cases, ISCT can improve the results of ISSCT slightly except for the transverse normal stress in the [0/90/0] laminate, shown in Figure 3.10. Studies show that the recovered transverse normal stress from ISSCT gives better prediction than those directly calculated from ISCT.

# 3.2.2 Laminates under Bidirectional Bending

Consider a simply-supported cross-ply laminate which has dimensions of  $a \times b$  and is subjected to bidirectionally sinusoidal loading, i.e.,

$$q(x, y) = q_0 \sin \frac{\pi x}{a} \sin \frac{\pi y}{b}$$

as shown in Figure 3.11. The three-dimensional elasticity solution has been obtained by Pagano and Hatfield [27]. It is the purpose of this study to compare the stress continuity theories with the exact solution. Although the results presented here are all for symmetric cross-ply layups, the theories have no difficulty in analyzing asymmetric or angle-ply laminates.

The material properties studied here are exactly the same as those used in cylindrical bending. Similarly, the following normalized quantities are used in the presentations

$$\overline{w} = \frac{100E_T h^3 w}{q_0 a^4} \quad ; \quad (\overline{\sigma}_1, \overline{\sigma}_2, \overline{\sigma}_6) = \frac{h^2}{q_0 a^2} (\sigma_x, \sigma_y, \sigma_{xy}) \quad ; \quad (\overline{\sigma}_4, \overline{\sigma}_5) = \frac{h}{q_0 a} (\sigma_{yz}, \sigma_{xz})$$

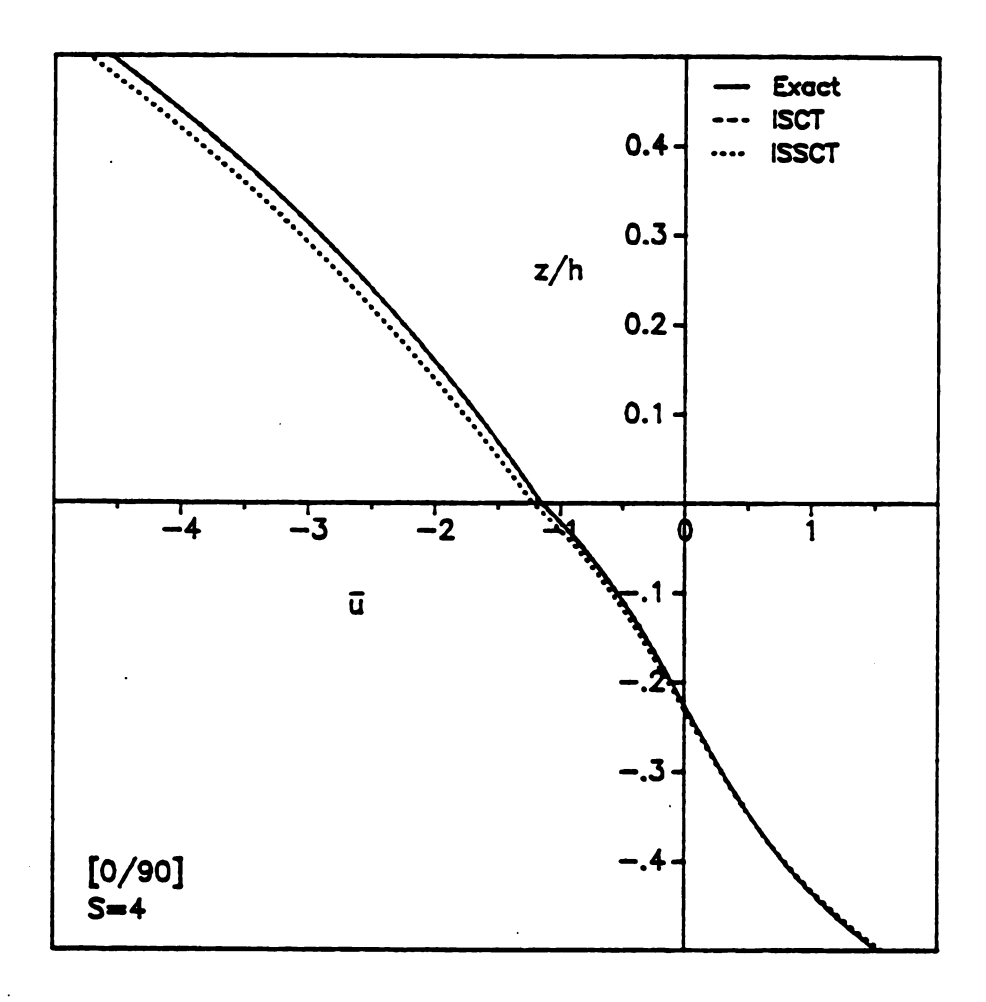


Figure 3.3 Normalized inplane displacement  $\bar{u}(0)$  of a simply-supported [0/90] laminate with S=4 under cylindrical bending.

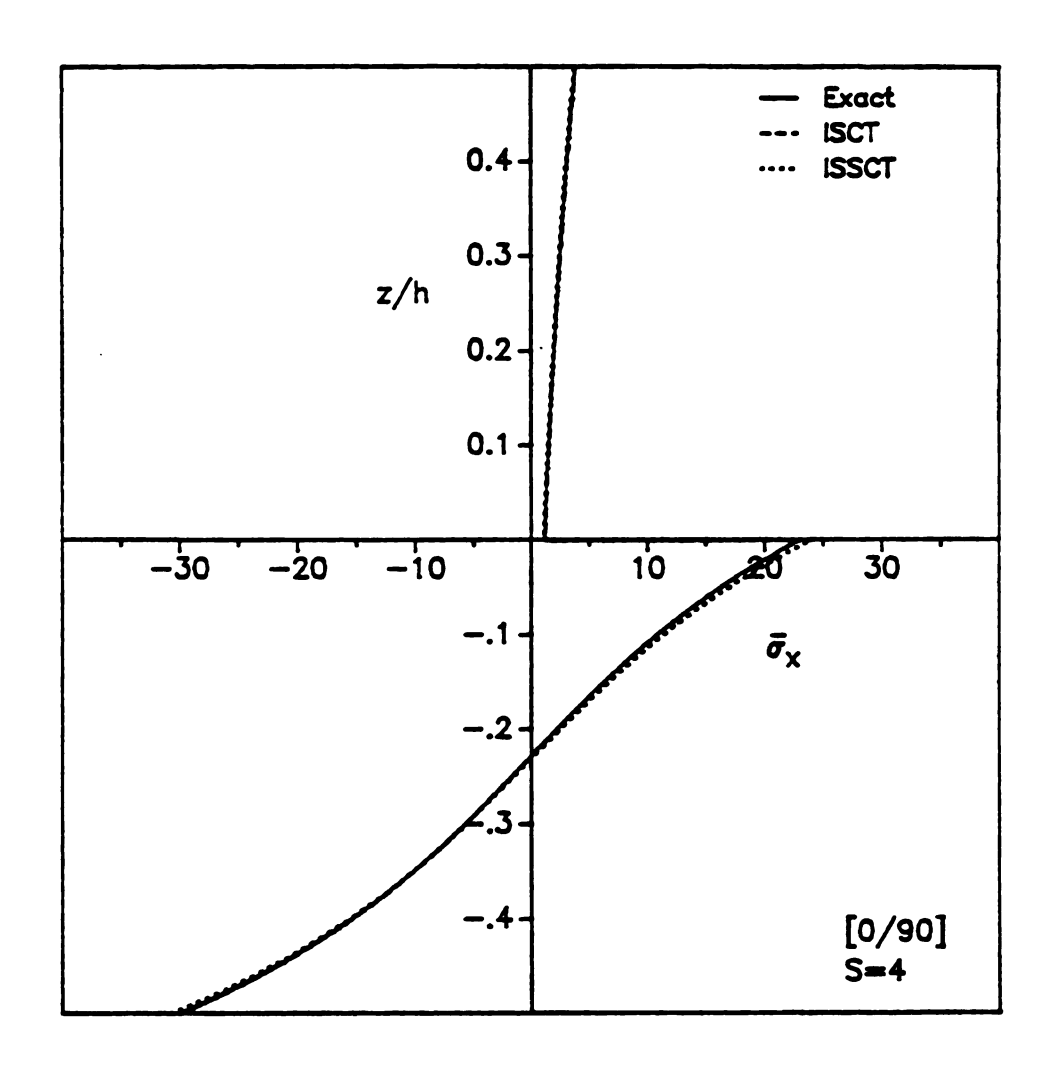


Figure 3.4 Normalized inplane normal stress  $\bar{\sigma}_x(l/2)$  of a simply-supported [0/90] laminate with S=4 under cylindrical bending.

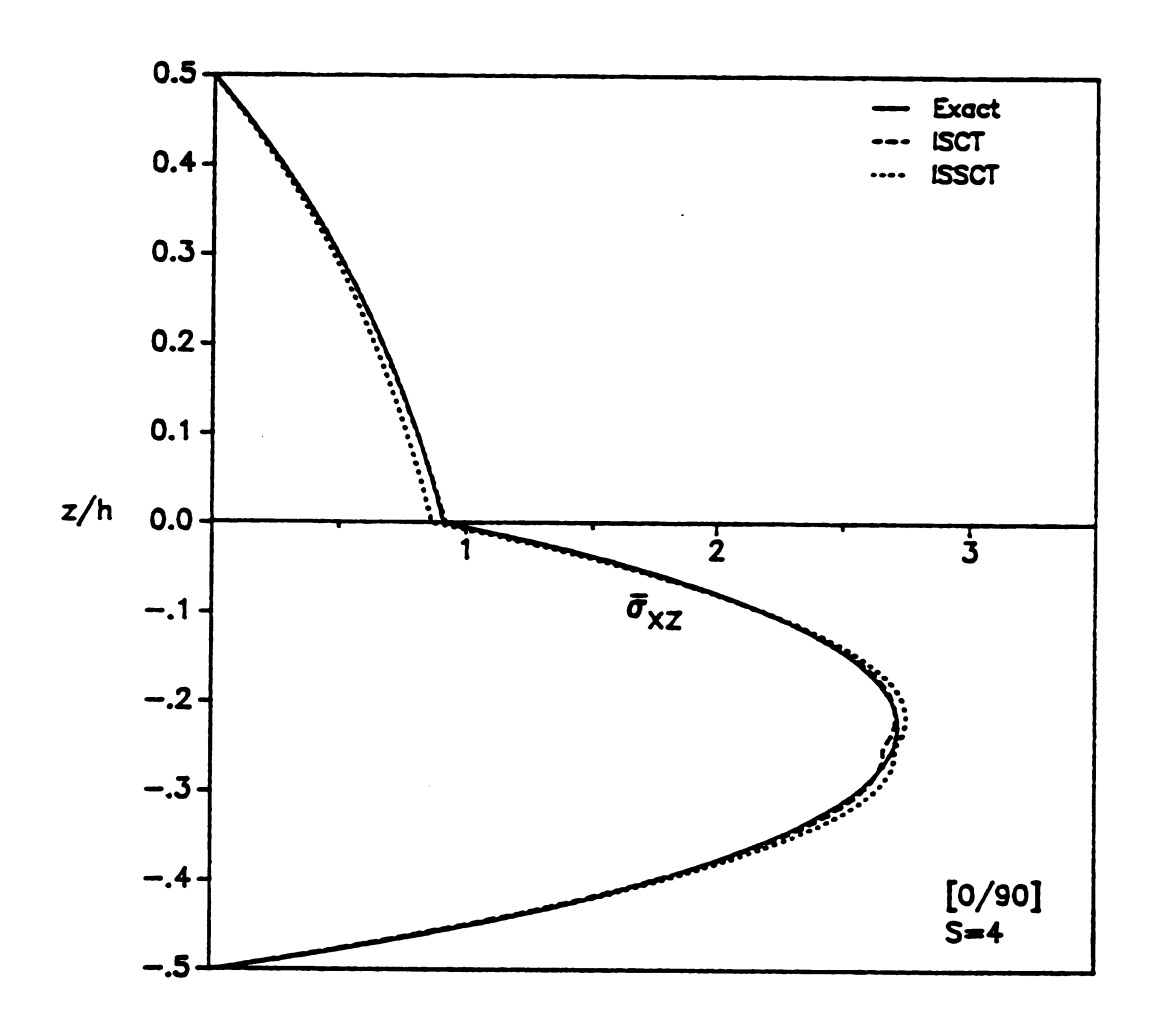


Figure 3.5 Normalized transverse shear stress  $\bar{\sigma}_{xz}(0)$  of a simply-supported [0/90] laminate with S=4 under cylindrical bending.

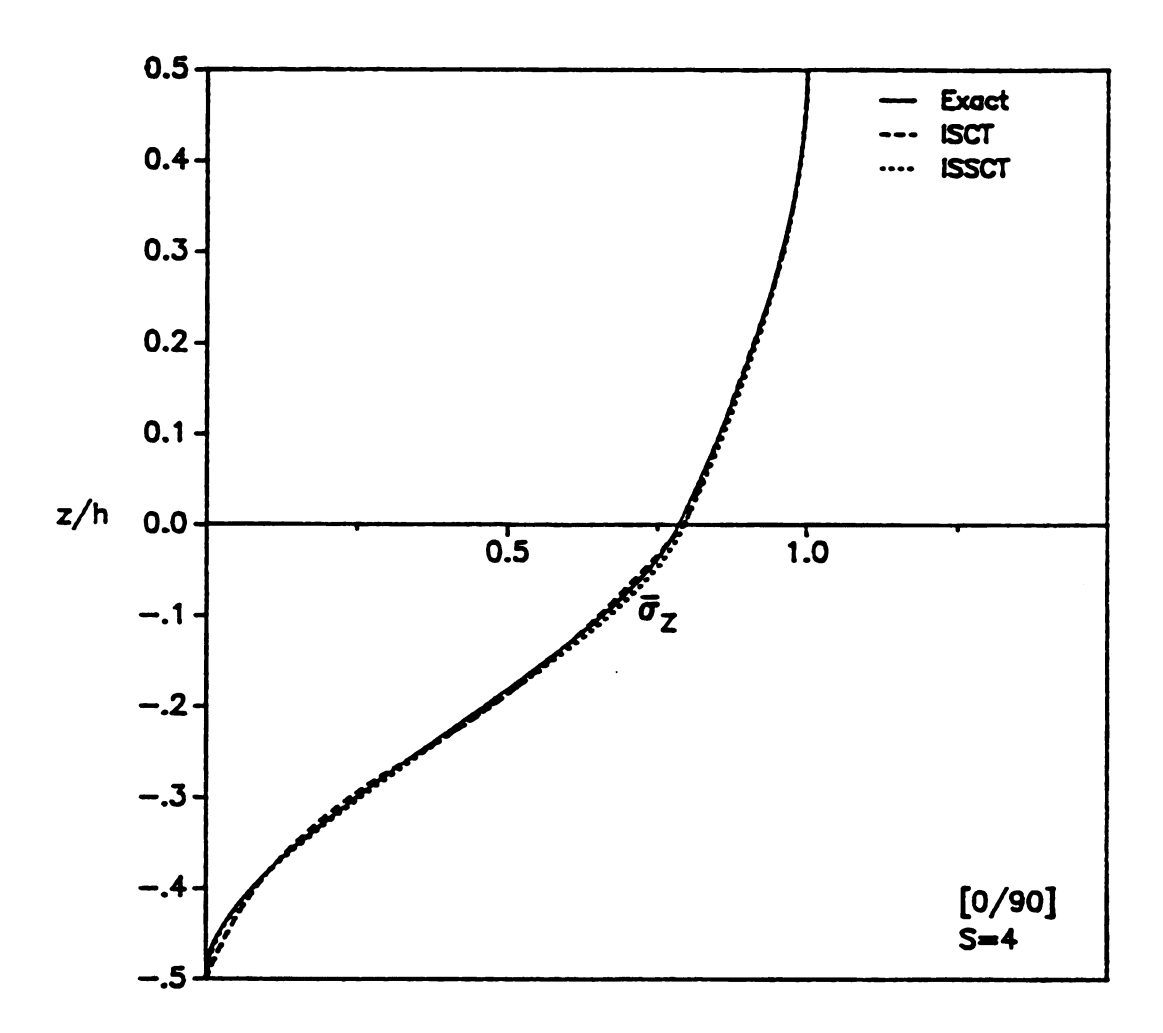


Figure 3.6 Normalized transverse normal stress  $\bar{\sigma}_z(l/2)$  of a simply-supported [0/90] laminate with S=4 under cylindrical bending.

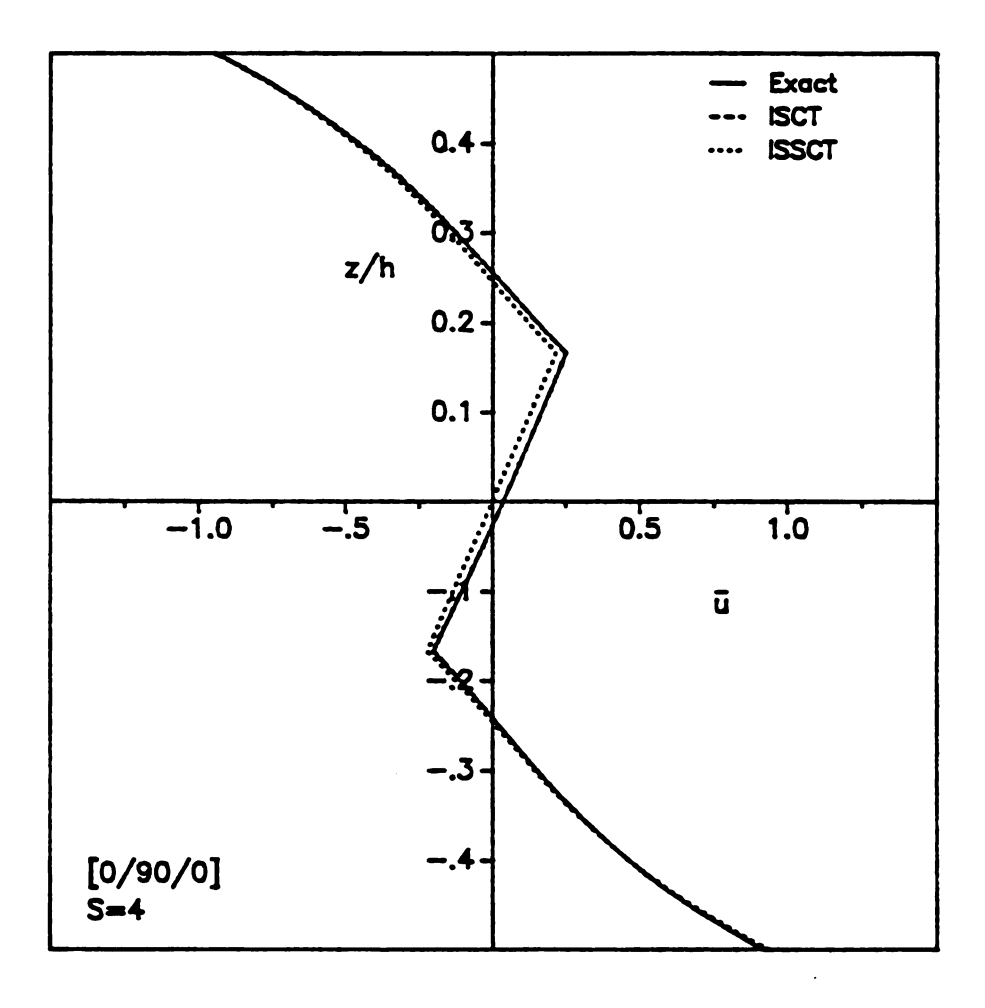


Figure 3.7 Normalized inplane displacement  $\bar{u}(0)$  of a simply-supported [0/90/0] laminate with S=4 under cylindrical bending.

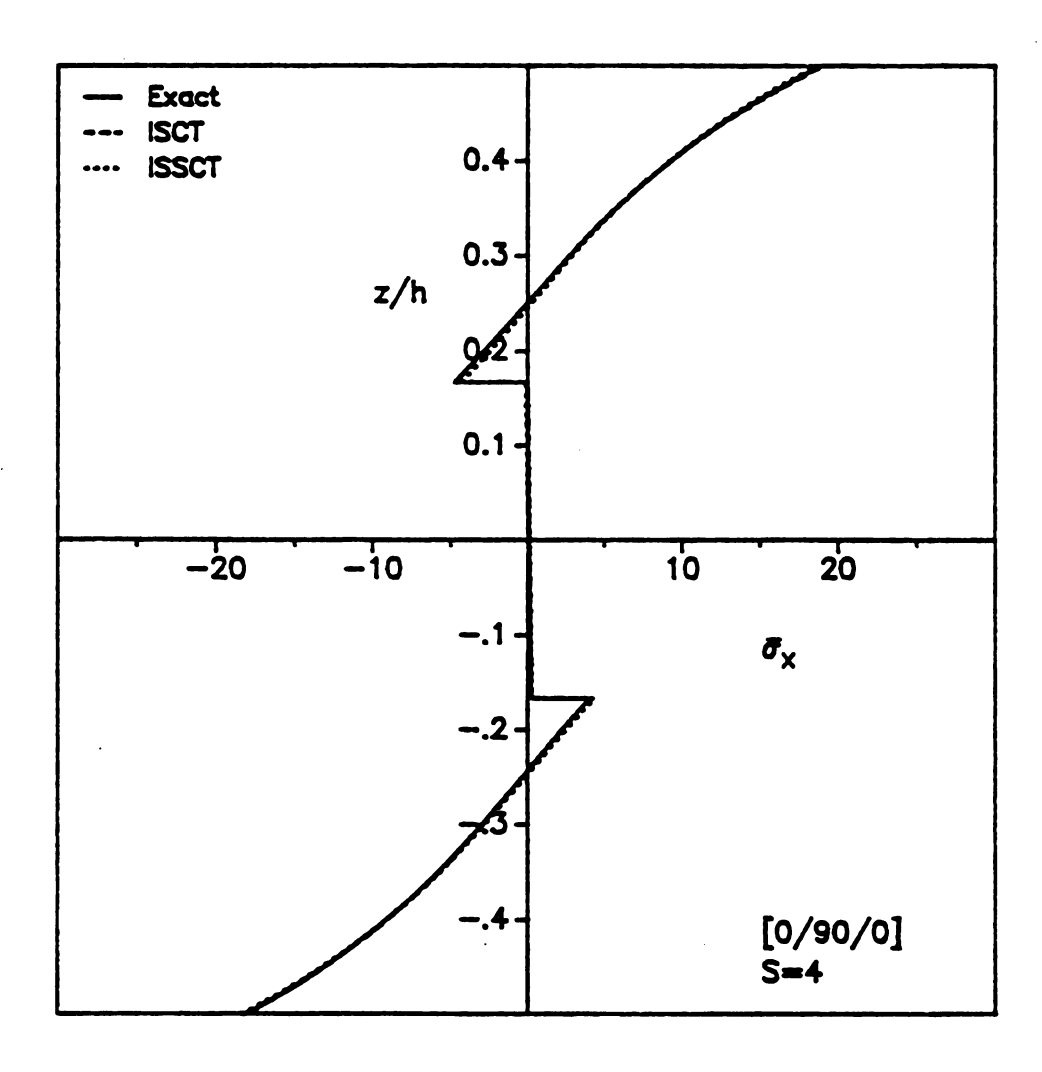


Figure 3.8 Normalized inplane normal stress  $\bar{\sigma}_x(l/2)$  of a simply-supported [0/90/0] laminate with S=4 under cylindrical bending.

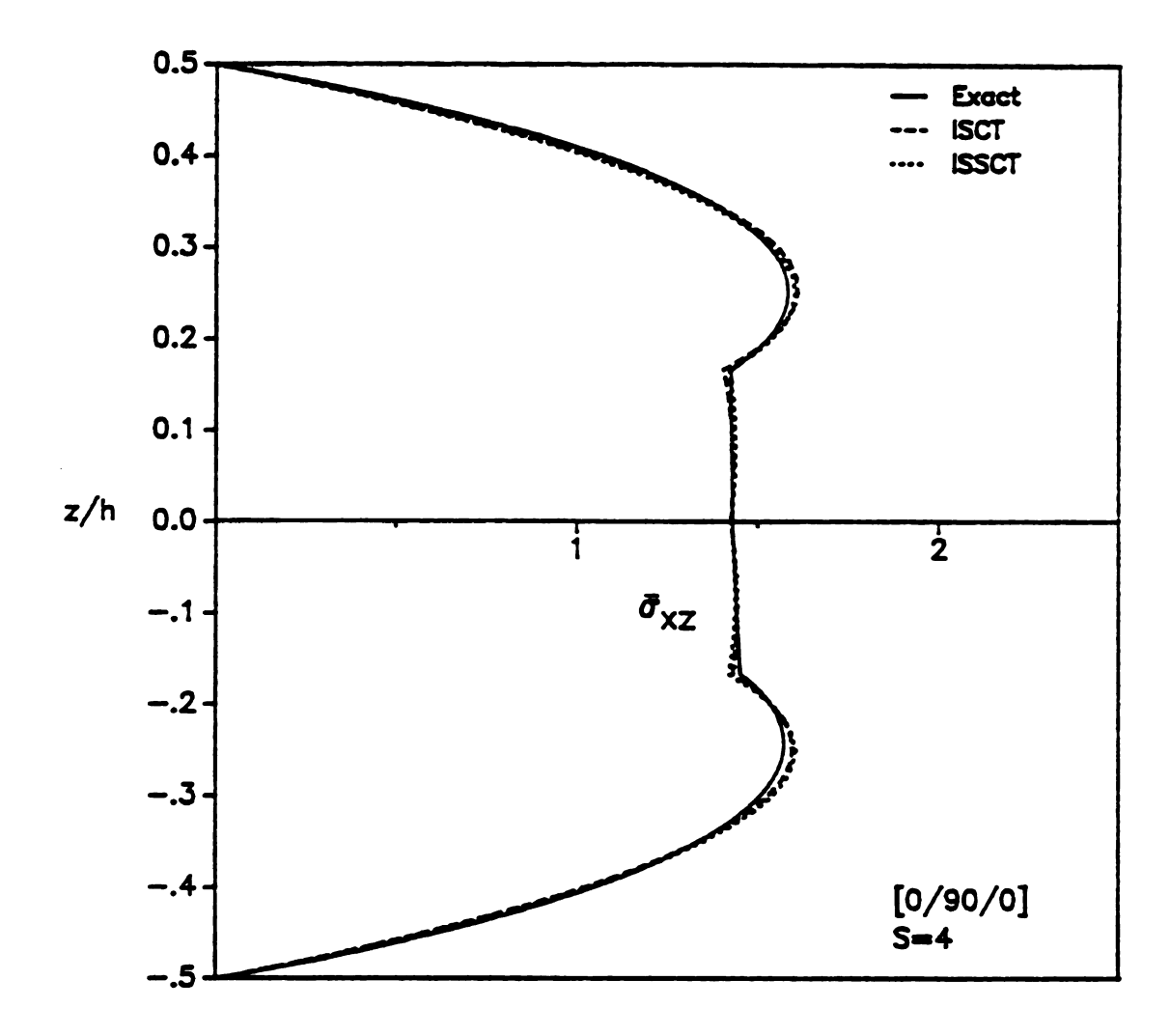


Figure 3.9 Normalized transverse shear stress  $\bar{\sigma}_{xz}(0)$  of a simply-supported [0/90/0] laminate with S=4 under cylindrical bending.

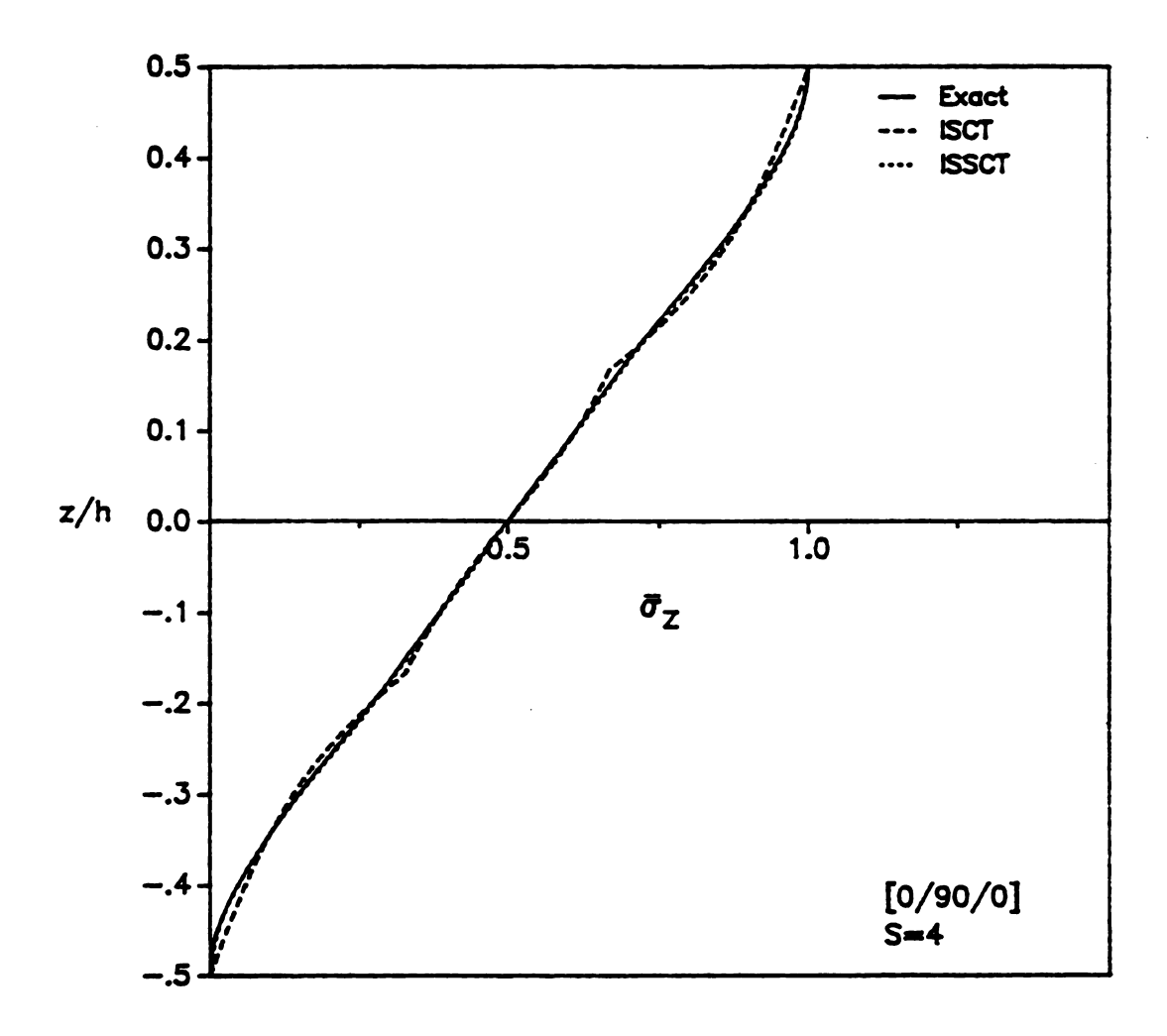


Figure 3.10 Normalized transverse normal stress  $\bar{\sigma}_z(l/2)$  of a simply-supported [0/90/0] laminate with S=4 under cylindrical bending.

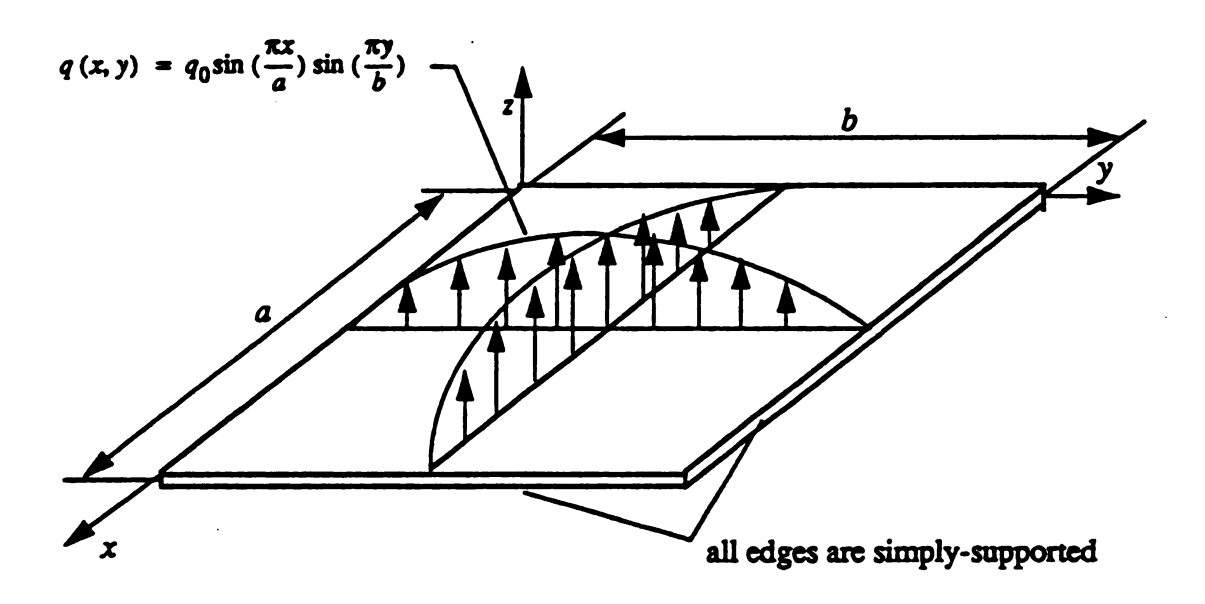


Figure 3.11 Simply-supported composite laminate under bidirectionally sinusoidal loading.

Since the maximum values of the displacement and stresses are of major concern, only the maximum values in the individual cases are reported. The studies are based on both closed-form solution and finite element analysis and are presented below.

## 1. Effect of Layer Number

The closed-form solutions of a square (a=b) [0/90/90/0] and a rectangular (b=3a) [0/90/0] laminates from ISSCT are given in Tables 3.5 and 3.6, respectively. Comparing the results, it is obvious that the increase of layer number introduces very small improvements to both displacement and stresses. This is also true for the analysis using ISCT shown in Tables 3.7 and 3.8.

#### 2. Effect of Laminate Thickness

From Table 3.5 to Table 3.8, it is clear that the conclusion drawn from the result of composite laminates under cylindrical bending is still valid in the case of bidirectional bending. More specifically, both ISSCT and ISCT are feasible for the analysis of both thin and thick composite laminates.

#### 3. Effect of Element Number

In the finite element analysis, because of the symmetry of the problem, only one quarter of the laminate needs to be examined. Table 3.9 presents the ISSCT results of a simply-supported [0/90/90/0] square laminate under bidirectional bending. In order to evaluate the influence of the order of interpolation functions on the inplane assembly, both linear and cubic interpolation functions are used. However, the assembly of the displacement components through the laminate thickness uses a 12-term cubic interpolation function. Based on these interpolation functions for element assembly, the degree-of-freedom of a four-node rectangular element is 16n + 12 for linear function while 48n + 12 for cubic. For a [0/90/90/0] composite laminate, if n = 4 is selected, the total number of degree-of-freedom for a finite element mesh can be calculated accordingly. The numbers for different cases are presented as with parentheses in Table 3.9. It then can be seen that with approximately the same number of degree-of-freedom used in the finite element analysis,

Table 3.5 Closed-form solutions of a simply-supported [0/90/90/0] square (a=b) laminate under bidirectional bending by using ISSCT.

a ħ	Solution	<u>w</u>	$ar{\sigma}_1$	$ar{\sigma}_2$	σ̄₄	σ̄₅	ō <sub>6</sub>
	4-layer	1.9555	±0.7048	±0.6703	0.2876	0.2187	∓0.0465
	8-layer	1.9555	±0.7035	±0.6695	0.2915	0.2192	∓0.0465
4	12-layer	1.9555	±0.7034	±0.6694	0.2918	0.2193	∓0.0465
	Exact	1.937	+0.720 -0.684	+0.663 -0.666	0.292	0.219	-0.0465 +0.0458
	4-layer	0.7324	±0.5583	±0.3999	0.1957	0.3006	∓0.0274
	8-layer	0.7324	±0.5583	±0.3999	0.1961	0.3007	∓0.0274
10	12-layer	0.7324	±0.5583	±0.3999	0.1962	0.3007	∓0.0274
	Exact	0.737	+0.559 -0.559	+0.401 -0.403	0.196	0.301	-0.0275 +0.0276
	4-layer	0.5078	±0.5411	±0.3071	0.1563	0.3272	∓0.0228
	8-layer	0.5078	±0.5411	±0.3078	0.1564	0.3272	∓0.0228
20	12-layer	0.5080	±0.5413	±0.3072	0.1564	0.3272	∓0.0228
	Exact	0.513	+0.543 -0.543	+0.308	0.156	0.328	-0.0230 +0.0230
	4-layer	0.4296	±0.5366	±0.2699	0.1400	0.3377	∓0.0211
	8-layer	0.4307	±0.5380	±0.2705	0.1398	0.3378	∓0.0212
100	12-layer	0.4318	±0.5394	±0.2713	0.1394	0.3381	<b>∓0.0212</b> √
_	Exact	0.435	+0.539	+0.271 -0.271	0.139	0.339	-0.0214 +0.0214

$$\begin{split} \overline{\sigma}_1 &= \overline{\sigma}_1(\frac{a}{2}, \frac{b}{2}, \pm \frac{h}{2}) \,, \ \overline{\sigma}_2 &= \overline{\sigma}_2(\frac{a}{2}, \frac{b}{2}, \pm \frac{h}{4}) \,, \ \overline{\sigma}_6 &= \overline{\sigma}_6(0, 0, \pm \frac{h}{2}) \\ \overline{\sigma}_4 &= \overline{\sigma}_4(\frac{a}{2}, 0, 0) \,, \ \overline{\sigma}_5 &= \overline{\sigma}_5(0, \frac{b}{2}, 0) \end{split}$$

Table 3.6 Closed-form solutions of a simply-supported [0/90/0] rectangular (3a=b) laminate under bidirectional bending by using ISSCT.

a h	Solution	W	$ar{\sigma}_1$	$ar{\sigma}_2$	σ̄₄	$\bar{\sigma}_{5}$	ਰ̄ <sub>6</sub>
	4-layer	2.8406	±1.1254	±0.1115	0.0319	0.3494	∓0.0277
	6-layer	2.8409	±1.1209	±0.1115	0.0320	0.3512	∓0.0277
4	10-layer	2.8409	±1.1205	±0.1115	0.0320	0.3512	∓0.0277
	Exact	2.820	+1.140 -1.100	+0.109 -0.119	0.0334	0.351	-0.0269 +0.0281
	4-layer	0.9178	±0.7265	±0.0424	0.0154	0.4196	∓0.0121
	6-layer	0.9178	±0.7264	±0.0424	0.0154	0.4199	∓0.0121
10	10-layer	0.9178	±0.7264	±0.0424	0.0154	0.4198	∓0.0121
	Exact	0.919	+0.726 -0.725	+0.0418 -0.0435	0.0152	0.420	-0.0120 +0.0123
	4-layer	0.6073	±0.6501	±0.0301	0.0124	0.4342	∓0.0092
	6-layer	0.6073	±0.6501	±0.0301	0.0124	0.4343	∓0.0092
20	10-layer	0.6073	±0.6501	±0.0301	0.0120	0.4340	∓0.0092
	Exact	0.610	+ 0.650 - 0.650	+0.0294	0.0119	0.434	-0.0093 +0.0093
	4-layer	0.5053	±0.6243	±0.0260	0.0114	0.4392	∓0.0083
	6-layer	0.5061	±0.6252	±0.0260	0.0114	0.4392	∓0.0083
100	10-layer	0.5061	±0.6253	±0.0260	0.0109	0.4389	∓0.0083
<u>.</u>	Exact	0.508	+ 0.624 - 0.624	+0.0253 -0.0253	0.0108	0.439	-0.0083 +0.0083

$$\begin{split} \overline{\sigma}_1 &= \overline{\sigma}_1(\frac{a}{2}, \frac{b}{2}, \pm \frac{h}{2}) \,, \ \overline{\sigma}_2 &= \overline{\sigma}_2(\frac{a}{2}, \frac{b}{2}, \pm \frac{h}{6}) \,, \ \overline{\sigma}_6 &= \overline{\sigma}_6(0, 0, \pm \frac{h}{2}) \\ \overline{\sigma}_4 &= \overline{\sigma}_4(\frac{a}{2}, 0, 0) \,, \ \overline{\sigma}_5 &= \overline{\sigma}_5(0, \frac{b}{2}, 0) \end{split}$$

Table 3.7 Closed-form solutions of a simply-supported [0/90/90/0] square (a=b) laminate under bidirectional bending by using ISCT.

$\frac{a}{h}$	Solution	w	$\bar{\sigma}_1$	₫2	σ̄₄	<b>ਰ</b> ̄₅	ਰੌ <sub>6</sub>
	4-layer	1.9377	+0.7216 -0.6856	+0.6642 -0.6671	0.2876	0.2189	-0.0467 +0.0459
4	8-layer	1.9369	+0.7203 -0.6843	+0.6628 -0.6657	0.2912	0.2193	-0.0467 +0.0458
	Exact	1.937	+0.720 -0.684	+0.663 -0.666	0.292	0.219	-0.0465 +0.0458
	4-layer	0.7371	+0.5587 -0.5591	+0.4010	0.1955	0.3013	-0.0275 +0.0276
10	8-layer	0.7370	+0.5586 -0.5591	+0.4010 -0.4026	0.1959	0.3014	-0.0275 +0.0276
	Exact	0.737	+0.559 -0.559	+0.401 -0.403	0.196	0.301	-0.0275 +0.0276
	4-layer	0.5130	+0.5428 -0.5432	+0.3084	0.1555	0.3281	-0.0230 +0.0231
20	8-layer	0.5130	+0.5428 -0.5432	+0.3084 -0.3088	0.1556	0.3282	-0.0230 +0.0231
	Exact	0.513	+0.543 -0.543	+0.308	0.156	0.328	-0.0230 +0.0230
	4-layer	0.4346	±0.5389	±0.2710	0.1389	0.3388	∓0.0214
100	8-layer	0.4346	±0.5389	±0.2710	0.1389	0.3388	∓0.0214
	Exact	0.435	±0.539	±0.271	0.139	0.339	∓0.0214

$$\begin{split} \vec{\sigma}_1 &= \vec{\sigma}_1(\frac{a}{2}, \frac{b}{2}, \pm \frac{h}{2}) \,, \; \vec{\sigma}_2 = \vec{\sigma}_2(\frac{a}{2}, \frac{b}{2}, \pm \frac{h}{4}) \,, \; \vec{\sigma}_6 = \vec{\sigma}_6(0, 0, \pm \frac{h}{2}) \\ \vec{\sigma}_4 &= \vec{\sigma}_4(\frac{a}{2}, 0, 0) \,, \; \vec{\sigma}_5 = \vec{\sigma}_5(0, \frac{b}{2}, 0) \end{split}$$

Table 3.8 Closed-form solutions of a simply-supported [0/90/0] rectangular (3a=b) laminate under bidirectional bending by using ISCT.

a h	Solution	w	$ar{\sigma}_1$	$ar{\sigma}_2$	$\bar{\sigma}_4$	<b>σ</b> ₅	ਰੋ <sub>6</sub>
	4-layer	2.8215	+1.1496 -1.1041	+0.1085 -0.1191	0.0332	0.3494	-0.0269 +0.0281
4	6-layer	2.8212	+1.1449 -1.0998	+0.1088 -0.1193	0.0333	0.3511	-0.0269 +0.0281
	Exact	2.820	+1.140 -1.100	+0.109	0.0334	0.351	-0.0269 +0.0281
:	4-layer	0.9189	+0.7261 -0.7256	+0.0417 -0.0435	0.0152	0.4198	-0.0120 +0.0123
10	6-layer	0.9189	+0.7260 -0.7254	+0.0418 -0.0435	0.0152	0.4201	-0.0120 +0.0123
	Exact	0.919	+0.726 -0.725	+0.0418	0.0152	0.420	-0.0120 +0.0123
	4-layer	0.6095	+0.6500 -0.6502	+0.0294	0.0119	0.4343	-0.0092 +0.0093
20	6-layer	0.6095	+0.6500 -0.6501	+0.0294 -0.0299	0.0119	0.4344	-0.0092 +0.0093
	Exact	0.610	+0.650 -0.650	+0.0294	0.0119	0.434	-0.0093 +0.0093
	4-layer	0.5077	±0.6244	±0.0253	0.0108	0.4393	∓0.0083
100	6-layer	0.5077	±0.6244	±0.0253	0.0108	0.4393	∓0.0083
	Exact	0.508	±0.624	±0.0253	0.0108	0.439	∓0.0083

$$\begin{split} \overline{\sigma}_1 &= \overline{\sigma}_1 \, (\frac{a}{2}, \frac{b}{2}, \pm \frac{h}{2}) \,, \ \overline{\sigma}_2 &= \overline{\sigma}_2 \, (\frac{a}{2}, \frac{b}{2}, \pm \frac{h}{6}) \,, \ \overline{\sigma}_6 &= \overline{\sigma}_6 \, (0, 0, \pm \frac{h}{2}) \\ \overline{\sigma}_4 &= \overline{\sigma}_4 \, (\frac{a}{2}, 0, 0) \,, \ \overline{\sigma}_5 &= \overline{\sigma}_5 \, (0, \frac{b}{2}, 0) \end{split}$$

Table 3.9 Finite element solutions of a simply-supported [0/90/90/0] square (a=b) laminate under bidirectional bending by using ISSCT.

a h	No. of elements	Interpolation function	W	ō₁	$\bar{\sigma}_2$	₫,	σ̄ <sub>5</sub>	₹6
	lxl	Linear(76) Cubic(204)	1.6979 1.9484	0.5420 0.8039	0.5136 0.7593	0.3223 0.3241	0.2498 0.2318	0.0367 0.0463
	2x2	Linear(171) Cubic(459)	1.9059 1.9516	0.6748 0.7149	0.6404 0.6795	0.3132 0.2908	0.2353 0.2197	0.0448 0.0464
4	3x3	Linear(324) Cubic(816)	1.9361 1.9527	0.6933 0.7072	0.6584 0.6723	0.3084 0.2879	0.2288 0.2186	0.0459 0.0465
	4x4	Linear(475) Cubic(1275)	1.9457 1.9537	0.6990 0.7065	0.6641 0.6709	0.3036 0.2876	0.2253 0.2186	0.0462 0.0465
	Close	ed-form	1.9555	0.7048	0.6703	0.2876	0.2187	0.0465
	lxl	Linear(76) Cubic(204)	0.5651 0.7204	0.3899 0.6607	0.2921 0.5032	0.0853 0.2766	0.3022 0.3306	0.0198 0.0267
	2x2	Linear(171) Cubic(459)	0.7043 0.7309	0.5281 0.5727	0.3823 0.4121	0.1764 0.2052	0.3189 0.3047	0.0261 0.0275
10	3x3	Linear(324) Cubic(816)	0.7211 0.7315	0.5463 0.5610	0.3929 0.4024	0.1969 0.1973	0.3175 0.3013	0.0269 0.0274
	4x4	Linear(475) Cubic(1275)	0.7265 0.7319	0.5520 0.5605	0.3963 0.4007	0.2039 0.1961	0.3154 0.3008	0.0271 0.0274
	Close	xd-form	0.7324	0.5583	0.3999	0.1957	0.3006	0.0274
	lxl	Linear(76) Cubic(204)	0.3107 0.4805	0.3122 0.6501	0.1815 0.4460	0.2361 0.2775	0.1827 0.4069	0.0133 0.0203
	2x2	Linear(171) Cubic(459)	0.4796 0.5062	0.5069 0.5623	0.2893 0.3277	0.0343 0.1836	0.3116 0.3413	0.0214 0.0229
20	3x3	Linear(324) Cubic(816)	0.4968 0.5071	0.5277 0.5487	0.3002 0.3134	0.1077 0.1620	0.3317 0.3300	0.0223 0.0228
	4x4	Linear(475) Cubic(1275)	0.5020 0.5074	0.5340 0.5461	0.3035 0.3098	0.1355 0.1580	0.3384 0.3280	0.0225 0.0228
	Close	d- form	0.5078	0.5411	0.3071	0.1563	0.3272	0.0228
	1x1	Linear(76) Cubic(204)	0.0403 0.2299	0.0489 0.5089	0.0246 0.3066	1.3249 0.9368	0.4703 0.1338	0.0019 0.0060
	2x2	Linear(171) Cubic(459)	0.3249 0.4177	0.4053 0.5977	0.2039 0.3170	2.3455 0.2904	0.6838 0.5130	0.0160 0.0204
100	3x3	Linear(324) Cubic(816)	0.4027 0.4276	0.5029 0.5615	0.2529 0.2913	1.2435 0.1933	0.1987 0.3940	0.0198 0.0210
	4x4	Linear(475) Cubic(1275)	0.4187 0.4291	0.5230 0.5471	0.2630 0.2805	0.6719 0.1699	0.0335 0.3597	0.0206 0.0211
	Close	d- form	0.4296	0.5366	0.2699	0.1400	0.3377	0.0211

<sup>\*</sup> numbers in parenthesis denote the corresponding degree-of-freedom for each mesh

elements with cubic interpolations show faster convergence at small aspect ratios. However, if the aspect ratio of the composite laminate becomes large, although cubic ones still have better results for transverse stresses, linear ones can give good predictions for inplane stresses. In addition, it is also interesting to know that as the aspect ratio of the laminate increases, more elements are required for convergence. Because of the excellent results from ISSCT and the requirement of a very large degree-of-freedom for ISCT, the finite element analysis based on ISCT is omitted.

## 3.3 Comparison of Different Laminate Theories

In addition to the stress continuity theories, a couple of other laminate theories also deserve some attention. The comparison of the laminate theories with the stress continuity theories becomes an important study in assessing ISSCT and ISCT.

## 3.3.1 Number of Degree-of-Freedom

Although the accuracy is an essential requirement for a good theory, the number of displacement variables used in the theory can affect the feasibility of the theory. Fortunately, the rapid renovation of computer has made the computational work easier and faster than ever before. Nevertheless, the reduction in the computational effort should never be ignored. In the following sections, two typical displacement-based laminate theories are compared with the stress continuity theories for feasibility evaluation. The first one stands for a single-layer approach. It is, in fact, a high-order shear deformation theory and has the following displacement field [11]:

$$u(x, y, z) = u_0(x, y) + z(\psi_x - \frac{4}{3}(\frac{z}{h})^2(\psi_x + \frac{\partial w_0}{\partial x}))$$

$$v(x, y, z) = v_0(x, y) + z(\psi_y - \frac{4}{3}(\frac{z}{h})^2(\psi_y + \frac{\partial w_0}{\partial y}))$$

$$w(x, y, z) = w_0(x, y)$$
(3.1)

In Equation (3.1),  $u_0$ ,  $v_0$  and  $w_0$  denote the displacements on the midplane in the x, y, and z coordinates, respectively, while  $\psi_x$  and  $\psi_y$  are the rotations of the normals to the midplane about y and x axes, respectively. It can be seen that the number of displacement variables is five regardless of the number of layers in the composite laminate.

The other approach is the generalized laminated plate theory [5]. This mutliplelayer approach has the following displacement field:

$$u(x, y, z) = u_0(x, y) + \sum_{j=1}^{N} U^{j}(x, y) \Phi_{j}(z)$$

$$v(x, y, z) = v_0(x, y) + \sum_{j=1}^{N} V^{j}(x, y) \Phi_{j}(z)$$

$$w(x, y, z) = w_0(x, y)$$
(3.2)

where the quantities with subscript 0 denote the midplane displacements, while  $\Phi_j$ 's are the global interpolation functions for thickness assembly. U' and V' are the nodal displacements relative to the midplane. It should be noted that the number of displacement variables used in Equation (3.2) totally depends on the order of the interpolation functions and the number of layers, n, in the laminate of interest. For instance, the order of a piecewise linear interpolation gives rise to N = n + 1. Since U' and V' vanish on the midplane according to definition, it then results in N = n. Hence the total number of displacement variables for linear interpolation is 2n + 1. With higher-order interpolation in each layer, the conditions for free shear tractions on top and bottom surfaces of the composite laminate can eliminate four more variables. This brings the total number of displacement variables to 4n - 1 and 6n - 1 for quadratic and cubic interpolations, respectively.

Table 3.10 gives the comparison of the degree-of-freedom among the theories of single-layer approach, multiple-layer approach, and the stress continuity theories presented in this thesis. In this table, GLPT<sup>1</sup> represents for GLPT based on quadratic interpolation function while GLPT<sup>2</sup> cubic interpolation function. It can be seen ISSCT and GLPT<sup>1</sup> have

Table 3.10 Comparison of different laminate theories for an n-layer laminate.

Theory	Number of displacement variables	Inplane stresses	Transverse shear stresses	Transverse normal stress
HSDT	5	constitutive	equilibrium	equilibrium
GLPT 1	4n-1	constitutive	equilibrium	equilibrium
GLPT <sup>2</sup>	6n-1	constitutive	equilibrium	equilibrium
ISSCT	4n+1	constitutive	constitutive	equilibrium
ISCT	6n	constitutive	constitutive	constitutive

nearly the same number of displacement variables. However, ISSCT can describe a cubic displacement field through the thickness of each layer while GLPT<sup>1</sup> only quadratic. Moreover, for the same cubic interpolation functions through each layer, GLPT<sup>2</sup> requires nearly 50% more displacement variables than ISSCT. As also shown in Table 3.10, ISCT demands much more displacement variables than ISSCT, though the former is rewarded with the simplicity of calculating the transverse normal stress directly from constitutive equations.

# 3.3.2 Recovery of Transverse Stresses

The recovery of transverse stresses from inplane stresses can be accomplished by using the equilibrium equations in the absence of body forces, i.e.,

$$\sigma_{yz} = -\int_{-\frac{h}{2}}^{z} \left(\frac{\partial \sigma_{xy}}{\partial x} + \frac{\partial \sigma_{y}}{\partial y}\right) dz$$
 (3.3a)

$$\sigma_{xz} = -\int_{-\frac{h}{2}}^{z} \left(\frac{\partial \sigma_{x}}{\partial x} + \frac{\partial \sigma_{xy}}{\partial y}\right) dz$$
 (3.3b)

$$\sigma_z = -\int_{-\frac{h}{2}}^{z} \left( \frac{\partial \sigma_{xz}}{\partial x} + \frac{\partial \sigma_{yz}}{\partial y} \right) dz$$
 (3.3c)

It must be mentioned that in the analysis of closed-form solution, the distribution of all unknown variables in the x-y plane are exact functions. In other words, there is no inplane assembly in the closed-form analysis. Hence, the derivatives involved in Equations (3.3) do not include any error due to numerical differentiation. However, in the finite element analysis, a composite laminate is discretized into many elements. The variables need to be assembled by interpolation functions and are not exact. The errors from numerical differentiations become unavoidable and always cause losses of accuracy. In addition, each integration in Equations (3.3) provides an integration constant to be determined by the boundary conditions. Usually one undetermined constant cannot satisfy the two traction boundary conditions at the top and bottom surfaces of the composite laminate. How-

ever, as the finite element result converges to closed-form solution, both traction boundary conditions can be satisfied.

## 3.3.3 Closed-Form Solutions for Different Laminate Theories

The basic difference of the laminate theories mentioned in Section 3.3.1 is due to the assumption of the displacement field through the thickness. Since the closed-form solution is based on a complete function for inplane deformation instead of section-by-section assembly, it then does not introduce error due to approximation and assembly. A direct insight into the different theories is possible. Therefore, closed-form solutions are performed for comparing the different laminate theories.

Table 3.11 presents the results of a [0/90] laminate under cylindrical bending. For HSDT, GLPT¹ and GLPT², since the transverse shear stresses calculated from the constitutive equations are not continuous across the laminate interface, two numerical values, one for the layer above the interface and the other below the interface, are reported in the table. The transverse shear stress distributions through the thickness for some of these theories are shown in Figure 3.12(a). In addition, the continuous transverse shear stress distributions from equilibrium equations can be found in Figure 3.12(b). Because the results from ISCT and elasticity are very close to each other and so are GLPT² and ISSCT, the results from ISCT and GLPT² are not presented in these figures for clearity. Similar results for [0/90/90/0] laminate are presented in Table 3.12, Figures 3.13(a), and (b). It should be noted that because of symmetric layup, the transverse shear stress at the midplane calculated by HSDT, GLPT¹, and GLPT² has only one value.

The comparison for different laminate theories can be addressed from the following viewpoints.

# 1. Transverse Deflection at Midspan

Comparing the results from the different theories, it is clear that ISCT gives the best prediction (error < 0.1%) of the transverse deflection at the midspan for the aspect

Table 3.11 Closed-form solutions of a [0/90] laminate under cylindrical bending by using different laminate theories.

Aspect ratio	Theory	¥	σ̄ <sub>z</sub> *	σ̄ <sub>x2</sub> *	ō <sub>xs</sub>	$\vec{\sigma}_z$
	HSDT	4.4445	-33.6062 3.0915	2.4769 0.9907	0.7147	0.8320
	GLPT <sup>1</sup>	4.2625	-33.4930 3.2913	3.2215 0.8623	0.7411	0.8220
S=4	GLPT <sup>2</sup>	4.7785	-31.0802 3.7159	0.8479 0.8553	0.8623	0.7957
	ISSCT	4.7785	-31.0844 3.7158	0.8530	*******	0.7897
	ISCT	4.6918	-30.2907 3.8362	0.9055	******	0.8468*
·	Elasticity	4.6953	-30.0293 3.8359	0.9135	,	0.7860
	HSDT	2.6933	-703.437 75.805	12.625 5.0501	3.8998	0.8202
	GLPT <sup>1</sup>	2.6867	-703.315 76.016	16.611 4.4181	3.9053	0.8198
S=20	GLPT <sup>2</sup>	2.7069	-700.464 76.563	3.9342 3.9340	3.9353	0.8184
	ISSCT	2.7069	-700.459 76.562	3.9340	*******	0.8182
	ISCT	2.7027	-699.737 76.652	3.9451	******	0.8875*
	Elasticity	2.7027	-699.734 76.653	3.9460	*******	0.8180
	HSDT	2.6375	-2796.29 303.03	25.266 10.106	7.8204	0.8198
	GLPT <sup>1</sup>	2.6359	-2796.41 303.26	33.257 8.8432	7.8241	0.8198
S=40	GLPT <sup>2</sup>	2.6409	-2793.39 303.80	7.8380 7.8375	7.8387	0.8194
	ISSCT	2.6408	-2793 <i>.27</i> 303.79	7.8373	******	0.8193
	ISCT	2.6398	-2792.56 303.88	7.8430		0.8891*
	Elasticity	2.6398	-2792.59 303.88	7.8436	******	0.8193

$$\overline{\sigma}_x = \overline{\sigma}_x(\frac{l}{2}, \mp \frac{h}{2}) \; \; ; \; \overline{\sigma}_{xz} = \overline{\sigma}_{xz}(0, 0) \; \; ; \; \overline{\sigma}_z = \overline{\sigma}_z(\frac{l}{2}, 0)$$

<sup>\*</sup> calculated from constitutive equations directly

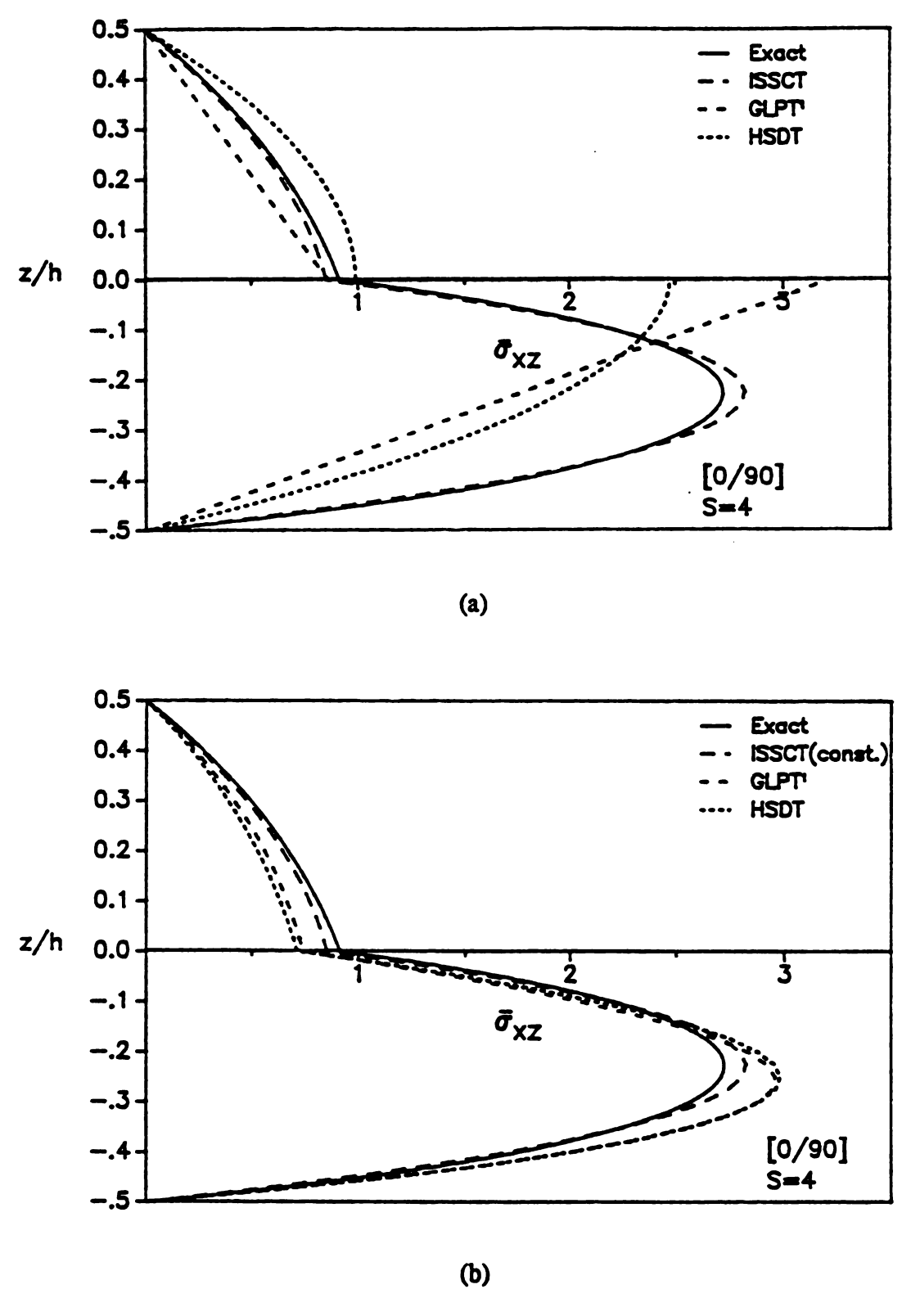


Figure 3.12 Normalized transverse shear stresses at the edge of a simply-supported [0/90] laminate with S=4 by using different laminate theories. (a) constitutive equations, (b) equilibrium equations.

Table 3.12 Closed-form solutions of a [0/90/90/0] laminate under cylindrical bending by using different laminate theories.

Aspect ratio	Theory	¥	<b>ਰ</b> ∗	σ̄ <u>*</u>	ō₂,	ਰ,
	HSDT	3.2020	<b>∓18.6276</b>	1.3636	1.5061	0.7960
	GLPT <sup>I</sup>	3.3325	<b>∓20.5875</b>	1.4383	1.4400	0.7834
	GLPT <sup>2</sup>	3.3581	∓19 <i>.</i> 9049	1.4541	1.4541	0.7862
S=4	ISSCT	3.3581	<b>∓19.9125</b>	1.4512		0.7855
	ISCT	3.3360	-19.7062 20.2398	1.4532	******	0.7776*
	Elasticity	3.3361	-19.6700 20.2020	1.4560	******	0.7858
	HSDT	0.6885	<b>∓284.205</b>	7.0885	8.2173	0.8213
	GLPT <sup>1</sup>	0.6796	<b>∓287.302</b>	8.2132	8.1964	0.8206
	GLPT <sup>2</sup>	0.6797	<b>∓287.079</b>	8.1973	8.1974	0.8206
S=20	ISSCT	0.6797	<b>∓287.080</b>	8.1966	******	0.8206
	ISCT	0.6793	-287.109 286.913	8.1977	*******	0.8185*
	Elasticity	0.6793	-287.108 286.912	8.1983	*******	0.8207
	HSDT	0.5861	<b>∓1113.21</b>	14.195	16.479	0.8222
	GLPT <sup>1</sup>	0.5889	<b>∓1116.35</b>	16.504	16.469	0.8220
	GLPT <sup>2</sup>	0.5889	<b>∓1116.14</b>	16.469	16.469	0.8220
S <del>=</del> 40	ISSCT	0.5889	<b>∓1116.15</b>	16.469	******	0.8220
	ISCT	0.5888	-1116.18 1115.95	16.469	*******	0.8201*
	Elasticity	0.5889	-1116.18 1115.96	16.470	******	0.8220

$$\overline{\sigma}_x = \overline{\sigma}_x(\frac{l}{2}, \mp \frac{h}{2}) \; \; ; \; \overline{\sigma}_{xz} = \overline{\sigma}_{xz}(0,0) \; \; ; \; \; \overline{\sigma}_z = \overline{\sigma}_z(\frac{l}{2},0)$$

<sup>\*</sup> calculated from constitutive equations

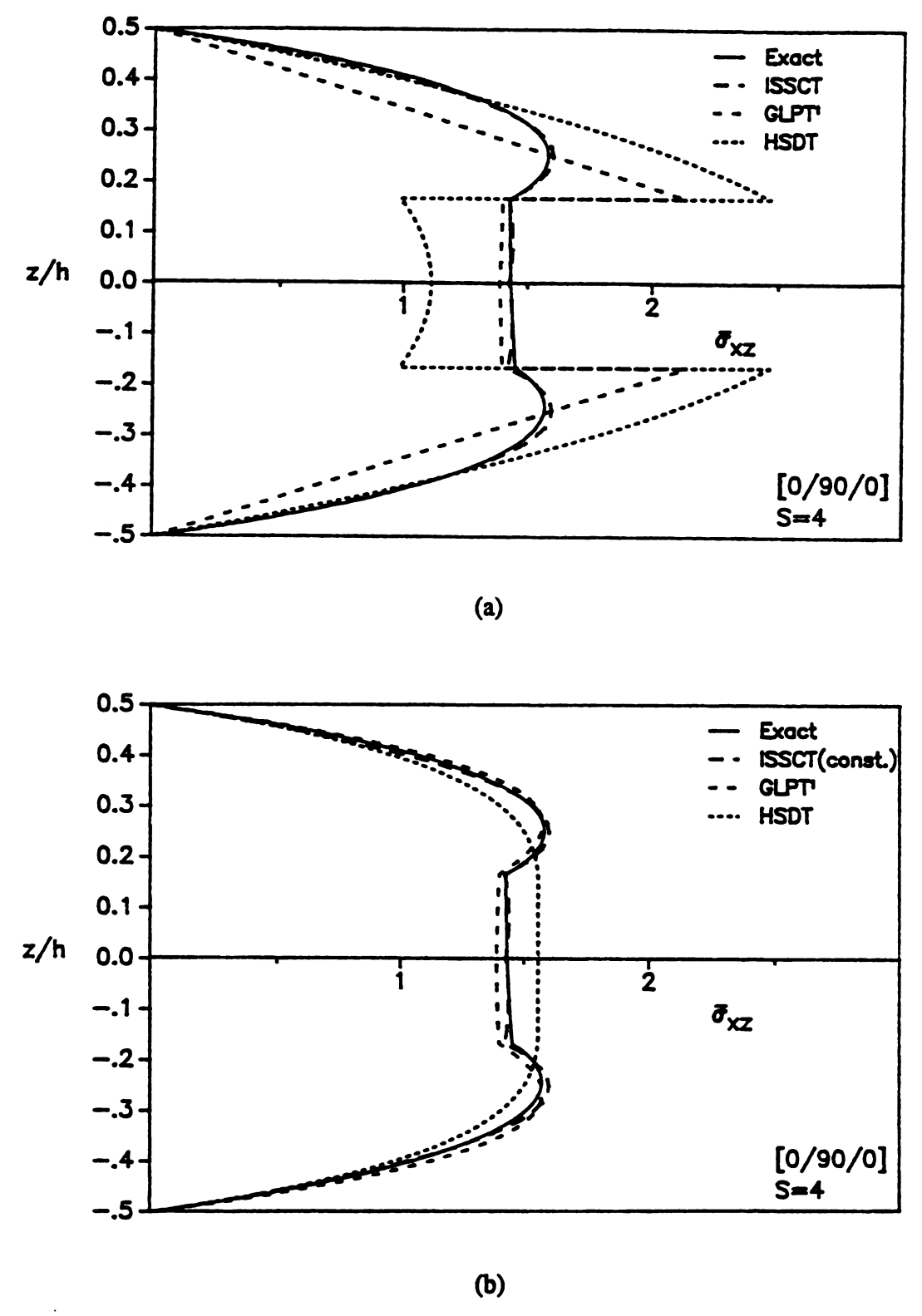


Figure 3.13 Normalized transverse shear stresses at the edge of a simply-supported [0/90/0] laminate with S=4 by using different laminate theories. (a) constitutive equations, (b) equilibrium equations.

ratios considered. However, there is no surprise to see that at large aspect ratio, HSDT can also give excellent result.

#### 2. Inplane Stress

The inplane stress considered in cylindrical bending is the normal stress in x-direction,  $\sigma_x$ . Although ISCT again shows the best result (error < 1%), the remaining theories can give accuracy within 0.5% at S=40. However, the error becomes very large, e.g., 12%, at S=4.

#### 3. Transverse Shear Stress

For the transverse shear stress, ISSCT and GLPT<sup>2</sup> have the same accuracy as those of ISCT except for a [0/90] laminate with S=4. However, since GLPT<sup>2</sup> has higher degree-of-freedom than ISSCT and its transverse shear stress has to be calculated from equilibrium equations, GLPT<sup>2</sup> is not as efficient as ISSCT. Although GLPT<sup>1</sup> has approximately the same degree-of-freedom as ISSCT, its result is not as good as ISSCT. In addition, from Figure 3.13(b), it is found that HSDT does not predict the correct trend of the transverse shear stress through the thickness when S=4.

#### 4. Transverse Normal Stress

Among the laminate theories discussed in this study, only ISCT can calculate the transverse normal stress directly from the constitutive equations. However, it is surprising to see that the results obtained by ISCT does not provide better accuracy than those recovered from equilibrium equations, especially for the asymmetric layup, [0/90] laminate. Although the accuracy can be improved by increasing the number of layers in the analysis as shown in Table 3.3, the penalty of increasing the degree-of-freedom may drastically overwhelm the support of using ISCT.

## 5. Bidirectional Bending

Beside the examples for laminates under cylindrical bending, laminates under bidirectional bending are also studied here. Since there is no advantage of using GLPT<sup>2</sup>, GLPT<sup>2</sup> is omitted in the following discussion. Thus, GLPT in the following tables denotes the GLPT<sup>1</sup>. The closed-form solutions of a square [0/90/90/0] laminate and a rectangular [0/90/0] laminate are presented in Tables 3.13 and 3.14, respectively. For the transverse shear stresses, the results obtained from equilibrium equations are reported within parentheses right under the quantities calculated directly from the constitutive equations. Moreover, due to the symmetric stacking sequence of the laminates studied, only one value of transverse shear stress is found at the midplane. With the results shown in Tables 3.13 and 3.14, it can be seen that HSDT has an error around 10% for both deflection and stresses at a/h = 4. The prediction can be improved as the aspect ratio of the composite laminate increases. In additions, the results obtained by GLPT are less accurate than ISSCT while ISCT gives excellent agreement with elasticity solutions.

## **3.3.4 Summary**

Based on the numerical results presented in the previous sections, the following summary can be drawn.

- 1. The importance of interlaminar shear stress continuity condition in composite laminate analysis can be recognized from the comparison between ISSCT and GLPT<sup>2</sup>, shown in Tables 3.11 and 3.12. In both theories, a cubic displacement field within each layer is used though only ISSCT satisfies the interlaminar shear stress continuity conditions at the composite interfaces. It can be seen from Tables 3.11 and 3.12, both theories predict almost the same results for displacement and stresses. In other words, they have about the same accuracy for composite analysis. However, as the computational effort is concerned, ISSCT has degree-of-freedom 30% lower than that of GLPT<sup>2</sup>, shown in Table 3.10.
- 2. As mentioned in Chapter 2, the major difference between ISCT and ISSCT lies in the assumption of transverse displacement w. The former varies in the thickness direction while the latter is constant through the thickness. If phrased differently, as can be recognized from Equations (2.14) and (2.29), the significance is the consideration of  $\sigma_{e}$  in the

Table 3.13 Closed-form solutions of a square (a=b) [0/90/90/0] laminate under bidirectional bending by using different laminate theories.

a k	Theory	w	<b>ਰ</b> ₁	₫2	σ̄₄	<b>შ</b> ₅	<b>ਰ</b> ̄ <sub>6</sub>
4	HSDT	1.8813	±0.6641	±0.6253	0.2398 (0.2977)*	0.2056 (0.2299)	∓0.0435
	GLPT	1.9433	±0.7323	±0.6632	0.3297 (0.2893)	0.2182 (0.2174)	∓0.0470
-	ISSCT	1.9555	±0.7048	±0.6703	0.2876	0.2187	∓0.0465
	ISCT	1.9377	+0.7216 -0.6856	+0.6642 -0.6671	0.2876	0.2189	-0.0467 +0.0459
	Elasticity	1.937	+0.720 -0.684	+0.663 -0.666	0.292	0.219	-0.0465 +0.0458
	HSDT	0.7079	±0.5433	±0.3863	0.1546 (0.1930)	0.2629 (0.3059)	∓0.0264
	GLPT	0.7319	±0.5606	±0.3996	0.2225 (0.1960)	0.3020 (0.3005)	∓0.0274
10	ISSCT	0.7324	±0.5583	±0.3999	0.1957	0.3006	∓0.0274
	ISCT	0.7371	+0.5587 -0.5591	+ 0.4010 -0.4027	0.1955	0.3013	-0.0275 +0.0276
	Elasticity	0.737	+0.559 -0.559	+0.401 -0.403	0.196	0.301	-0.0275 +0.0276
	HSDT	0.5004	±0.5369	±0.3027	0.1251 (0.1550)	0.2814 (0.3289)	∓0.0225
	GLPT	0.5077	±0.5415	±0.3071	0.1771 (0.1564)	0.3288 (0.3272)	∓0.0228
20	ISSCT	0.5078	±0.5411	±0.3071	0.1563	0.3272	∓0.0228
	ISCT	0.5130	+0.5428 -0.5432	+0.3084 -0.3088	0.1555	0.3281	-0.0230 +0.0231
	Elasticity	0.513	+0.543 -0.543	+0.308 -0.309	0.156	0.328	-0.0230 +0.0230
100	HSDT	0.4293	±0.5365	±0.2697	0.1134 (0.1400)	0.2887 (0.3380)	∓0.0211
	GLPT	0.4297	±0.5368	±0.2700	0.1580 (0.1401)	0.3395 (0.3380)	∓0.0211
	ISSCT	0.4296	±0.5366	±0.2699	0.1400	0.3377	∓0.0211
	ISCT	0.4346	+0.5389 -0.5389	+0.2710 -0.2710	0.1389	0.3388	-0.0214 +0.0214
	Elasticity	0.435	+0.539 -0.539	+0.271 -0.271	0.139	0.339	-0.0214 +0.0214

<sup>\*</sup> quantity in parenthesis denotes the result obtained by equilibrium equations

Table 3.14 Closed-form solutions of a rectangular (3a=b) [0/90/0] laminate under bidirectional bending by using different laminate theories.

a k	Theory	W	σ <sub>ι</sub>	₹ <b>7</b> 2	ਰ੍4	$\bar{\sigma}_{5}$	ਰ <sub>6</sub>
	HSDT	2.6366	±1.0372	±0.1026	0.0356 (0.0309)*	0.2722 (0.3822)	∓0.0262
4	GLPT	2.7800	±1.1866	±0.1093	0.0331 (0.0313)	0.3405 (0.3408)	∓0.0278
	ISSCT	2.8406	±1.1254	±0.1115	0.0319	0.3494	∓0.0277
	ISCT	2.8215	+1.1496 -1.1041	+0.1085 -0.1191	0.0332	0.3494	-0.0269 +0.0281
	Elasticity	2.820	+ 1.14 -1.10	+0.109 -0.119	0.0334	0.351	-0.0269 +0.0281
	HSDT	0.8594	±0.6923	±0.0404	0.0177 (0.0150)	0.2858 (0.4298)	∓0.0115
	GLPT	0.9159	±0.7320	±0.0423	0.0161 (0.0154)	0.4192 (0.4190)	∓0.0121
10	ISSCT	0.9178	±0.7265	±0.0424	0.0154	0.4196	∓0.0121
	ISCT	0.9189	+0.7261 -0.7256	+0.0417 -0.0435	0.0152	0.4198	-0.0120 +0.0123
	Elasticity	0.919	+0.726 -0.725	+0.0418 -0.0435	0.0152	0.420	-0.0120 +0.0123
	HSDT	0.5911	±0.6404	±0.0295	0.0147 (0.0123)	0.2879 (0.4370)	<b>∓0.0091</b>
	GLPT	0.6070	±0.6511	±0.0301	0.0129 (0.0124)	0.4345 (0.4341)	∓0.0092
20	ISSCT	0.6073	±0.6501	±0.0301	0.0124	0.4342	∓0.0092
	ISCT	0.6095	+ 0.6500 -0.6502	+0.0294 -0.0299	0.0119	0.4343	-0.0092 +0.0093
	Elasticity	0.610	+0.650 -0.650	+0.0294 -0.0299	0.0119	0.434	-0.0093 +0.0093
100	HSDT	0.5045	±0.6238	±0.0260	0.0137 (0.0114)	0.2886 (0.4394)	<b>∓0.008</b> 3
	GLPT	0.5051	±0.6241	±0.0260	0.0118 (0.0114)	0.4395 (0.4392)	∓0.0083
	ISSCT	0. <i>5</i> 053	±0.6243	±0.0260	0.0114	0.4392	∓0.0083
	ISCT	0.5077	+0.6244 -0.6244	+0.0253 -0.0253	0.0108	0.4393	-0.0083 +0.0083
	Elasticity	0.508	+0.539 -0.539	+0.0253 -0.0253	0.0108	0.439	-0.0083 +0.0083

<sup>\*</sup> quantity in parenthesis denotes the result obtained by equilibrium equations

thickness direction. In order to illustrate the significance, Figures 3.14 to 3.17 present the closed-form solutions obtained from different laminate theories. The investigations are for a simply-supported [0/90] laminate under cylindrical bending and has aspect ratios ranging from three to 200. In these figures, the midspan deflection, maximum inplane stress at midspan, interfacial shear stress at laminate edge, and the transverse normal stress at the interface of midspan are normalized with respect to associated exact solutions [6]. It should be mentioned that the results with asterisk denote the stresses recovered from equilibrium equations, otherwise they are calculated directly from constitutive equations.

As can be seen from these figures, all theories predict excellent results except for the transverse normal stress  $\sigma_z$  from ISCT when the aspect ratio of the composite laminate is greater than 10. However, the results from ISCT can converge to the exact solution as the number of layers used in the analysis increases (see Table 3.11). In spite of this offset difference in  $\sigma_z$ , the results of ISCT have excellent agreement with the exact solutions even for S<10. However, it should be noted that ISSCT can also predict very good result for S=5. Based on the numerical analysis, it can be concluded that ISCT is necessary only when laminates have aspect ratio lower than five. In other words, when the composite laminate is very thick, especially when  $\sigma_z$  is of major concern, the variation of transverse displacement with respect to the thickness needs to be considered.

3. Beside the comparison of accuracy described above, another important aspect needs to be considered is the feasibility of finite element analysis. Unlike ISSCT, the finite element analysis using ISCT suffers from the element aspect ratio problem as pointed out in Tables 3.3 and 3.4. As the aspect ratio of the element is away from one, the results of ISCT diverge. Furthermore, the ISCT demands 50% higher degree-of-freedom than ISSCT. Therefore, it is believed that ISSCT is superior to ISCT for finite element analysis. In the following chapters, only ISSCT is used to demonstrate the feasibility of using the stress continuity theory for composite analysis.

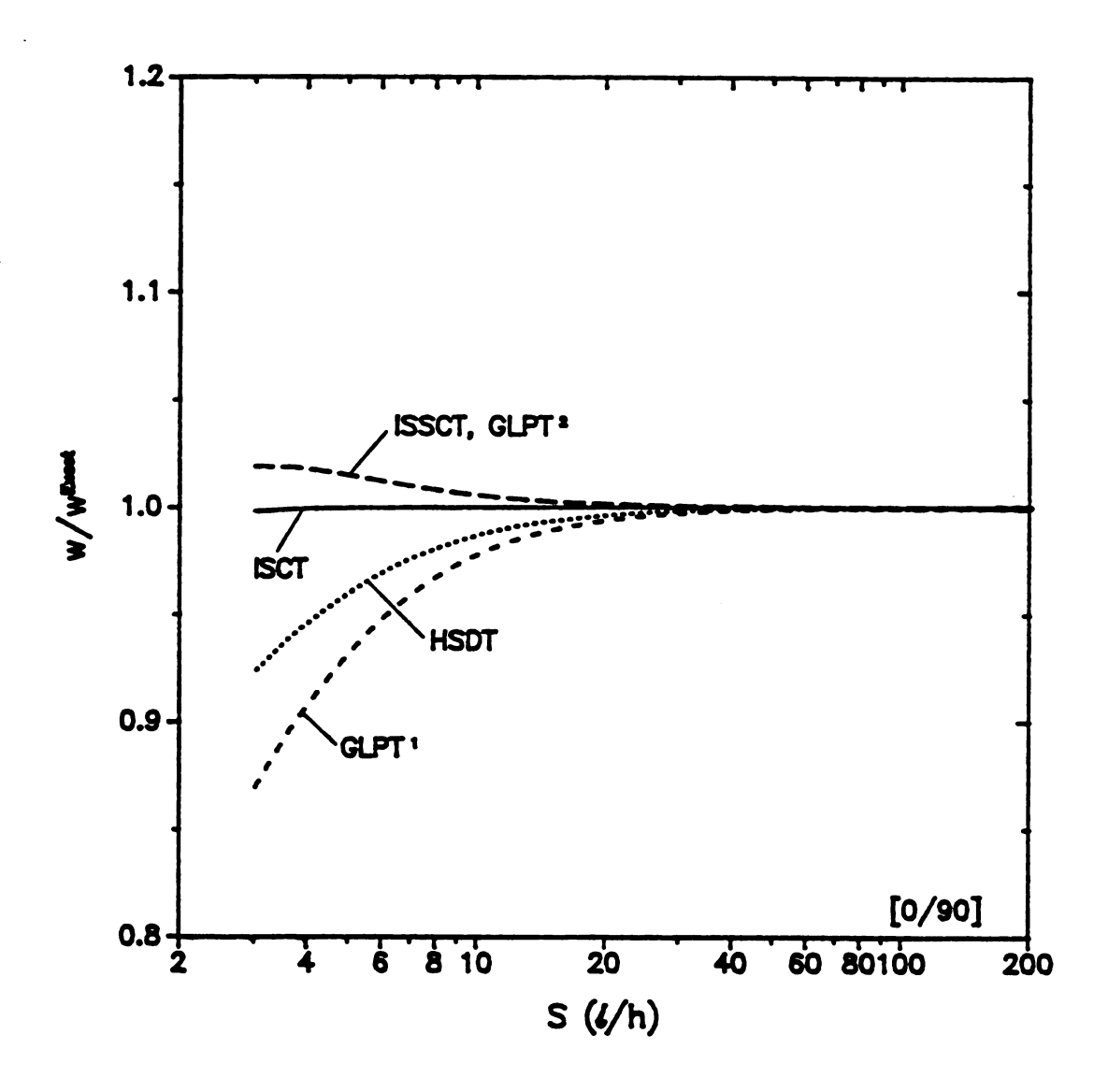


Figure 3.14 Normalized midspan deflections w(U2,0) of a simply-supported [0/90] laminate under cylindrical bending by using different laminate theories.

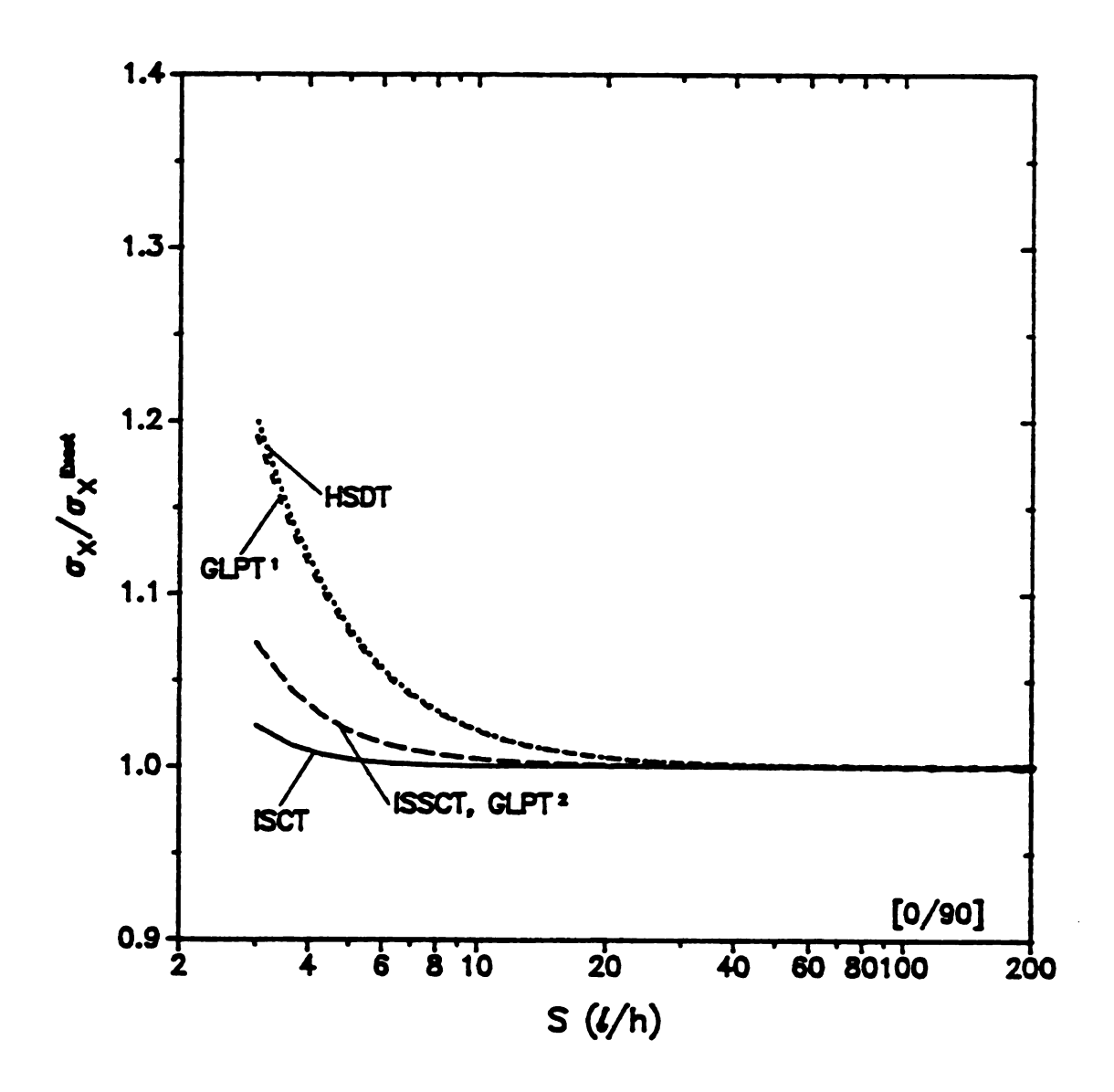


Figure 3.15 Normalized inplane normal stresses  $\sigma_x(U2, W2)$  of a simply-supported [0/90] laminate under cylindrical bending by using different laminate theories.

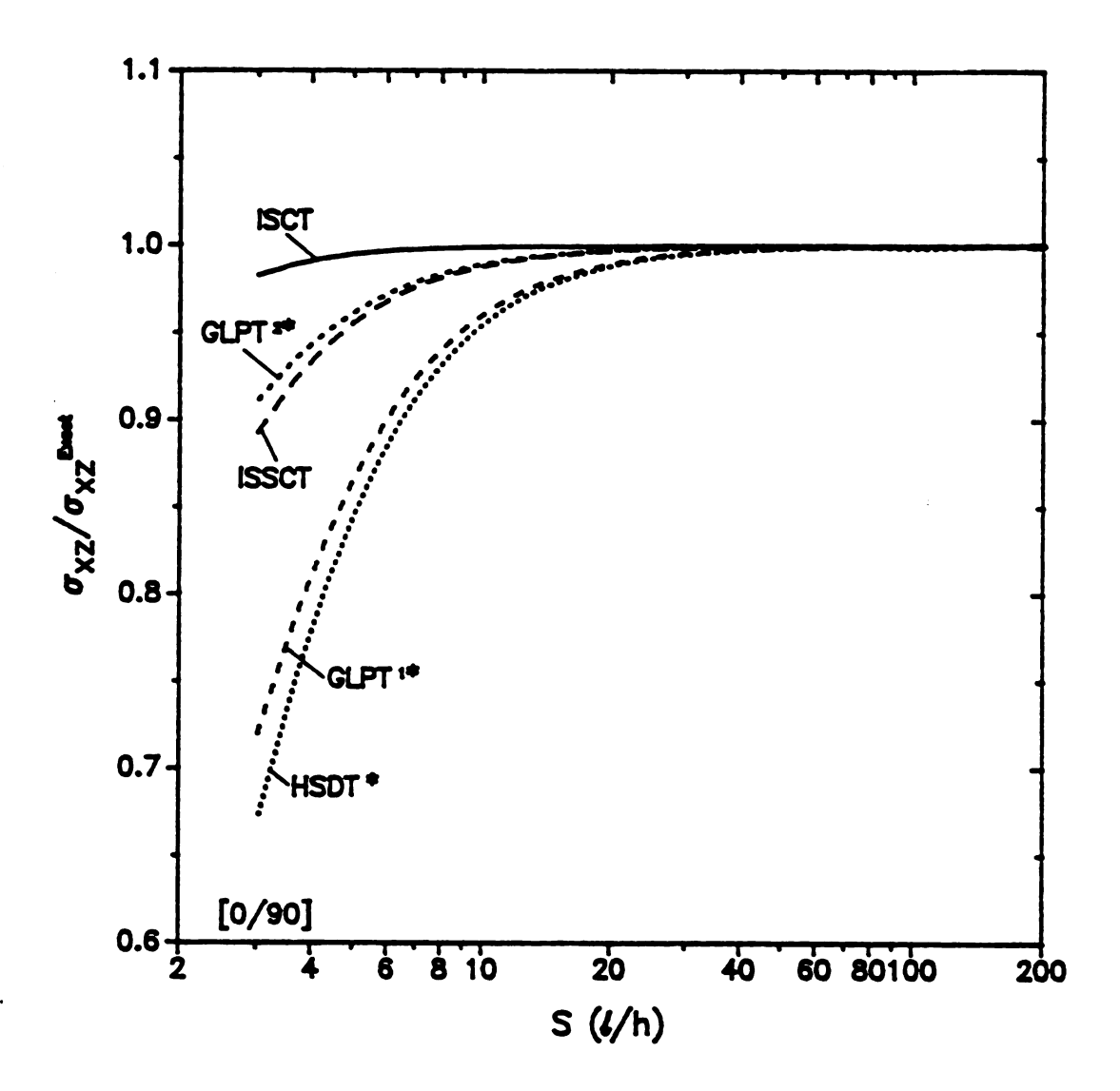


Figure 3.16 Normalized transverse shear stresses  $\sigma_{xx}(0,0)$  of a simply-supported [0/90] laminate under cylindrical bending by using different laminate theories. (\* indicates the results are from equilibrium equations)

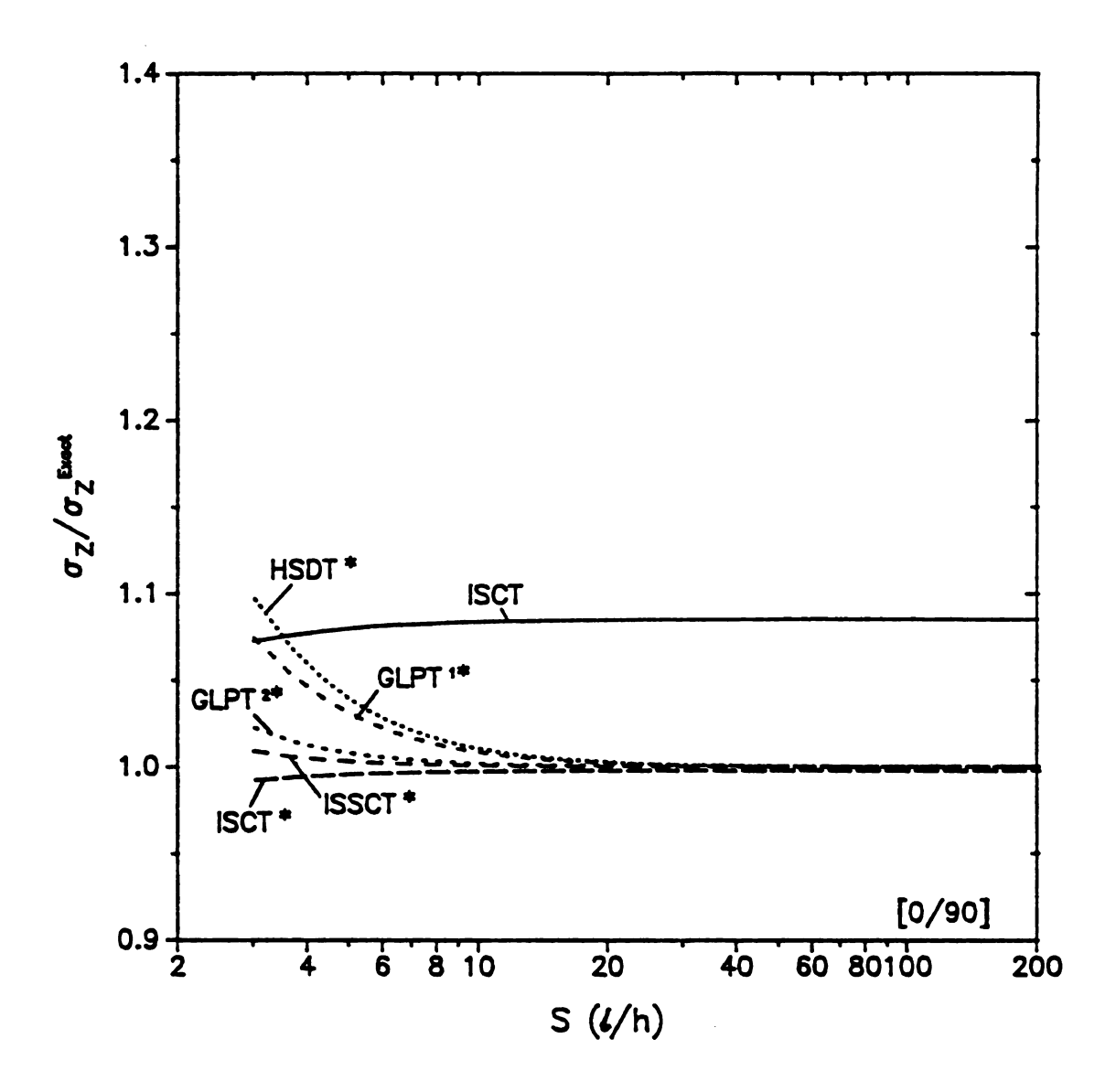


Figure 3.17 Normalized transverse normal stresses  $\sigma_z(1/2,0)$  of a simply-supported [0/90] laminate under cylindrical bending by using different laminate theories. (\* indicates the results are from equilibrium equations)

#### **CHAPTER 4**

## TECHNIQUES FOR LAYER REDUCTION

#### 4.1 Introduction

As discussed in the previous chapter, different laminate theories have different aspects of advantage and disadvantage. For instance, HSDT is simple and has low degree-of-freedom. However, its results for small aspect ratio (S<10) are poor. In addition, the calculation of transverse stresses in this technique needs to resort to the equilibrium equations. On the other hand, ISSCT and ISCT are suitable for both thick and thin composite laminates, and the calculation of transverse stresses can be obtained directly from constitutive equations without extra effort. However, the number of degree-of-freedom in these theories increases with the number of composite layer. A large number of degree-of-freedom can result in costly computation if not impossible. Fortunately, in most design cases, instead of the whole stress distributions through the thickness, frequently only the stress states at some particular interfaces are of interest. This indicates a possibility of combining different theories together to reduce the computational effort while still retain the accuracy in predicting stresses and deformations.

#### 4.2 Fundamental Techniques

The goal of layer reduction is to combine the simplicity of single-layer approach and the accuracy and easiness for stress calculation of the interlaminar shear stress continuity theory. Figure 4.1 illustrates the idea of layer reduction. The original n-layer laminate is reduced to a four-layer laminate. The decision of the layer reduction is dependent on the interface where the stress state is of interest. As pointed out in the previous chapter, every laminate theory can predict inplane stresses more accurately than transverse stress-

es. Hence, the interface of interest should be retained in the layup after layer reduction. Consequently, the two layers adjacent to the interested interface remain unchanged while the layers above and below these two layers are lumped into two single layers. It can be seen that this technique reduces the composite laminate from an n-layer one to a four-layer one. As shown in Figure 4.1, the second and third layers remain unchanged. The material properties used in these two layers are exactly the same as those used in the original case. The determination of the material properties in the reduced layers, i.e., the first and fourth layers, are proposed in the following sections. In this study, only ISSCT is used to demonstrate the feasibility of the layer reduction technique. If ISCT is of interest, similar procedure can be followed.

## 1. Lumping the Reduced Layers by CLT

The first approach of lumping the material properties for the reduced layers is to find an equivalent inplane stiffnesses by CLT and an equivalent shear moduli by averaging the shear modulus through the thickness. Due to this homogenization of the first and fourth layers, both the inplane stresses and transverse shear stresses are continuous through the thickness of each reduced layer.

## 2. Lumping the Reduced Layers by HSDT

As can be shown in Appendix B, ISSCT can be reduced to HSDT for single-layer laminates. Hence, HSDT can be viewed as a single-layer version of ISSCT. It then is possible to model ISSCT and HSDT with a consistent displacement field. That is, the reduced layers can be modeled by HSDT while the unchanged layers by ISSCT. If the reduced layer is modeled by HSDT, the transverse shear stresses calculated from constitutive equations cannot be continuous at the interfaces of the reduced layer. However, because ISSCT is virtually used in assembling the reduced and the unchanged layers, the continuity of transverse shear stresses at their interfaces is guaranteed.

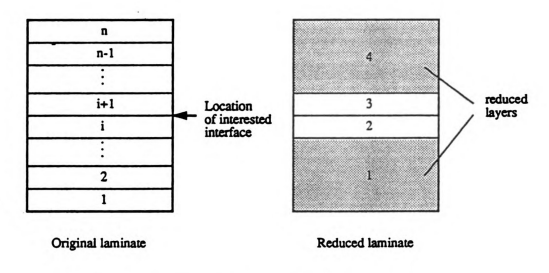


Figure 4.1 Cross-sections of original and reduced layups.

3. Lumping Inplane Stiffnesses by HSDT and Transverse Shear Moduli by Parallel Averaging

The transverse shear stresses calculated from constitutive equations in HSDT are not continuous through the interfaces inside a reduced layer in the second approach while the inplane stresses calculated from the first approach are continuous. These results do not fit the real situation since the inplane stress should be discontinuous through the thickness while the transverse shear stress continuous. However, by lumping the inplane stiffness with HSDT and averaging the transverse shear moduli through the thickness of a reduced layer, the distributions of the stresses through the thickness of the composite laminate become consistent with the exact solutions. In other words, discontinuous inplane stresses and continuous transverse shear stresses through the thickness can be obtained from this approach. The averaging technique for the transverse shear moduli is called parallel averaging and implies

$$Q_{xx} = (\sum_{i} (Q_{xx}^{(i)} h_i)) / (\sum_{i} h_i)$$
 (4.1a)

$$Q_{yz} = (\sum_{i} (Q_{yz}^{(i)} h_{i})) / (\sum_{i} h_{i})$$
 (4.1b)

4. Lumping Inplane Stiffnesses by HSDT and Transverse Shear Moduli by Serial Averaging

Same argument as proposed in the above approach except that serial averaging is employed for transverse shear moduli, i.e.,

$$Q_{xz} = \left(\sum_{i} h_{i}\right) / \left(\sum_{i} h_{i} / Q_{xz}^{(i)}\right) \tag{4.2a}$$

$$Q_{yz} = (\sum_{i} h_{i}) / (\sum_{i} h_{i} / Q_{yz}^{(i)})$$
 (4.2b)

## 4.3 Numerical Examples

The feasibility of the aforementioned techniques for layer reduction is evaluated

with the investigation of several numerical examples. Since the techniques only involve the alternation of layup in the thickness direction without any change in property or geometry in the x-y plane, closed-form solutions are available.

## 4.3.1 Cylindrical Bending

Consider a simply-supported 10-layer [0/90/0/90/0]s laminate subjected to cylindrical bending, and assume the midspan deflection, the maximum inplane stress at midspan, and the midplane transverse shear stress at the laminate boundary are of interest. As can be noted that these are also critical stresses for the composite laminate. The ten-layer laminate is then reduced to a four-layer one, i.e., [R/0]s, where R denotes the reduced layers. The normalizations of the numerical results with respect to ISSCT for the four approaches at different aspect ratios are presented in Figures 4.2-4.4. In these figures, superscripts o and r represent for the results obtained from the original and the reduced laminates, respectively. Since HSDT is the one-layer version of ISSCT, i.e., the simplest reduction of ISSCT, the results from HSDT are included in the following figures for comparison. Figure 4.2 shows clearly that the midspan deflections from all approaches converge to those of ISSCT as the aspect ratio increases. Among the four approaches, the fourth approach gives the best results for all S. For the inplane normal stress as shown in Figure 4.3, all approaches except the first one agree very well with ISSCT. The normalized result for the transverse shear stress is shown in Figure 4.4. It should be pointed out that although HSDT gives fair results in shear stress, the results are obtained by stress recovery technique. If the constitutive equations are used to calculate the shear stress, poor result can be expected.

## 4.3.2 Bidirectional Bending

The same 10-layer [0/90/0/90/0]s laminate is used again in the analysis of bidirectional bending. The displacements and stresses of the simply-supported, square laminate

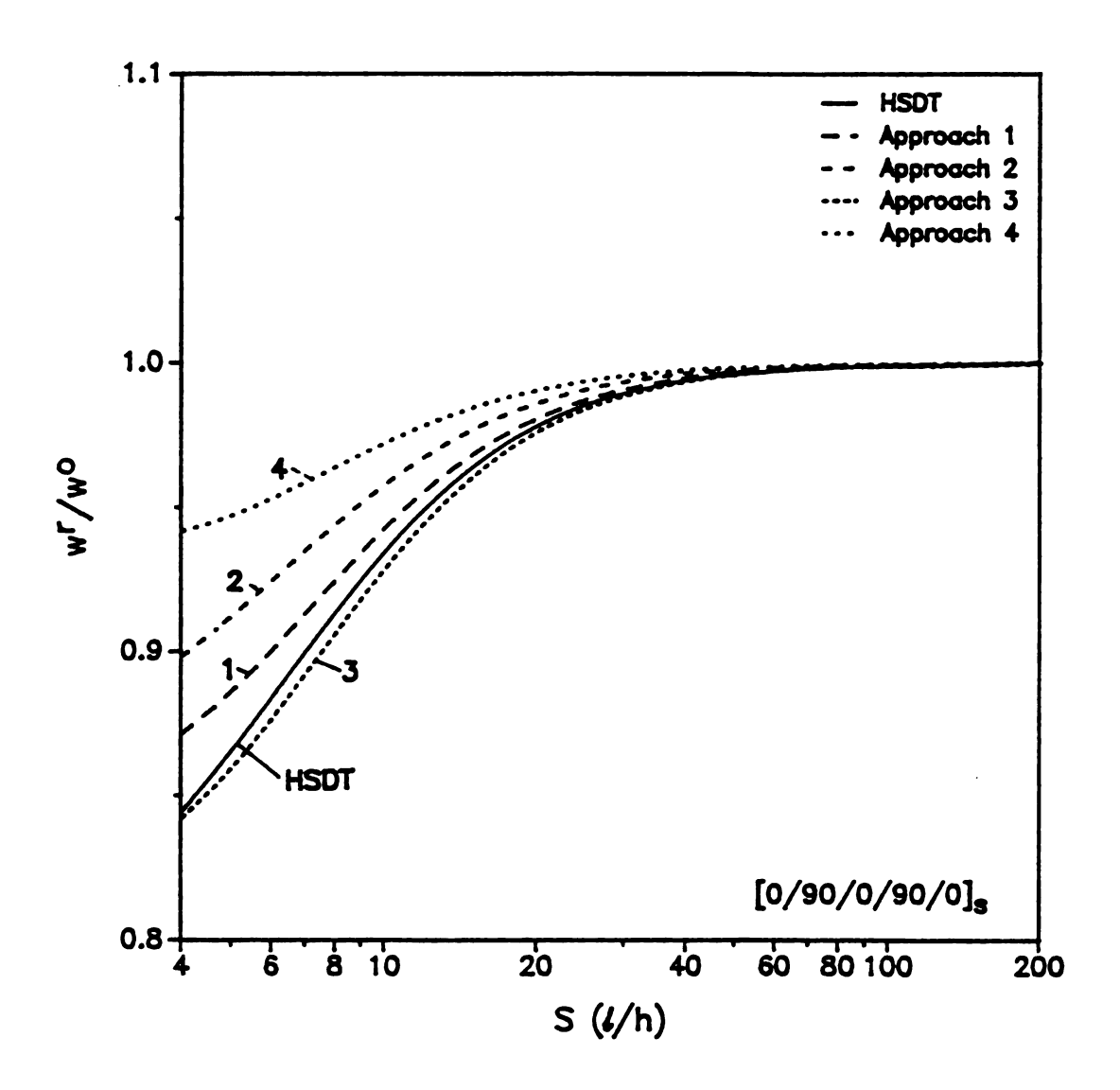


Figure 4.2 Normalized midspan deflections of a [0/90/0/90/0]s laminate under cylindrical bending at different aspect ratios from different layer reduction approaches.

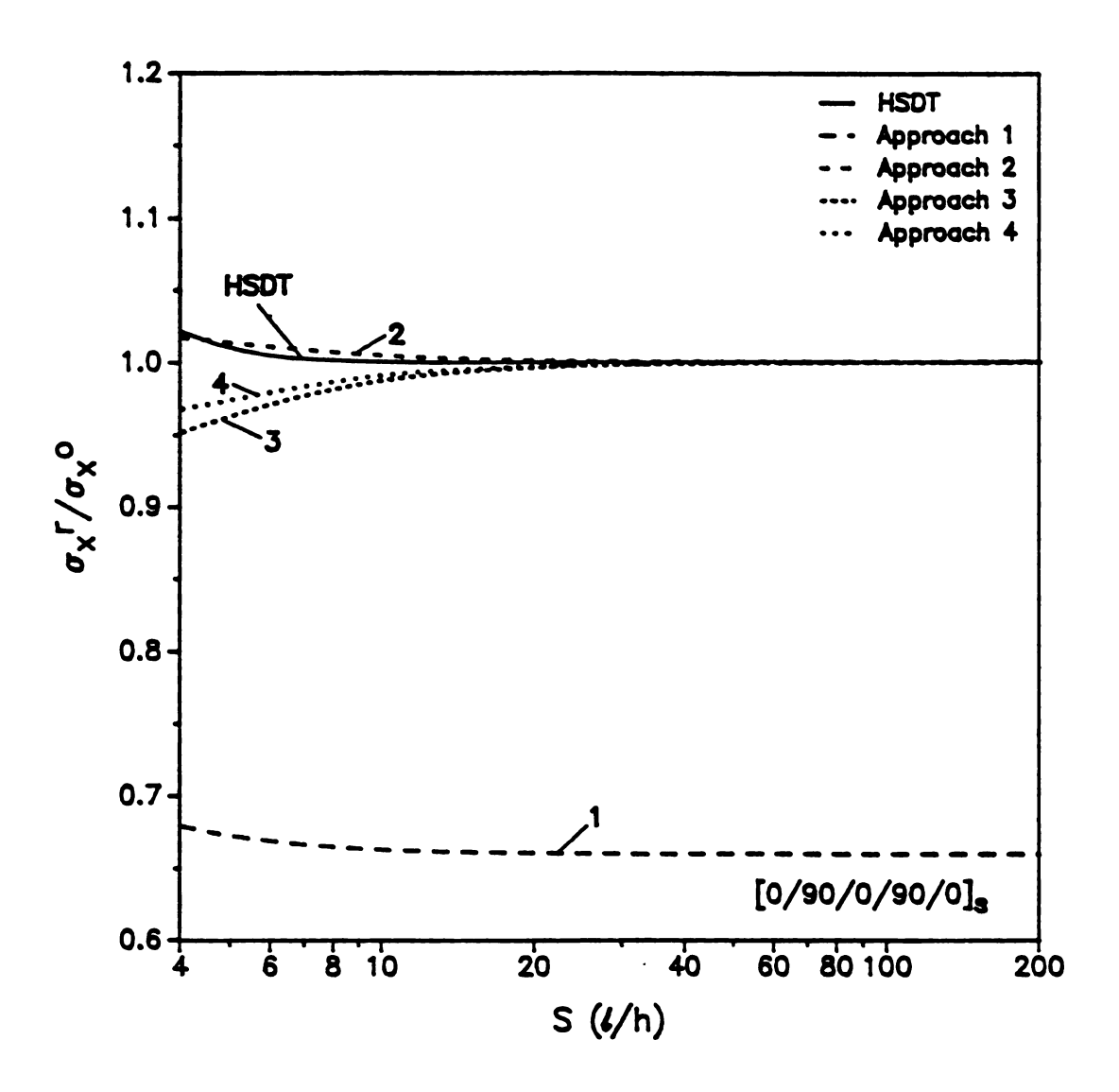


Figure 4.3 Normalized inplane normal stress  $\bar{\sigma}_x(l/2,\pm h/2)$  of a [0/90/0/90/0]s laminate under cylindrical bending at different aspect ratios from different layer reduction approaches.

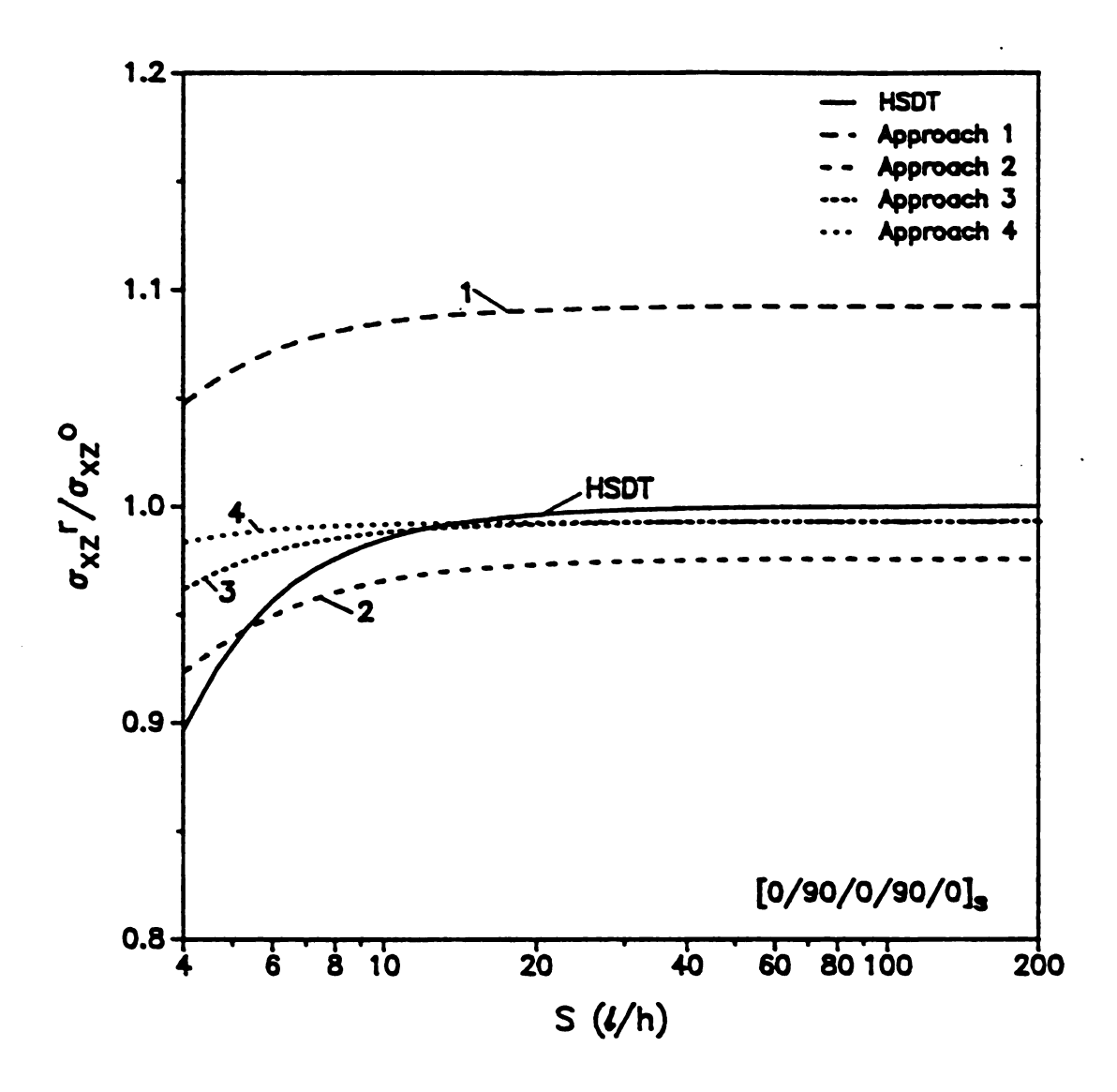


Figure 4.4 Normalized transverse shear stress  $\bar{\sigma}_{xz}(0,0)$  of a [0/90/0/90/0]s laminate under cylindrical bending at different aspect ratios from different layer reduction approaches.

subjected to bidirectionally sinusoidal loading are investigated. Since HSDT needs to resort to equilibrium equations to calculate the transverse shear stresses, it is different from other approaches and is dropped out from the discussion. Furthermore, since the biggest difference among the different approaches appears at small aspect ratio, only the results at S=4 are presented herein.

The normalized inplane displacements through the thickness are shown in Figures 4.5 and 4.6. The solid lines represent for the results obtained by the original 10-layer laminate with the use of ISSCT. It is clear that the displacements predicted by the layer reduction techniques are continuous through the thickness. Figures 4.7, 4.8, and 4.9 present the normalized inplane stresses,  $\bar{\sigma}_{x}$ ,  $\bar{\sigma}_{y}$  and  $\bar{\sigma}_{xy}$ , respectively. As pointed out in the cylindrical bending case, the first approach predicts continuous inplane stress distributions through the reduced layer which obviate from the exact distribution significantly. The normalized results of the transverse shear stresses are shown in Figures 4.10 and 4.11. The second approach gives a discontinuous shear stress through the reduced layer due to the use of HSDT and constitutive equations. In general, both the third and fourth approaches show good approximations through the thickness.

#### 4.4 Discussions

Of the four approaches and the numerical examples presented in the previous sections, the third and the fourth approaches seem to give better results for both displacement and stresses. Both approaches also give the same trends of inplane and transverse stresses as the elasticity solutions.

As can be seen in Figures 4.2 to 4.4, HSDT is accurate for laminates with aspect ratio greater than 10. However, as mentioned in Reference [33], if the stress state near the free edge of the laminate is of concern, the stress recovery technique using equilibrium equations is not satisfactory. On the contrary, as will be seen in the next chapter, the interlaminar stress continuity theory gives very good descriptions of displacement and stress

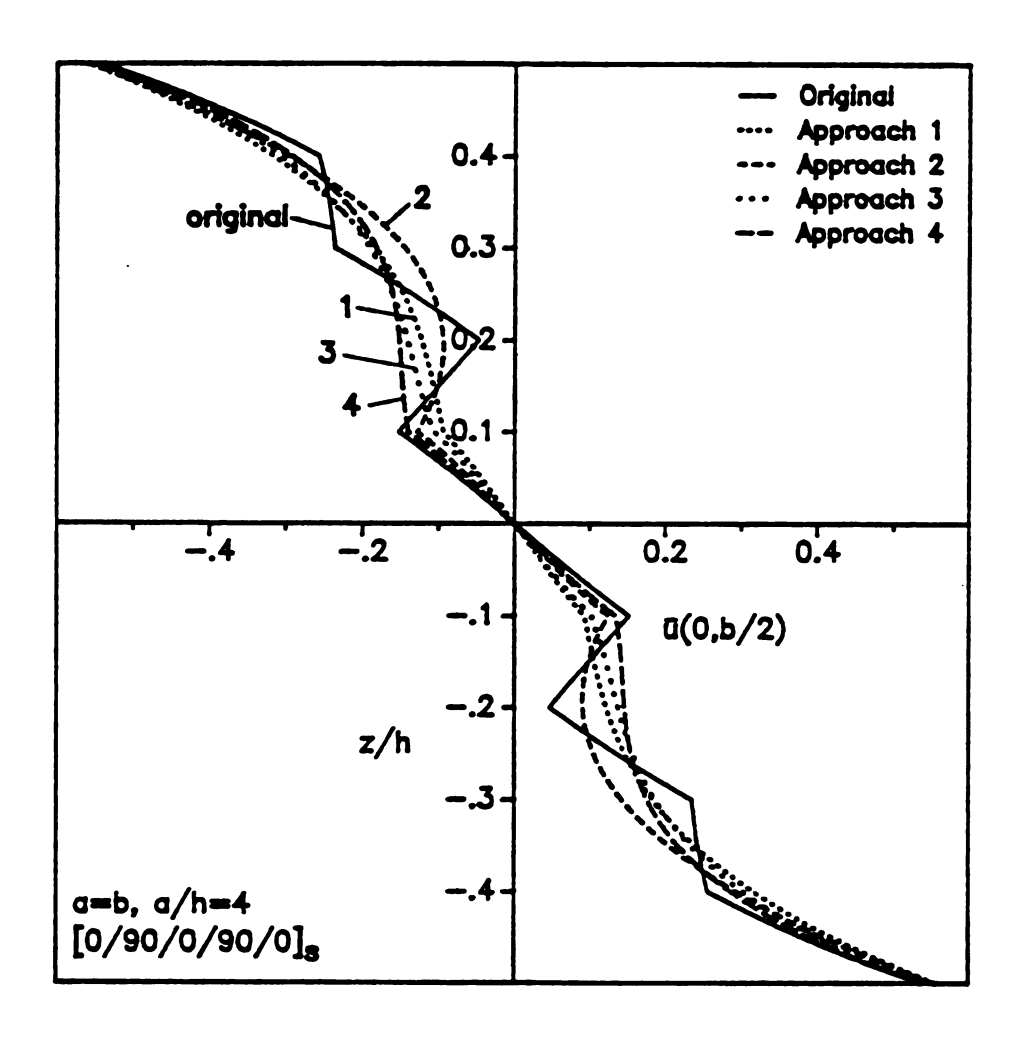


Figure 4.5 Normalized inplane displacement  $\bar{u}(a/2,0)$  of a square [0/90/0/90/0]s laminate subjected to bidirectional bending at S=4 from different layer reduction approaches..

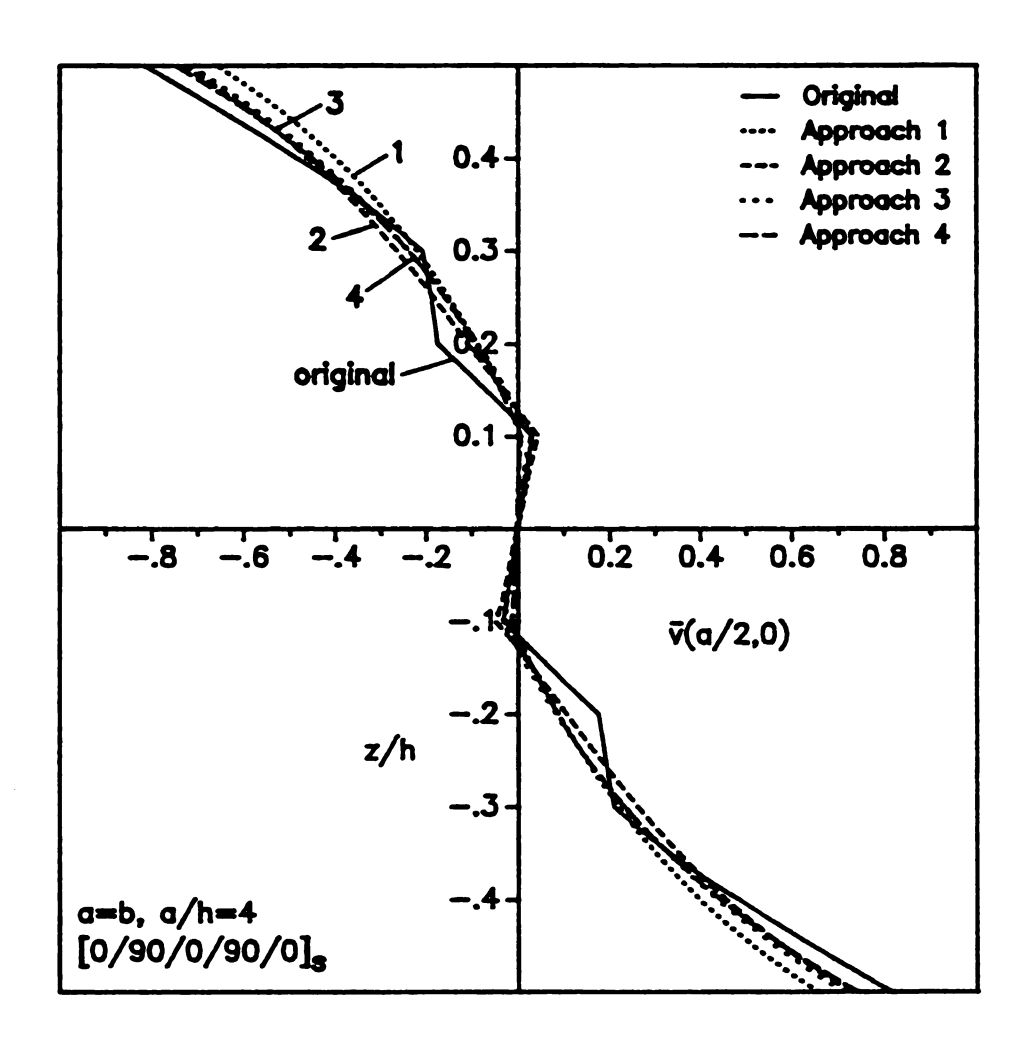


Figure 4.6 Normalized inplane displacement  $\bar{v}(0, b/2)$  of a square [0/90/0/90/0]s laminate subjected to bidirectional bending at S=4 from different layer reduction approaches.

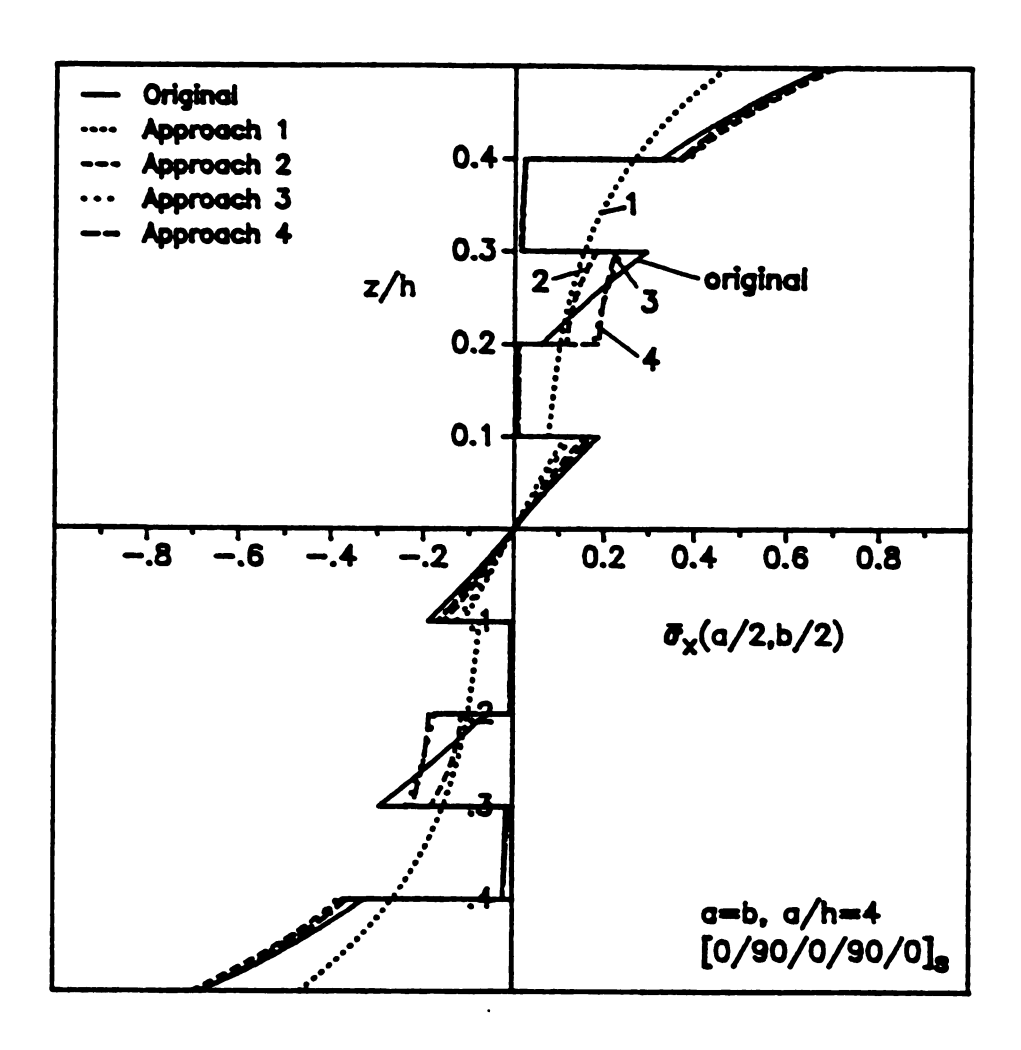


Figure 4.7 Normalized inplane normal stress  $\bar{\sigma}_x(a/2,b/2)$  of a square [0/90/0/90/0]s laminate subjected to bidirectional bending at S=4 from different layer reduction approaches.

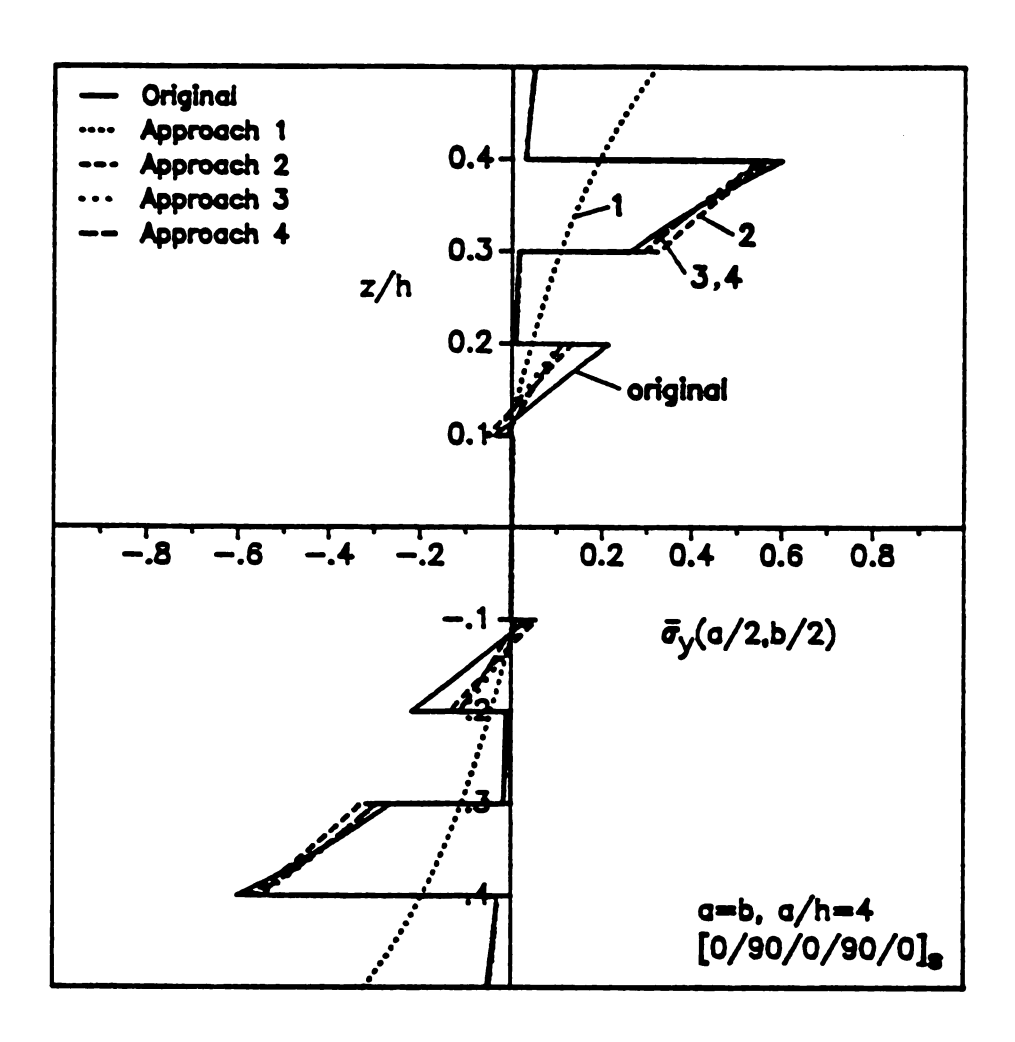


Figure 4.8 Normalized inplane normal stress  $\bar{\sigma}_y(a/2,b/2)$  of a square [0/90/0/90/0]s laminate subjected to bidirectional bending at S=4 from different layer reduction approaches..

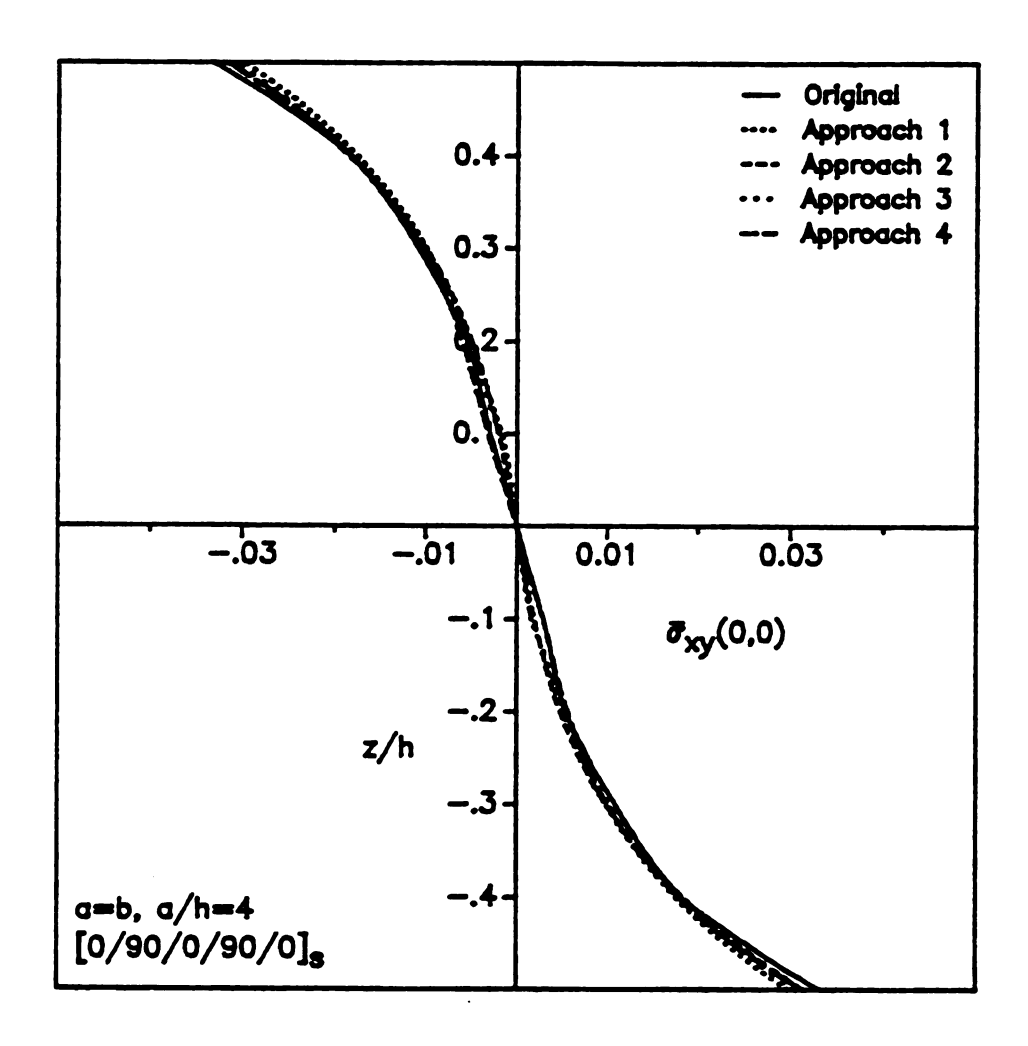


Figure 4.9 Normalized inplane shear stress  $\vec{\sigma}_{xy}(0,0)$  of a square [0/90/0/90/0]s laminate subjected to bidirectional bending at S=4 from different layer reduction approaches.

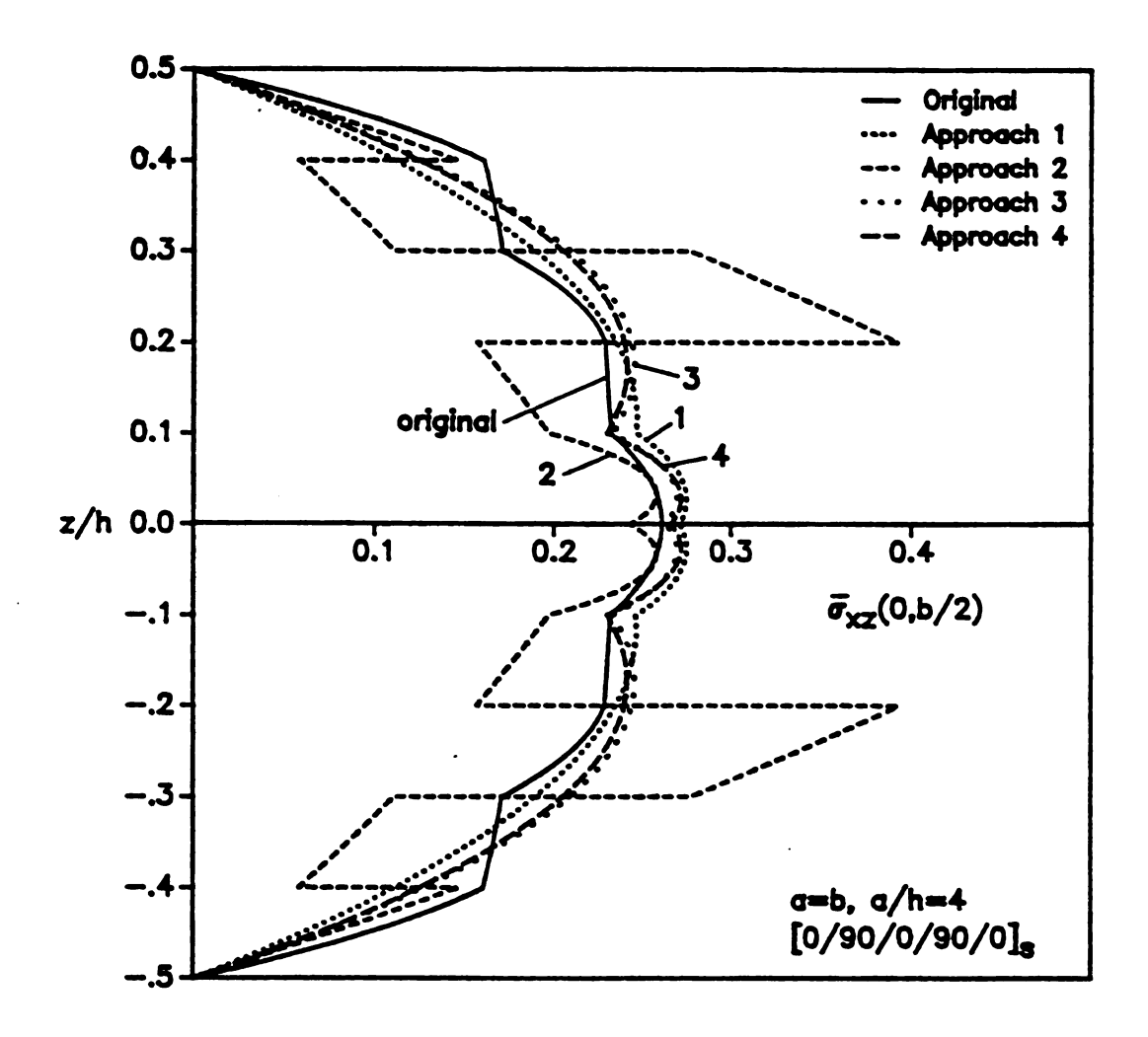


Figure 4.10 Normalized transverse shear stress  $\bar{\sigma}_{xz}(0, b/2)$  of a square [0/90/0/90/0]s laminate subjected to bidirectional bending at S=4 from different layer reduction approaches.

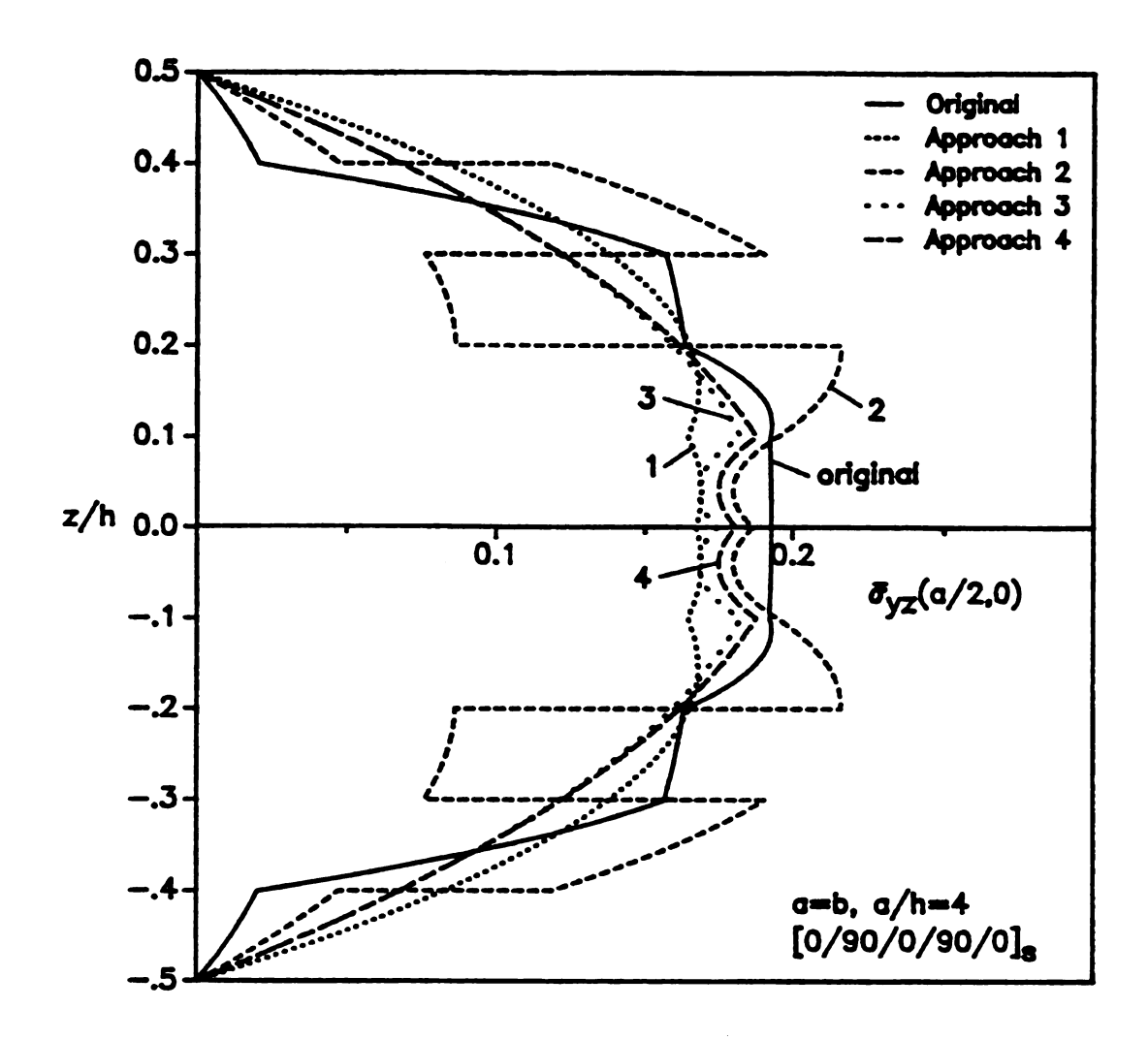


Figure 4.11 Normalized transverse shear stress  $\bar{\sigma}_{yz}(a/2,0)$  of a square [0/90/0/90/0]s laminate subjected to bidirectional bending at S=4 from different layer reduction approaches.

near the free edge. Therefore, it is believed that ISSCT is superior to HSDT in this respect.

Another technique in reducing the computational effort can be achieved by combining ISSCT and HSDT together. This technique implies the use of different types of elements in structural discretization. It is suggested that the ISSCT will be employed only where the stress state is of interest, and the remaining part of laminate can be modeled by HSDT. This mixed technique can reduce the total number of degree-of-freedom considerably, especially for the composite laminate with many layers. However, special attention should be paid to the compatibility between the two different theories. Since this technique is very similar to the traditional finite element analysis for a complicated structure, e.g., a structure composed of truss, beam, and plate substructures, it is not included in this study.

## **CHAPTER 5**

# APPLICATIONS OF ISSCT IN VIBRATION, BUCKLING, AND NONLINEAR ANALYSIS

#### 5.1 Introduction

In Chapters 2 and 3, the derivations and assessments of ISCT and ISSCT are accomplished. Static bending is used to demonstrate the merit of these new theories. It is concluded that for very thick composite laminate (S<5) and for very high accuracy ISCT is necessary. Otherwise, ISSCT is more efficient for computation. In order to further investigate the applicability of ISSCT for engineering analysis, the governing equations of laminated structures in natural vibration, buckling, nonlinear bending, and nonlinear vibration are obtained. Some numerical examples need to be solved and compared with elasticity solutions to assess the new theory. Moreover, the feasibility of using ISSCT for free-edge analysis is presented.

#### 5.2 Natural Vibration

For a composite laminate with some particular boundary conditions, linear free vibration analysis gives the resonant frequencies and associated mode shapes. These kinds of information provide a valuable insight into the structure performance under dynamic loading. Hence, in this section, the governing equation for linear, undamped, free vibration will be derived. In addition, some examples will be examined to justify the accuracy of the laminate theory.

The Lagrangian of a rectangular composite laminate with dimensions of  $a \times b$  under free vibration can be written as

$$L = \int_{0}^{a} \int_{0}^{b} \int_{-\frac{1}{2}}^{\frac{1}{2}} \frac{1}{2} \left\{ \begin{cases} \sigma_{x} \\ \sigma_{y} \\ \sigma_{xy} \end{cases} \right\}^{T} \left\{ \begin{array}{c} \varepsilon_{x} \\ \varepsilon_{y} \\ 2\varepsilon_{xy} \end{array} \right\} + \left\{ \begin{array}{c} \sigma_{yz} \\ \sigma_{xz} \end{array} \right\}^{T} \left\{ \begin{array}{c} 2\varepsilon_{yz} \\ 2\varepsilon_{xz} \end{array} \right\} dz dy dx$$
$$- \int_{0}^{a} \int_{0}^{b} \int_{-\frac{1}{2}}^{\frac{1}{2}} 2\rho \left( \dot{u}^{2} + \dot{v}^{2} + \dot{w}^{2} \right) dz dy dx \tag{5.1}$$

where the first term is the strain energy stored in the structure while the second term is the kinetic energy associated with the time-varying response. In addition, (') denotes time derivative and  $\rho$  stands for mass density. By using constitutive equations, the stresses can be substituted by strains. Employing the strain-displacement relations and carrying out the integration through the thickness, the Lagrangian then becomes

$$L = \frac{1}{2} \int_{0}^{a} \int_{0}^{b} (\{\hat{X}_{n}\}^{T} [S\hat{K}_{n}] \{\hat{X}_{n}\} + \{\hat{X}_{s}\}^{T} [S\hat{K}_{s}] \{\hat{X}_{s}\} - \{\hat{X}_{s}\}^{T} [S\hat{M}_{d}] \{\hat{X}_{s}\} - m\dot{w}^{2}) \, dy dx \qquad (5.2)$$

In the above equation, all the notations used in Chapter 2 are followed. Some new notations are defined below,

$$[S\hat{M}_d] = \sum_{i=1}^n \left( \int_{z_{i-1}}^{z_i} \rho^{(i)} \left[ N_d^{(i)} \right]^T \left[ N_d^{(i)} \right] dz \right)$$
 (5.3)

$$\begin{bmatrix}
N_d^{(1)} \\
\end{bmatrix} = \begin{bmatrix}
\phi_1 & 0 & \phi_2 & 0 & \phi_3 & 0 & A_{22}\phi_4 & A_{21}\phi_4 & B_{22}\phi_4 & B_{21}\phi_4 \\
0 & \phi_1 & 0 & \phi_2 & 0 & \phi_3 & A_{12}\phi_4 & A_{11}\phi_4 & B_{12}\phi_4 & B_{11}\phi_4
\end{bmatrix} (5.4)$$

$$m = \sum_{i=1}^{n} \rho^{(i)} (z_i - z_{i-1})$$
 (5.5)

To satisfy the shear traction free conditions on the laminate surfaces, the same constraint matrices used in Chapter 2, i.e., Equations (2.37a,b), can be introduced into Equation (5.2). The Lagrangian then results in

$$L = \frac{1}{2} \int_{0}^{a} \int_{0}^{b} \left( \left\{ \tilde{X}_{n} \right\}^{T} \left[ S \tilde{K}_{n} \right] \left\{ \tilde{X}_{n} \right\} + \left\{ \tilde{X}_{s} \right\}^{T} \left[ S \tilde{K}_{s} \right] \left\{ \tilde{X}_{s} \right\} - \left\{ \tilde{X}_{s} \right\}^{T} \left[ S \tilde{M}_{d} \right] \left\{ \tilde{X}_{s} \right\} - m \dot{w}^{2} \right) dy dx \qquad (5.6)$$

In the case of closed-form solution, since there exists an exact modal function for this particular problem, the displacement matrices can be assumed as

$$\{\bar{X}_n\} = [D_n] \{\bar{X}\} e^{j\omega t} \tag{5.7a}$$

$$\{\bar{X}_s\} = [D_s] \{\bar{X}\} e^{i\omega t} \tag{5.7b}$$

where [D<sub>a</sub>] and [D<sub>a</sub>] are matrices containing assumed modal functions and their derivatives with respect to the inplane axes. The matrix  $\{\bar{X}\}$  consists of unknown magnitudes of the displacement variables of the particular mode shape. In addition,  $e^{j\omega t}$  represents for the time variant part of the displacement functions where  $j = \sqrt{-1}$  and  $\omega$  is the circular frequency. By plugging Equations (5.7a,b) into Equation (5.6) and using the Lagrange's equations

$$\frac{d}{dt}\left(\frac{\partial L}{\partial \vec{X}_i}\right) - \frac{\partial L}{\partial \vec{X}_i} = \{0\}, \quad i = 1, 2, ..., 4n + 1$$
 (5.8)

the governing equation for this eigenvalue problem can be obtained, i.e.,

$$[D] \{ \bar{X} \} - \omega^2 [G] \{ \bar{X} \} = \{ 0 \}$$
 (5.9)

In Equation (5.8),  $\bar{X}_i$  is the *i*-component of the column matrix  $\{\bar{X}\}$ .

As the static bendings examined in Chapter 2, finite element analysis is required to study the structures with general geometry and boundary condition. For this type of eigenvalue problem, a set of interpolation functions are introduced

$$\{\tilde{X}_n\} = [\psi_n] \{X\} e^{j\omega t}$$

$$\{\tilde{X}_n\} = [\psi_n] \{X\} e^{j\omega t}$$

$$(5.10a)$$

$$\{X_s\} = [\psi_s] \{X\} e^{j\omega t} \tag{5.10b}$$

Substituting these functions into Equation (5.6) and employing Lagrange's equations, Equation (5.8), the following finite element equation for a single element can be achieved,

$$[K] \{X\} - \omega^2[M] \{X\} = \{0\}$$
 (5.11)

where [K] is the same stiffness matrix as used in static case while [M] the consistent mass matrix associated with the assumed interpolation functions.

Once the governing equation for the modal analysis is obtained, several examples are used to demonstrate the accuracy of ISSCT in vibration analysis. The fundamental frequencies of simply-supported [0], [0/90], and [0/90/0] laminates with aspect ratio ranging from four to 200 under cylindrical bending are shown in Figure 5.1. The same material properties as used in Chapter 2 are examined in the simulation. In this figure, the exact frequencies [28] are obtained using two-dimensional elasticity analysis while the ISSCT results are obtained from finite element analysis using four layers and four elements. It is clear that the ISSCT results agree very well with the exact solutions in both thin and thick composite laminates.

Table 5.1 presents the normalized fundamental frequency of a simply-supported [0/90/90/0] square laminate with aspect ratio a/h=5. Different anisotropic ratios,  $E_1/E_2$ , for the material is also investigated and compared with three-dimensional elasticity results [32]. In the finite element analysis, because of laminate symmetry, only a quarter of the plate is examined. It can be seen that with a  $4\times4$  mesh, the finite element solutions converge very well to the closed-form solutions.

## 5.3 Critical Buckling Load

For a composite laminate subjected to inplane loading, the critical buckling load is the essential information for stability analysis. The buckling phenomenom occurs due to the coupling between the applied inplane loading and lateral deflection. In this study, the principle of minimum potential energy is used. The total potential energy of a rectangular laminate subjected to uniformly compressive and shear loads along its boundaries can be written as follows [36], i.e.,

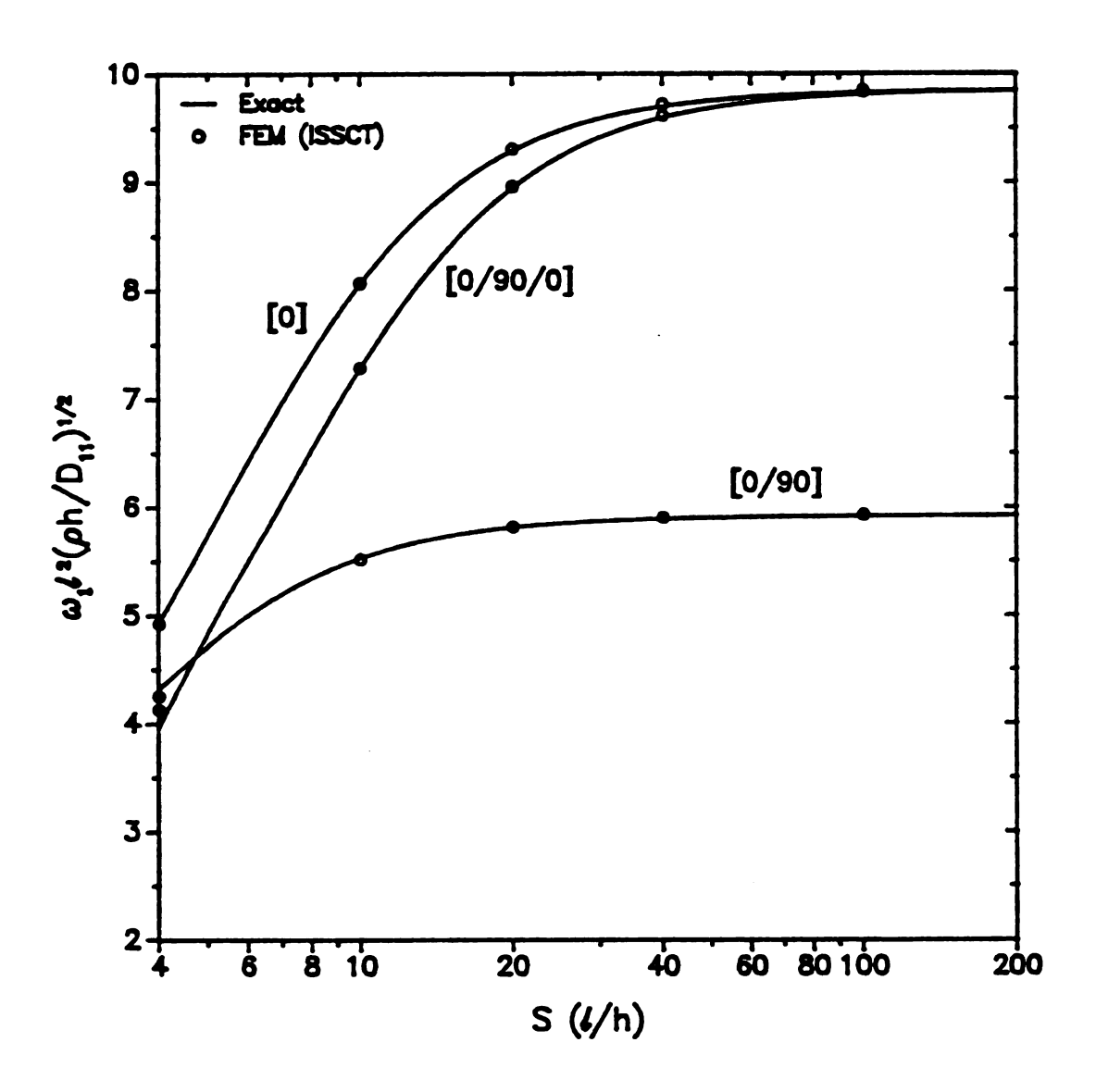


Figure 5.1 Fundamental frequencies of simply-supported [0],[0/90] and [0/90/0] laminates with different aspect ratios under cylindrical bending.

Table 5.1 Normalized fundamental frequency  $\lambda_{\star}$  of a simply-supported [0/90/90/0] square laminate.

E /E	Floorisis M01	ISSCT			
$E_1/E_2$	Elasticity[32]	Closed-form	FEM(4x4)		
40	10.752	10.698	10.724		
30	10.272	10.228	10.255		
20	9.5603	9.5310	9.5604		
10	8.2103	8.3366	8.3679		
3	6.6185	6.7062	6.7354		

$$\lambda_{v} = \frac{\omega a^{2}}{h} \sqrt{\frac{\rho}{E_{T}}}; \qquad a = b = 5; h = 1$$

$$E_{2} = E_{3} = 1 \times 10^{6} psi; G_{12} = G_{13} = 0.6 \times 10^{6} psi; G_{23} = 0.5 \times 10^{6} psi$$

$$v_{12} = v_{13} = v_{23} = 0.25$$

$$\pi = \int_{0}^{a} \int_{0}^{b} \int_{-\frac{1}{2}}^{\frac{1}{2}} \frac{1}{2} \left\{ \begin{bmatrix} \sigma_{x} \\ \sigma_{y} \\ \sigma_{xy} \end{bmatrix}^{T} \begin{bmatrix} \varepsilon_{x} \\ \varepsilon_{y} \\ 2\varepsilon_{xy} \end{bmatrix} + \begin{bmatrix} \sigma_{yz} \\ \sigma_{xz} \end{bmatrix}^{T} \begin{bmatrix} 2\varepsilon_{yz} \\ 2\varepsilon_{xz} \end{bmatrix} \right\} dz dy dx$$

$$- \int_{0}^{a} \int_{0}^{b} \int_{-\frac{1}{2}}^{\frac{1}{2}} \frac{1}{2} f_{x} \left( \left( \frac{\partial u}{\partial x} \right)^{2} + \left( \frac{\partial v}{\partial x} \right)^{2} + \left( \frac{\partial w}{\partial x} \right)^{2} \right) dz dy dx$$

$$- \int_{0}^{a} \int_{0}^{b} \int_{-\frac{1}{2}}^{\frac{1}{2}} \frac{1}{2} f_{y} \left( \left( \frac{\partial u}{\partial y} \right)^{2} + \left( \frac{\partial v}{\partial y} \right)^{2} + \left( \frac{\partial w}{\partial y} \right)^{2} \right) dz dy dx$$

$$- \int_{0}^{a} \int_{0}^{b} \int_{-\frac{1}{2}}^{\frac{1}{2}} f_{xy} \left( \frac{\partial u \partial u}{\partial x \partial y} + \frac{\partial v \partial v}{\partial x \partial y} + \frac{\partial w \partial w}{\partial x \partial y} \right) dz dy dx$$

$$- \int_{0}^{b} \int_{-\frac{1}{2}}^{\frac{1}{2}} \left( f_{x} u^{i}_{x=a} - f_{x} u^{i}_{x=0} \right) dz dy - \int_{0}^{a} \int_{-\frac{1}{2}}^{\frac{1}{2}} \left( f_{y} v^{i}_{y=b} - f_{y} v^{i}_{y=0} \right) dz dx$$

$$- \int_{0}^{b} \int_{-\frac{1}{2}}^{\frac{1}{2}} \left( f_{xy} v^{i}_{x=a} - f_{xy} v^{i}_{x=0} \right) dz dy - \int_{0}^{a} \int_{-\frac{1}{2}}^{\frac{1}{2}} \left( f_{xy} u^{i}_{y=b} - f_{xy} u^{i}_{y=0} \right) dz dx$$

$$- \int_{0}^{b} \int_{-\frac{1}{2}}^{\frac{1}{2}} \left( f_{xy} v^{i}_{x=a} - f_{xy} v^{i}_{x=0} \right) dz dy - \int_{0}^{a} \int_{-\frac{1}{2}}^{\frac{1}{2}} \left( f_{xy} u^{i}_{y=b} - f_{xy} u^{i}_{y=0} \right) dz dx$$

$$(5.12)$$

In the above equation, the first term is the strain energy stored in the structure. The second, third, and fourth terms are the coupled potential energy components due to inplane loading  $f_x$ ,  $f_y$ , and  $f_{xy}$ , respectively. The final four terms are the potential energy of external forces exerted on the boundaries. Since these four terms correspond to the inhomogeneous term, i.e., the force vector, in the final eigenvalue equation, they are not relevant to the calculation of the homogeneous eigenvalue problem. Therefore, they are omitted in the following derivation. In addition, for simplicity, only the compressive loading  $f_x$  is considered herein. The terms associated with  $f_y$  and  $f_{xy}$  are removed from the total potential energy.

Following the notations used in the previous section, the displacement field for a composite layer and its derivative can be written as

$$\left\{\begin{array}{c} u\\ v \end{array}\right\}^{(i)} = \left[N_d^{(i)}\right] \left\{\hat{X}_s^{(i)}\right\}$$
 (5.13)

$$\left\{\begin{array}{l}
\frac{\partial u}{\partial x} \\
\frac{\partial v}{\partial x}
\end{array}\right\}^{(i)} = \frac{\partial}{\partial x} [N_d^{(i)}] \left\{\hat{X}_s^{(i)}\right\}$$
(5.14)

Substituting these expressions into the potential energy and manipulating the strain energy term as in the vibration study, the total potential energy after integration through the thickness becomes

$$\pi = \frac{1}{2} \int_0^a \int_0^b \left( \left\{ \bar{X}_n \right\}^T \left[ S \bar{K}_n \right] \left\{ \bar{X}_n \right\} + \left\{ \bar{X}_s \right\}^T \left[ S \bar{K}_s \right] \left\{ \bar{X}_s \right\} - f_x \frac{\partial}{\partial x} \left\{ \bar{X}_s \right\}^T \left[ S \bar{B}_x \right] \frac{\partial}{\partial x} \left\{ \bar{X}_s \right\}$$

$$- f_x h \left( \frac{\partial w}{\partial x} \right)^2 \right) dy dx \tag{5.15}$$

where

$$[S\tilde{B}_{z}] = \sum_{i=1}^{n} \left( \int_{z_{i-1}}^{z_{i}} [N_{d}^{(i)}]^{T} [N_{d}^{(i)}] dz \right)$$
 (5.16)

is the assembled matrix through the thickness.

The closed-form solution for the critical buckling load is also valid for the problems with simply-supported boundary conditions and cross-ply layup. The buckling mode shape in the x-y plane can be assumed either a sine or cosine function with unknown magnitudes, i.e.,

$$\{\tilde{X}_n\} = [D_n] \{\overline{X}\} \tag{5.16a}$$

$$\{\vec{X}_s\} = [D_s] \{\vec{X}\} \tag{5.16b}$$

and

$$\frac{\partial}{\partial x} \{ \bar{X}_s \} = (\frac{\partial}{\partial x} [D_s]) \{ \bar{X} \}$$
 (5.16c)

Again,  $\{\overline{X}\}$  consists of unknown magnitudes of the displacement variables. Then, by employing the principle of minimum total potential energy,

$$\delta \pi = 0 \tag{5.17}$$

the homogeneous eigenvalue equation can be obtained

$$[D] \{ \vec{X} \} - f_x[B] \{ \vec{X} \} = 0$$
 (5.18)

In a similar way, a finite element equation can be derived for a more general analysis. Instead of the exact mode shapes as assumed in the closed-form solution, a set of interpolation functions in the x-y plane is introduced in the finite element method.

$$\{\tilde{X}_n\} = [\psi_n] \{X\} \tag{5.19a}$$

$$\{\tilde{X}_{x}\} = [\psi_{x}]\{X\} \tag{5.19b}$$

Substituting these interpolation functions into Equation (5.15) and employing the principle of minimum potential energy, the finite element equation in terms of the nodal displacement variables can be obtained

$$[K] \{X\} - f_{\tau}[G_R] \{X\} = 0 (5.20)$$

The normalized first buckling load of a simply-supported [0/90/90/0] square laminate with aspect ratio a/h=10 is shown in Table 5.2. Because of the symmetry of the rectangular laminate, only a quarter is required in the finite element analysis. The quarter laminate is discretized into 16 equal elements. The results from both closed-form solution and finite element analysis are presented with different anisotropic ratios along with three-dimensional elasticity solutions [33]. Similar analysis is performed on an asymmetric [0/90] laminate and the results are given in Table 5.3. These results show that the ISSCT analysis yields satisfactory predictions for both symmetric and asymmetric laminates. For another asymmetric laminate [0/90/0/90/0/90], Table 5.4 presents the closed-form solutions. Comparing these results with those obtained from elasticity analysis, it is clear that ISSCT predicts the buckling loading of the first mode very accurately.

Table 5.2 Normalized first buckling load  $\lambda_b$  of a simply-supported [0/90/90/0] square laminate.

F /F	Electicies (22)	ISSCT			
$E_1/E_2$	Elasticity[33]	Closed-form	FEM(4x4)		
40	22.8807	23.1262	23.1360		
30	19.3040	19.5545	19.5385		
20	15.0191	15.2759	15.2198		
10	9.7621	10.0283	9.9038		
3	5.2944	5.5957	5.3707		
1					

$$\lambda_{v} = \frac{f_{x}a^{3}}{E_{T}h^{2}}; \qquad a = b = 10; h = 1$$

$$E_{2} = E_{3} = 1 \times 10^{6}psi; G_{12} = G_{13} = 0.6 \times 10^{6}psi; G_{23} = 0.5 \times 10^{6}psi$$

$$\nu_{12} = \nu_{13} = \nu_{23} = 0.25$$

Table 5.3 Normalized first buckling load  $\lambda_b$  of a simply-supported [0/90] square laminate.

E /E	Electicis (22)	ISS	CT
$E_1/E_2$	Elasticity[33]	Closed-form	FEM(4x4)
40	22.8807	23.1262	23.1360
20	15.0191	15.2759	15.2198
10	9.7621	10.0283	9.9038

$$\lambda_{v} = \frac{f_{x}a^{3}}{E_{T}h^{2}};$$
  $a = b = 10; h = 1$ 

$$E_{2} = E_{3} = 1 \times 10^{6}psi; G_{12} = G_{13} = 0.6 \times 10^{6}psi; G_{23} = 0.5 \times 10^{6}psi$$

$$v_{12} = v_{13} = v_{23} = 0.25$$

Table 5.4 Normalized first buckling load  $\lambda_b$  of a simply-supported [0/90/0/90/0/90] square laminate.

$E_1/E_2$	Elasticity[33]	ISSCT Closed-form
40	23.6689	23.6673
20	15.0014	15.0126
10	9.6501	9.6289

$$\lambda_{\nu} = \frac{f_{x}a^{3}}{E_{T}h^{2}}; \qquad a = b = 10; h = 1$$

$$E_{2} = E_{3} = 1 \times 10^{6}psi; G_{12} = G_{13} = 0.6 \times 10^{6}psi; G_{23} = 0.5 \times 10^{6}psi$$

$$\nu_{12} = \nu_{13} = \nu_{23} = 0.25$$

## 5.4 Nonlinear Bending

As pointed out in Reference [36], the composite laminates containing the coupling effect between the transverse deflection and inplane force are more sensitive to the nonlinear ear effect. Even in the range of small deformation defined by conventional analysis, the laminate can behave in a nonlinear fashion. Many investigations have used different laminate theories and different types of nonlinearity [24,36-39] for this study. In this section, a laminate subjected to moderately large deflections is examined with the use of interlaminar shear stress continuity theory.

# 5.4.1 Formulation of Nonlinear Equation

The material is assumed to behave linearly and elastically though the linear relationships between strains and displacements are no longer valid. In fact, a nonlinear relationship of vonKármán sense is considered, i.e.,

$$\varepsilon_{x} = \frac{\partial u}{\partial x} + \frac{1}{2} \left(\frac{\partial w}{\partial x}\right)^{2}; \qquad \varepsilon_{y} = \frac{\partial v}{\partial y} + \frac{1}{2} \left(\frac{\partial w}{\partial y}\right)^{2}; \qquad 2\varepsilon_{xy} = \frac{\partial u}{\partial y} + \frac{\partial v}{\partial x} + \frac{\partial w}{\partial x} \frac{\partial w}{\partial y}$$

$$2\varepsilon_{yz} = \frac{\partial v}{\partial x} + \frac{\partial w}{\partial y}; \qquad 2\varepsilon_{xz} = \frac{\partial u}{\partial x} + \frac{\partial w}{\partial x}$$
(5.21)

It can be noted that the expressions for the transverse shear strains remain the same as linear case while the inplane strain components are modified with quadratic terms which involve the first derivatives of transverse displacement component. Since the reduction of displacement variables from Equation (2.27) to Equation (2.28) is achieved by imposing the shear stress continuity on the interface, this manipulation remains the same for both linear and nonlinear analysis. Thus, following the linear analysis and Equation (5.21), the strains in each layer can be written as

$$\left\{\begin{array}{c}
2\varepsilon_{yz} \\
2\varepsilon_{xz}
\end{array}\right\}^{(i)} = [N_s^{(i)}] \{\hat{X}_s^{(i)}\}$$
(5.22b)

where

$$[N_{NL}] = \begin{bmatrix} \frac{1}{2} \frac{\partial w}{\partial x} & 0 \\ 0 & \frac{1}{2} \frac{\partial w}{\partial y} \\ \frac{1}{2} \frac{\partial w}{\partial y} & \frac{1}{2} \frac{\partial w}{\partial x} \end{bmatrix}$$
(5.23)

$$\{X_{w}\} = \begin{cases} \frac{\partial w}{\partial x} \\ \frac{\partial w}{\partial y} \end{cases}$$
 (5.24)

The same notations defined in Equations (2.31) and (2.32) are also used. It should be noted that  $[N_{NL}]$  is a function of the derivatives of transverse displacement. It constitutes the nonlinear part of the analysis.

Again, the principle of virtual displacement is employed for deriving the governing equation. Substituting the stresses by strains of Equation (2.29), plugging Equations (5.22a,b) into Equation (2.29), and integrating through the thickness yields

$$\int_{0}^{a} \int_{0}^{b} (\{\delta \hat{X}_{n}\}^{T} [S\hat{K}_{n}] \{\hat{X}_{n}\} + \{\delta \hat{X}_{s}\}^{T} [S\hat{K}_{s}] \{\hat{X}_{s}\} + \{\delta X_{w}\}^{T} [S\hat{K}_{NL1}] \{\hat{X}_{n}\}$$

$$+ \{\delta \hat{X}_{n}\}^{T} [S\hat{K}_{NL2}] \{X_{w}\} + \{\delta X_{w}\}^{T} [S\hat{K}_{NL3}] \{X_{w}\} - q\delta w \} dy dx = 0$$
(5.25)

In the above equation, the following notations are used to denote the assembled matrices through the thickness,

$$[S\hat{K}_{NL1}] = \sum_{i=1}^{n} \left( \int_{z_{i-1}}^{z_i} 2[N_{NL}]^T [Q_n^{(i)}] [N_n^{(i)}] dz \right)$$
 (5.26a)

$$[\hat{SK}_{NL2}] = \sum_{i=1}^{n} \left( \int_{z_{i-1}}^{z_i} [N_n^{(i)}]^T [Q_n^{(i)}] [N_{NL}] dz \right)$$
 (5.26b)

$$[S\hat{K}_{NL3}] = \sum_{i=1}^{n} \left( \int_{z_{i-1}}^{z_i} 2 [N_{NL}]^T [Q_n^{(i)}] [N_{NL}] dz \right)$$
 (5.26c)

The introduction of vanished shear tractions on both top and bottom surfaces of the laminate results in the reduced displacement vectors,

$$\{\hat{X}_n\} = [E_n] \{\hat{X}_n\} \tag{5.27a}$$

$$\{\hat{X}_x\} = [E_x]\{\bar{X}_x\} \tag{5.27b}$$

These are the same matrices as used in Equations (2.37a,b). Substitute the reduced matrices into Equation (5.25), the principle of virtual displacement becomes,

$$\int_{0}^{a} \int_{0}^{b} \left( \left\{ \delta \tilde{X}_{R} \right\}^{T} \left[ S \tilde{K}_{R} \right] \left\{ \tilde{X}_{R} \right\} + \left\{ \delta \tilde{X}_{S} \right\}^{T} \left[ S \tilde{K}_{S} \right] \left\{ \tilde{X}_{S} \right\} + \left\{ \delta \tilde{X}_{w} \right\}^{T} \left[ S \tilde{K}_{NL1} \right] \left\{ \tilde{X}_{R} \right\} + \left\{ \delta \tilde{X}_{m} \right\}^{T} \left[ S \tilde{K}_{NL2} \right] \left\{ \tilde{X}_{w} \right\} + \left\{ \delta \tilde{X}_{w} \right\}^{T} \left[ S \tilde{K}_{NL3} \right] \left\{ \tilde{X}_{w} \right\} - q \delta w \right) dy dx = 0$$
 (5.28)

in which

$$[S\tilde{K}_n] = [E_n]^T [S\hat{K}_n] [E_n]$$
 (5.29a)

$$[S\tilde{K}_{s}] = [E_{s}]^{T}[S\hat{K}_{s}][E_{s}]$$
 (5.29b)

$$[S\bar{K}_{NL1}] = [S\hat{K}_{NL1}][E_{\pi}]$$
 (5.29c)

$$[S\tilde{K}_{NL2}] = [E_n]^T [S\hat{K}_{NL2}]$$
 (5.29d)

As in the linear case, the following interpolation functions in an element are assumed.

$$\{\bar{X}_n\} = [\psi_n] \{X\} \tag{5.30a}$$

$$\{\tilde{X}_s\} = [\psi_s] \{X\} \tag{5.30b}$$

$$\{X_{\mathbf{w}}\} = [\psi_{\mathbf{w}}] \{X\}$$
 (5.30c)

$$w = [\psi] \{X\} \tag{5.30d}$$

where  $\{X\}$  is the nodal displacement vector while  $[\psi_n]$ ,  $[\psi_n]$ ,  $[\psi_w]$ , and  $[\psi]$  are the interpolation functions corresponding to the displacement vectors. By using these interpo-

lation functions, the principle of virtual displacement, Equation (5.28), leads to the following finite element equation,

$$([K] + [K_{NL}(w)]) \{X\} = \{F\}$$
 (5.31)

where

$$[K] = \int_0^a \int_0^b (\{\psi_n\}^T [S\hat{K}_n] \{\psi_n\} + \{\psi_s\}^T [S\hat{K}_s] \{\psi_s\}) \, dy dx$$
 (5.32)

$$[K_{NL}(w)] = \int_0^a \int_0^b (\{\psi_w\}^T [S\hat{K}_{NL1}] \{\psi_n\} + \{\psi_n\}^T [S\hat{K}_{NL2}] \{\psi_w\} + \{\psi_w\}^T [S\hat{K}_{NL3}] \{\psi_w\}) dydx$$
 (5.33)

$$\{F\} = \int_0^a \int_0^b [\Psi] \, q \, dy \, dx \tag{5.34}$$

It should be noted that the linear part of the stiffness matrix and the external loading vector are the same as those derived in the linear analysis in Chapter 2. The major difference between the nonlinear and linear studies is the nonlinear part of the stiffness matrix which is a function of the transverse displacement.

In the solution phase of the nonlinear governing equation, a standard Newton-Raphson method is used. First, the governing equation is rewritten as

$$\{f\} = ([K] + [K_{NL}])\{X\} - \{F\} = \{0\}$$
 (5.35)

Then the Jacobian can be calculated. The component at ith row and jth column of the Jacobian matrix is defined as

$$J_{ij} = \frac{\partial f_i}{\partial X_i} \tag{5.36}$$

where the subscripts of the column vectors represent for the corresponding components accordingly. Once the Jacobian matrix is formulated, the numerical iteration scheme follows. A brief analysis is given below,

$$\{f\}^{(k)} = ([K] + [K_{NL}(\{X\}^{(k)})])\{X\}^{(k)} - \{F\}$$
 (5.37a)

$$[J(\{X\}^{(k)})]\{\Delta X\}^{(k)} = -\{f\}^{(k)}$$
(5.37b)

$${X}^{(k+1)} = {X}^{(k)} + {\Delta X}^{(k)}$$
 (5.37c)

where the superscript k denotes the result of kth iteration. The first iteration starting from the null nodal displacement vector gives the linear solution of the equation. As the iterations continue, the analysis is assumed to converge when the successive change of the displacement is less than 0.1%.

In the following sections, several examples are used to examine the feasibility of using ISSCT for nonlinear bending.

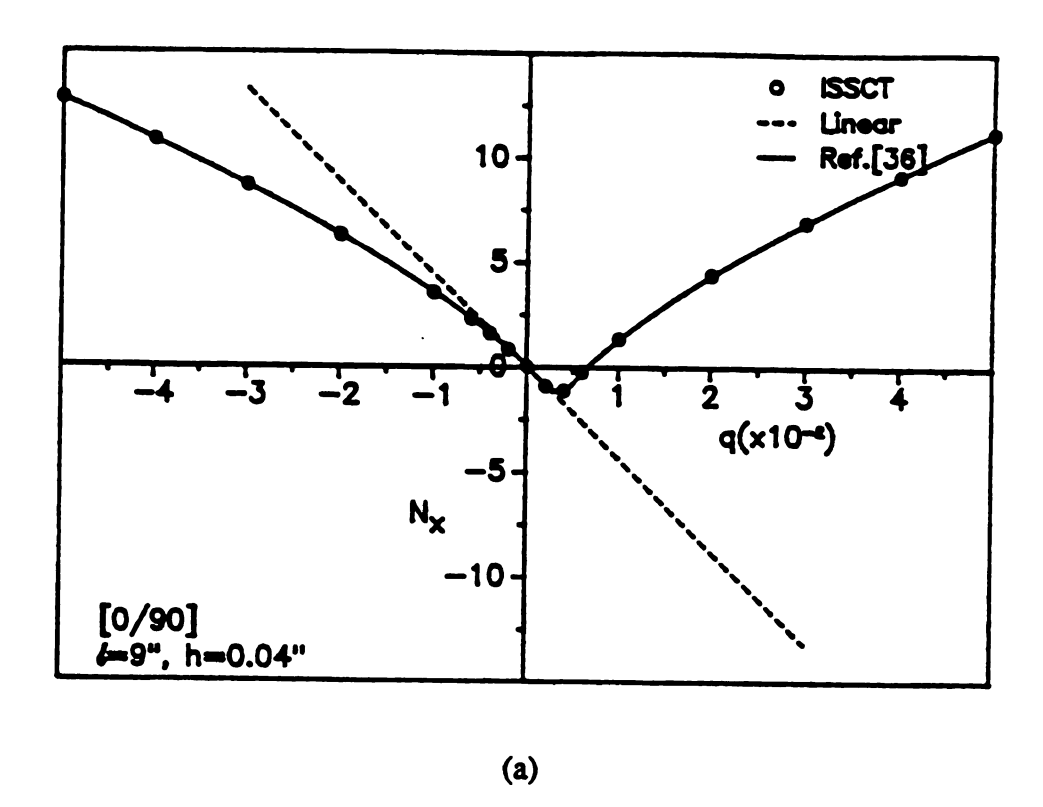
### 5.4.2 Laminates Subjected to Transverse Loadings

First, a pinned-pinned [0/90] laminate under uniform loading over the entire span is studied. This problem was investigated by CLT [36] for aspect ratio equals to 225. For such thin composite laminate, the transverse shear effect can be neglected. Therefore, the ISSCT is expected to yield a result close to CLT. Figures 5.2a and 5.2b present the midspan deflection and the inplane force resultant at different loading magnitudes. The material properties used are the same as those in Reference [36], i.e.,

$$E_L = 20 \times 10^6 psi$$
,  $E_T = 1.4 \times 10^6 psi$ ,  $G_{LL} = G_{LT} = 0.7 \times 10^6 psi$ ,  $V_{LT} = 0.30$ 

The ISSCT results are obtained by using four layers and four elements for finite element analysis. The dashed lines in Figures 5.2a and 5.2b represent for the linear results calculated from the same ISSCT model. It is clear that nonlinear analysis from ISSCT coincides with with that in Reference [36] while the linear analysis erroneously predicts both the midspan deflection and the inplane force resultant. It should also be noted that the structure behaves differently for upward and downward loading. This is due to the inplane forces caused by the couplings of asymmetric layup and geometrical nonlinearity.

One advantage of using ISSCT is the simplicity and accuracy in the calculation of



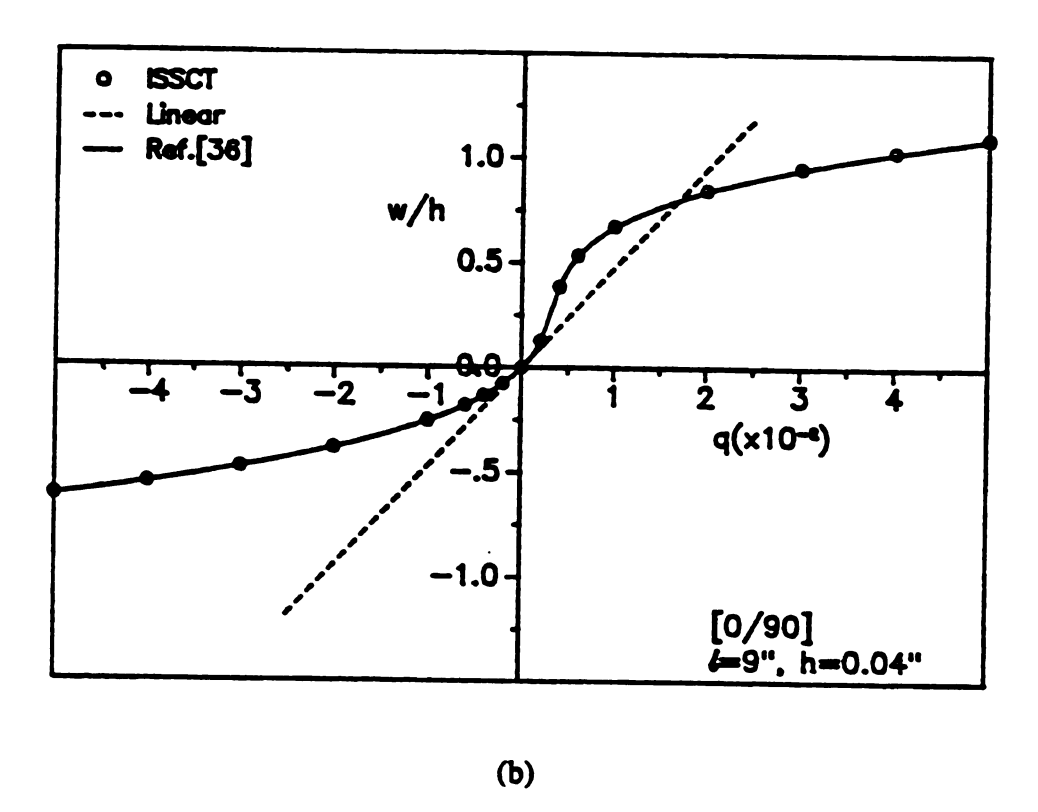
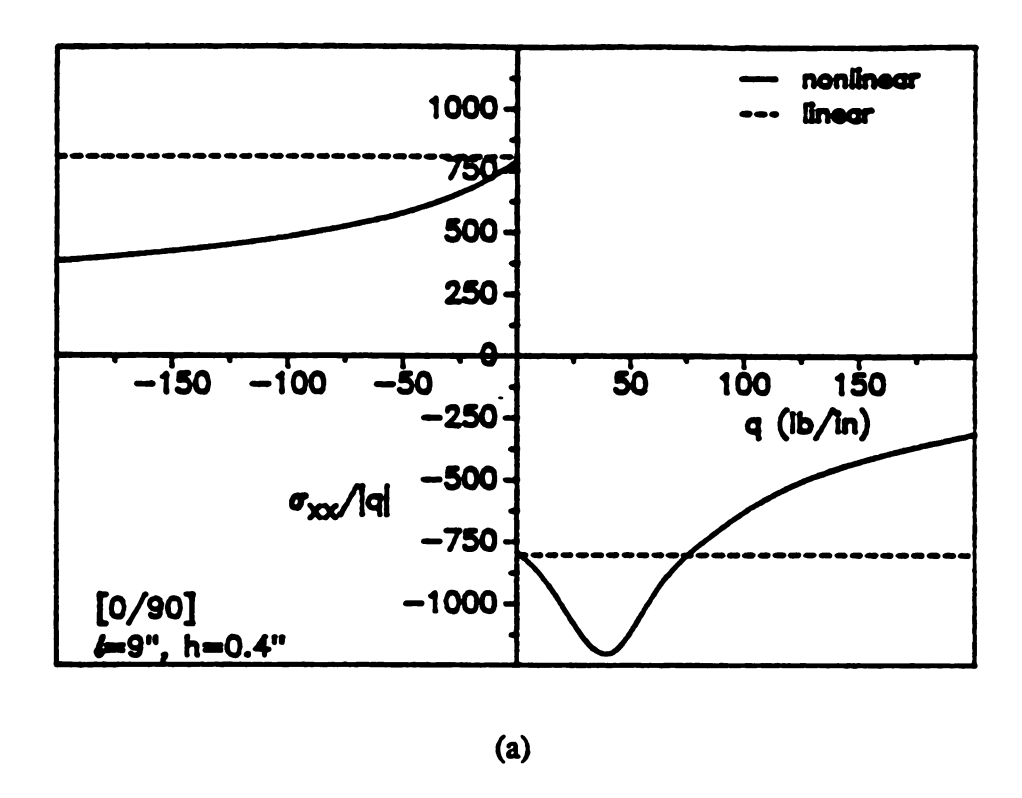


Figure 5.2 Pinned-pinned [0/90] laminate with aspect ratio S=225 subjected to uniformly distributed loading: (a) inplane force resultant; (b) midspan deflection.

transverse shear stresses. This is also true for the stresses from nonlinear analysis. Figures 5.3a and 5.3b present the maximum inplane normal stress at the midspan and the transverse shear stress at the midplane of the laminate edge, respectively. Figure 5.3a shows the inplane normal stress obtained from linear analysis may overpredict or underpredict the actual stress depending upon the loading range. The same observation applies to the transverse shear stress, shown in Figure 5.3b. Moreover, it is interesting to see that the transverse shear stress at the interface even changes its sign as the loading is higher than a certain value, 75 lb/in in this example. These unusual results can become a very important issue in composite design and need to be carefully examined.

The stress distributions through the thickness for the same locations as shown in Figures 5.3a and 5.3b are given in Figures 5.4a and 5.4b. In these figures, the stress distributions at different deflection levels are presented. It is seen that the profiles of the inplane stress distribution remain the same at different loading levels, however, those of the transverse shear stress alter dramatically as the loading increases. The nonlinear analysis gives a tremendously different stress state than the linear analysis and can result in a completely different prediction for failure mode.

As mentioned in a previous paragraph, the unusual nonlinear behavior of the structure arises from two inplane forces caused by the couplings due to asymmetric layup and geometrical nonlinearity. And it is known that the magnitude of the inplane force depends on the boundary conditions. Therefore, it is interesting to study the effect of different boundary conditions on the nonlinear structural behavior. Figures 5.5a and 5.5b give the normalized midspan deflection and coupled inplane force resultant as a function of transverse deflection. The composite laminate is of [0/90] and is subjected to a uniform loading. Three different boundary conditions are of interest. The subscripts L and NL denote the results from linear and nonlinear analysis, respectively. Among the three boundary conditions studied, i.e., pinned-pinned, pinned-clamped, and clamped-clamped, the pinned-pinned one gives the most significant nonlinear effect and should recieve more



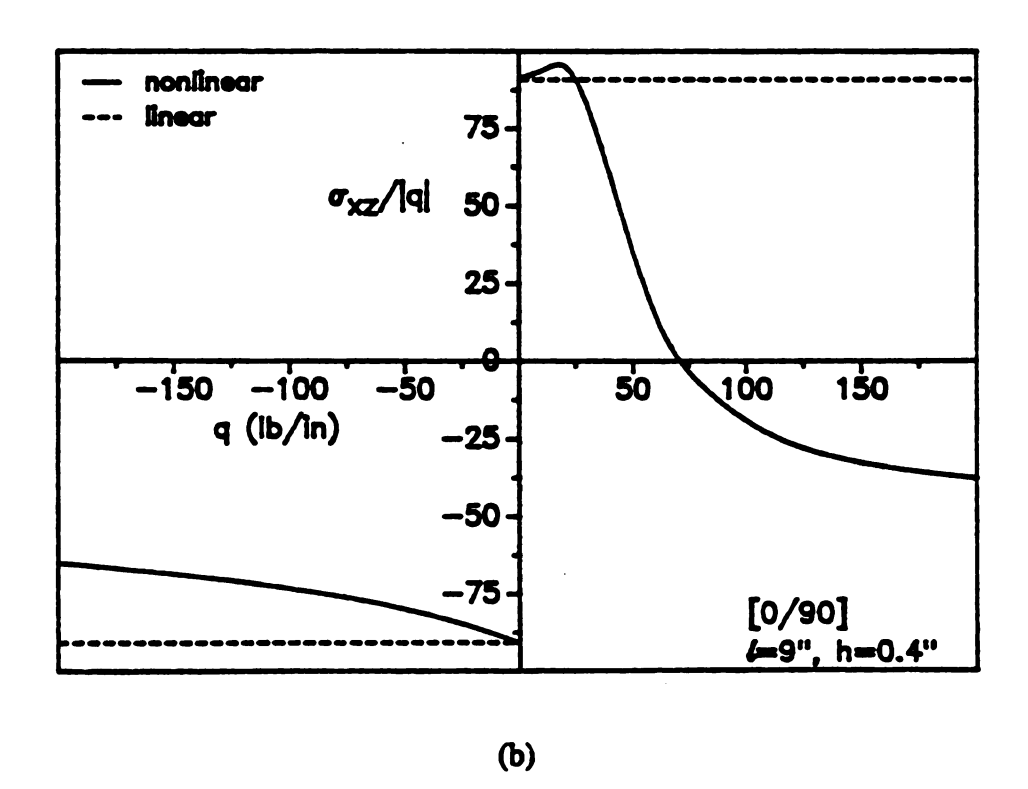
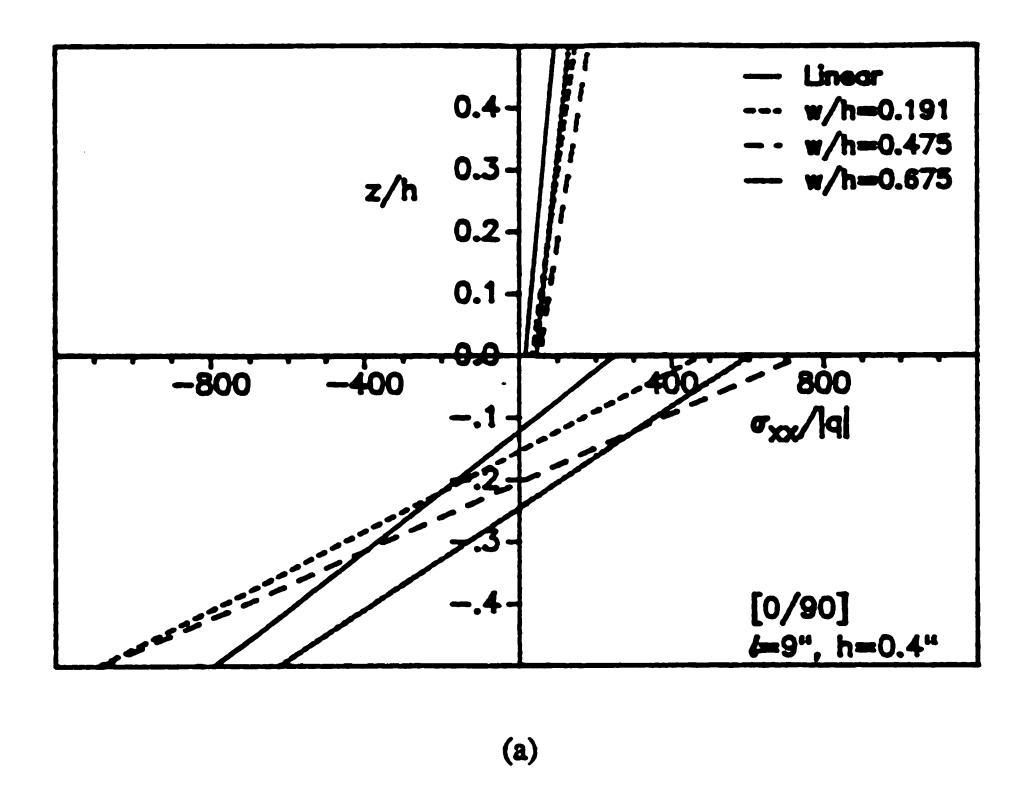


Figure 5.3 Normalized stresses of a pinned-pinned [0/90] laminated with S=22.5 subjected to uniformly distributed loading: (a)  $\sigma_x$  ( U2,-h/2); (b)  $\sigma_{xx}$  (0,0).



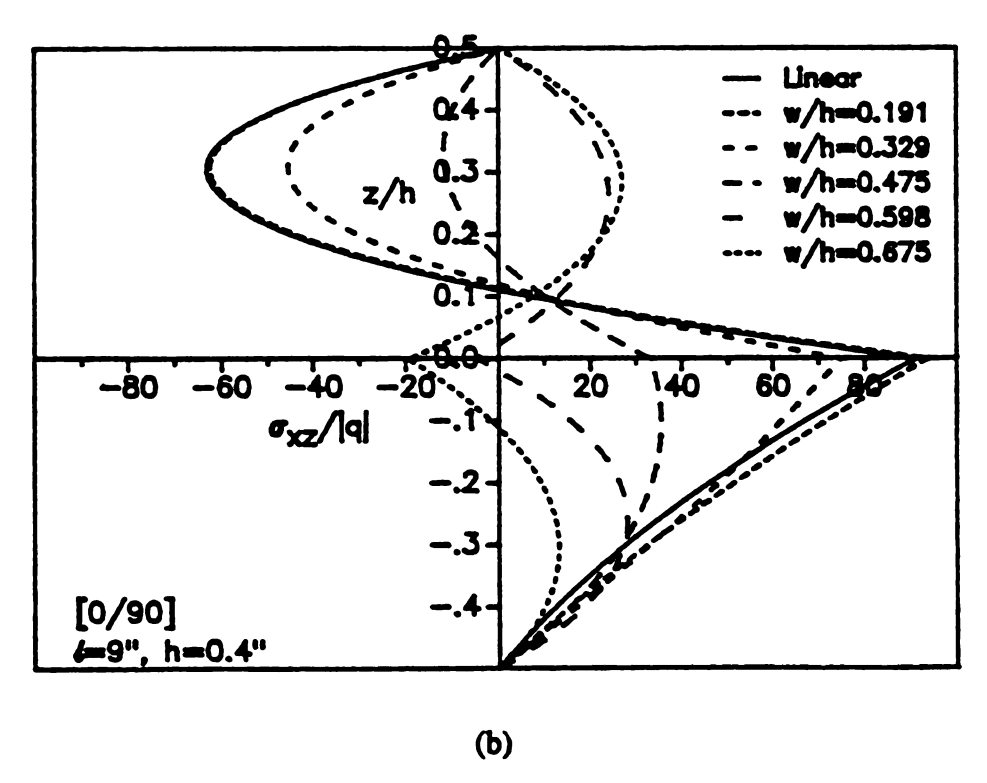
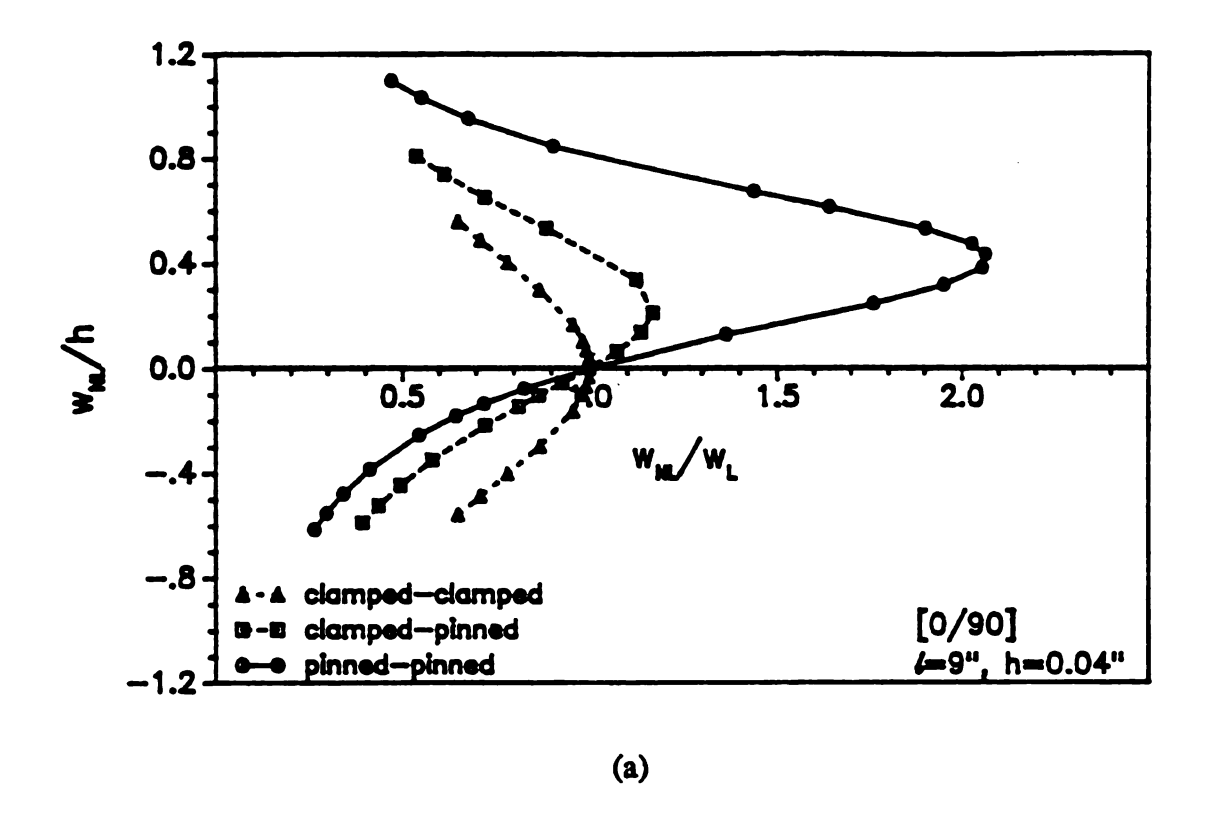


Figure 5.4 Normalized stresses of a pinned-pinned [0/90] laminate with S=22.5 subjected to uniformly distributed loading: (a)  $\sigma_x$  ( U2, z); (b)  $\sigma_{xz}$  ( 0, z).



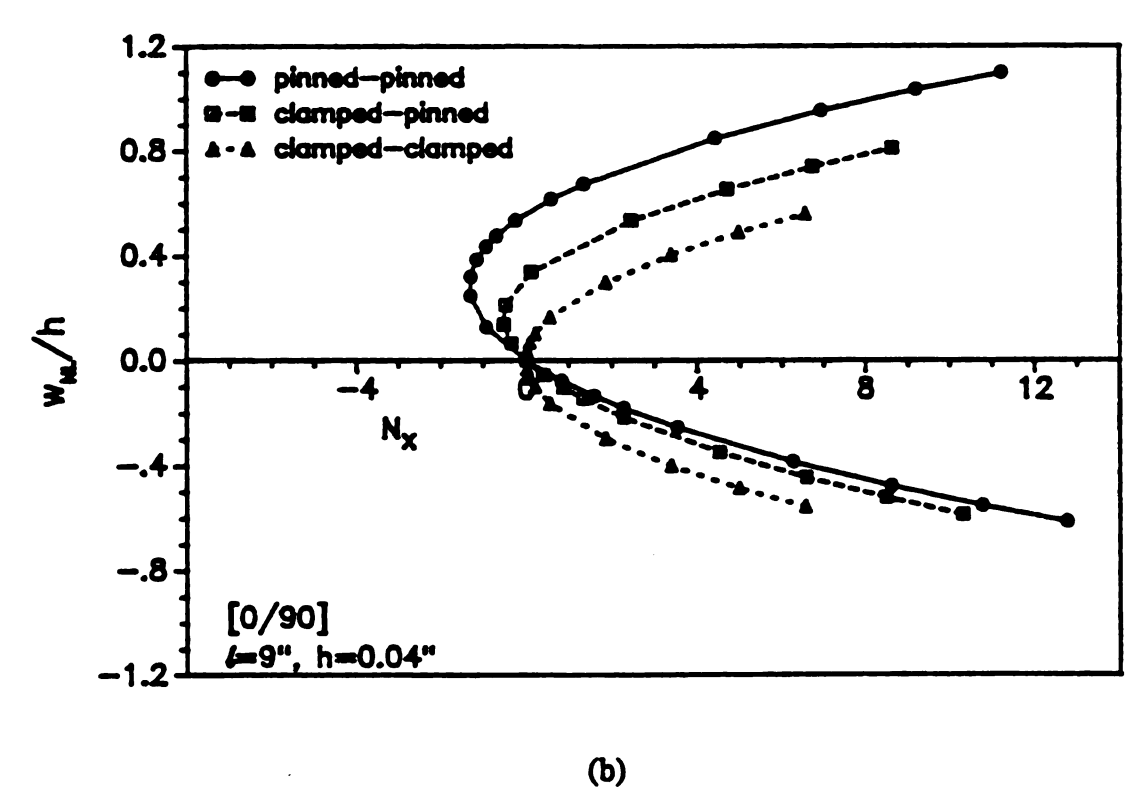


Figure 5.5 Normalized nonlinear results of [0/90] laminate with S=225 subjected to uniformly distributed loading in three different boundary conditions: (a) midspan deflections; (b) inplane force resultants.

attention. In addition, it is interesting to see that in the clamped-clamped boundary condition, even the stacking sequence is asymmetric, the laminate behaves like a symmetric one. In other words, the direction of transverse loading does not change the magnitude of deflection. This is believed to be due to the vanished inplane force in the [0/90] layup [37]. Since the clamped-pinned boundary condition has the intermediate coupling force between the two extreme cases, it behaves as a compromise of those two.

Once the cylindrical bending is examined, it is to investigate bidirectional bending.

A square [0] laminate with aspect ratio of 100 is of interest. The composite laminate has the following material properties

$$E_L/E_T = 3.0, G_{LT}/E_T = 0.5, v_{LT} = 0.25.$$

It is clamped around four edges and is subjected to a transversely uniform load. Because of the large aspect ratio, the laminate is analyzed by CLT in Reference [38]. The load-deflection curve is shown in Figure 5.6. The solid line represents for the result of normalized central deflection obtained by perturbation method in Reference [38]. The open circles are the results of ISSCT using quarter laminate and a 4x4 mesh. It is obvious that these two predictions compare very well with each other.

# 5.4.3 Laminates Subjected to Inplane Loadings

All the examples shown above are the laminates with transverse loading. The same analysis can be performed for structures with inplane loading. The same [0/90] laminate with pinned-pinned boundary condition is subjected to inplane compressive loading. The ISSCT result is based on finite element analysis. It is shown in Figure 5.7 with that obtained from Reference [36]. Good agreement is concluded. Besides, it should be noted that the linear buckling load obtained from linear analysis gives the upper bound of the load-deflection curve.

Similar analysis is performed for a simply-supported [0/90] square laminate with

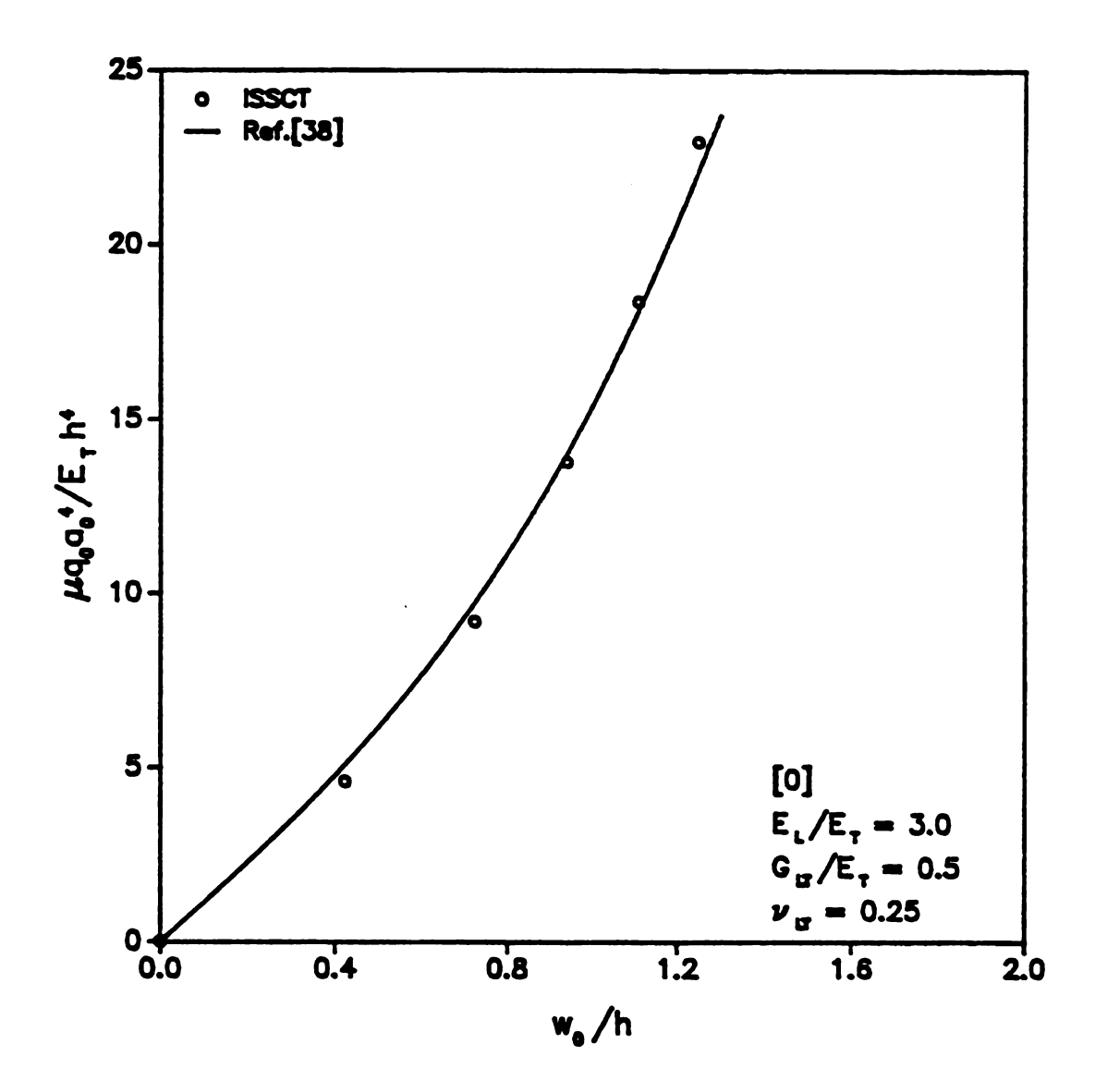


Figure 5.6 The load-deflection curve of a square [0] laminate with all edge clamped and a/h = 100 is subjected to uniformly distributed loading.

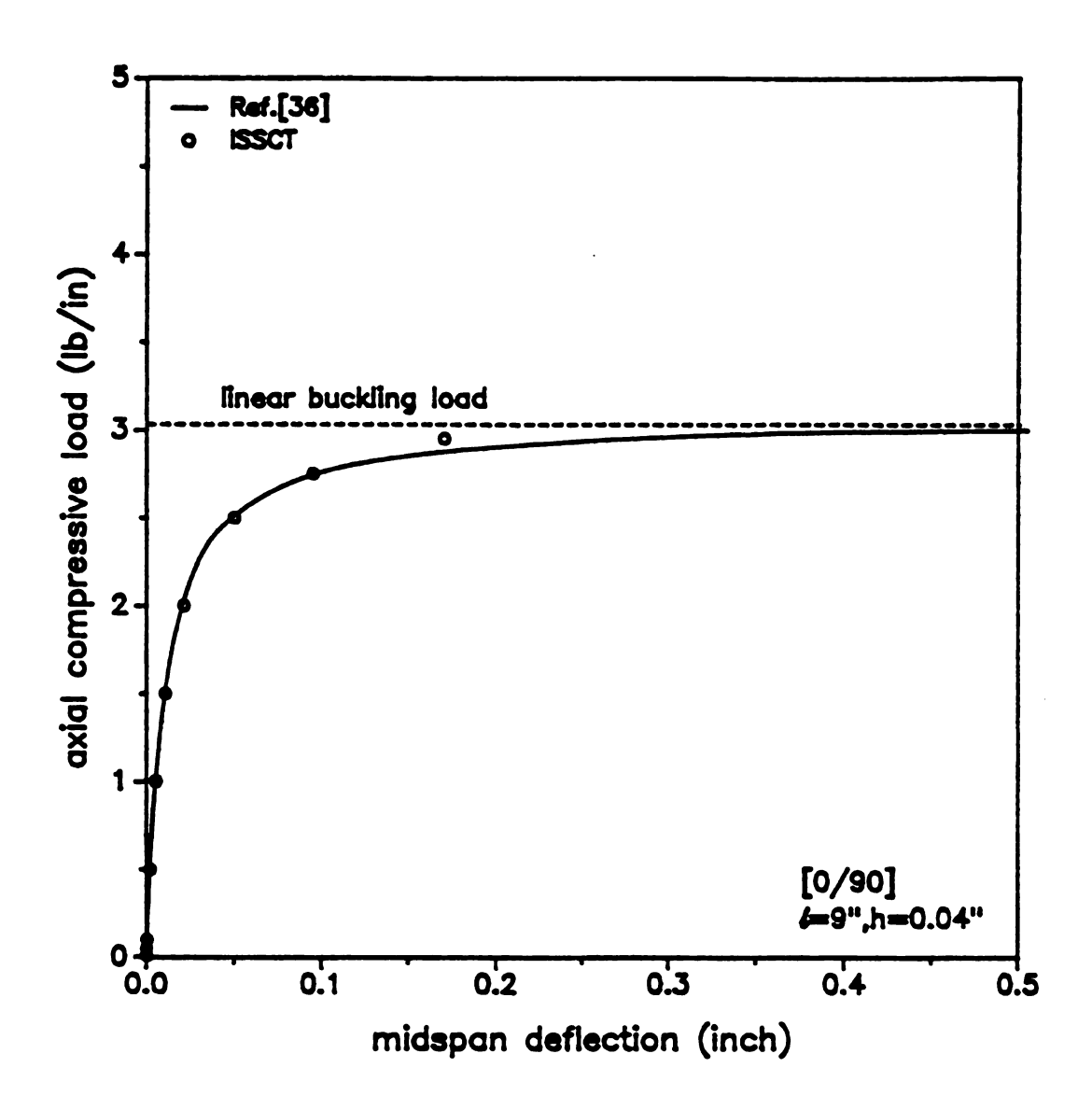


Figure 5.7 The load-deflection curve of a simply-supported [0/90] laminate under cylindrical bending with S=225 is subjected to inplane compressive loading.

aspect ratio of 1000. The material properties used in the simulation are as follows.

$$E_1 = 250GPa$$
,  $E_2 = E_3 = 20GPa$ ,  $G_{12} = G_{13} = 10GPa$ ,  $G_{23} = 4GPa$ ,  $V_{12} = V_{13} = V_{23} = 0.25$ 

Figure 5.8 presents the load-deflection curve of the analysis. A 2x2 mesh is used for a quarter of the laminate. Unlike the laminate under cylindrical bending, the laminate under inplane compression does not buckle as the load increases. The linear buckling load as indicated in the diagram is no more than a small deformation.

# 5.5 Large-Amplitude Vibration

The normal mode phenomenon has been shown to occur for beam and plate structures in large amplitude vibration [41]. It is also presented in Reference [42] that for composite laminate with aspect ratio greater than five and is subjected to nonlinear vibration with amplitude-to-thickness ratio close to one, the nonlinear analysis using vonKármán nonlinearity can provide satisfactory results compared to those using full nonlinearity. Therefore, by combining the nonlinear stiffness matrix obtained in the previous section and the consistent mass matrix established in Section 5.2, the governing equation of the undamped eigenvalue problem for amplitude-dependent vibration can be written as

$$([K] + [K_{NL}]) \{X\} - \omega^2[M] \{X\} = \{0\}$$
 (5.38)

To analyze the amplitude-dependent eigenvalue problem, a matrix iteration method [43] is used. First, the eigenvalue problem in Equation (5.38) is transformed into a standard form, i.e.,

$$([K] + [K_{NL}])^{-1}[M] \{X\} = \frac{1}{m^2} \{X\}$$
 (5.39)

Then, the iteration scheme takes the following steps

$$([K] + [K_{NL}(\{X\}^{(k)})])^{-1}[M] \{X\}^{(k)} = \frac{1}{(\omega^2)^{(k+1)}} \{X\}^{(k+1)}$$
 (5.40)

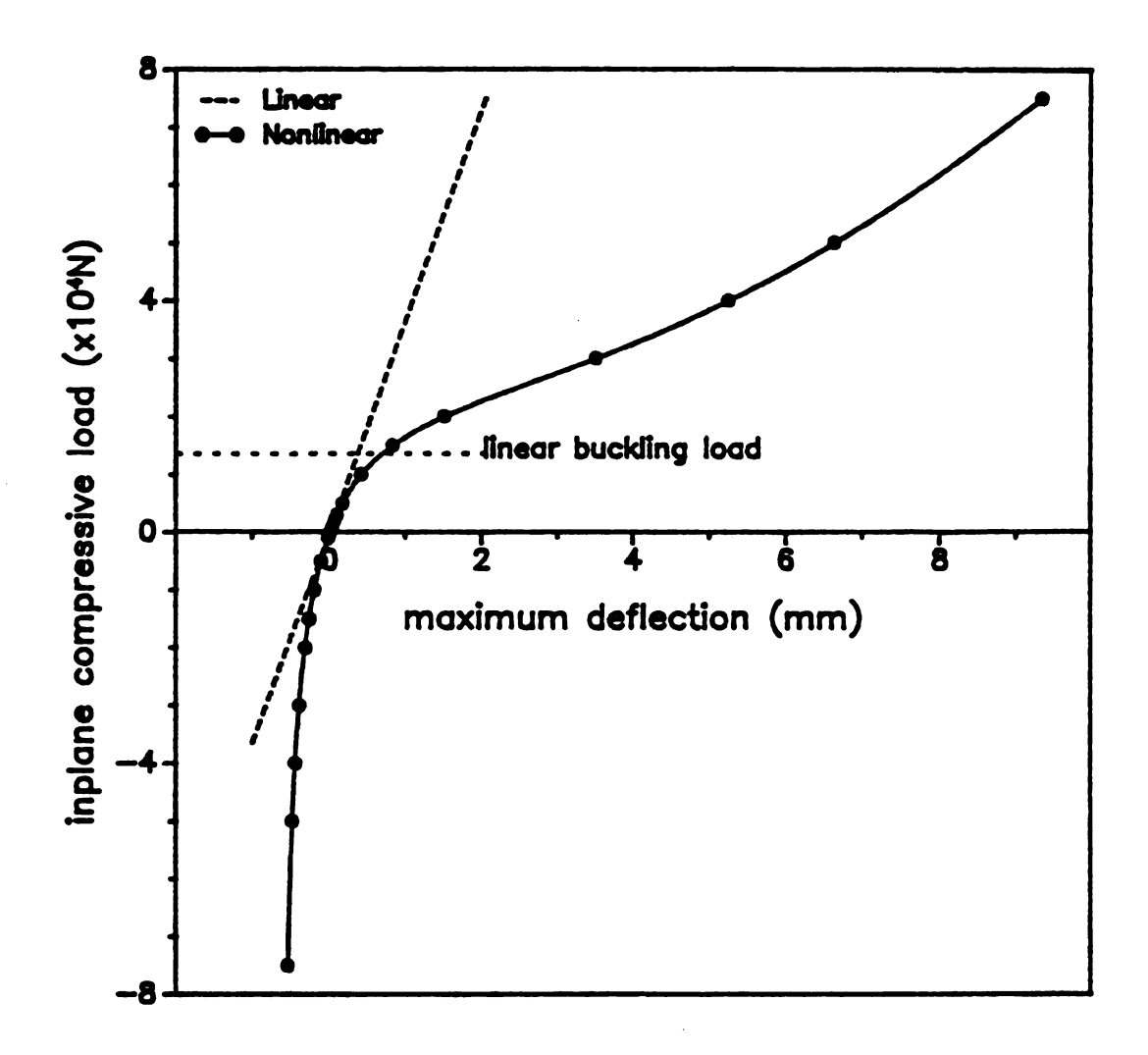


Figure 5.8 The load-deflection curve of a simply-supported square [0/90] laminate with a/h = 1000 is subjected to inplane compressive loading along the x-direction.

In the above equation, the resulting vector of the left-hand side is normalized to give the desired amplitude of vibration for a particular mode and the normalization constant related to the reciprocal of the associated eigenvalue. The iterations continue until the convergence of the eigenvalue within a preset tolerance is reached. After obtaining the first mode frequency and mode vector, the second mode frequency and mode vector can be found similarly. However, for the second mode, a sweeping matrix needs to be introduced to incorporate an orthogonal constraint in between the first and second mode vectors. Details of the procedure can be found in Reference [43]. In most situations, only the fundamental mode is of interest, therefore, the solution for the higher modes are not pursued in this study.

In order to verify the feasibility of ISSCT for large-amplitude vibration, the fundamental frequency of a thin [0/90/90/0] laminate is of interest. This composite laminate has an aspect ratio of 100 and a pinned-pinned boundary condition is subjected to cylindrical bending. Figure 5.9 presents the amplitude-dependent fundamental frequency of the laminate. In the ordinate, A represents for the amplitude of the funamental mode while r the radius of gyration of the cross-section. For a rectangular cross-section  $r = h/(\sqrt{12})$ . The results obtained by using CLT from Reference [44] is shown by a solid line. Clearly, it has a very good agreement with those from ISSCT.

As concluded in the study of nonlinear bending, the boundary conditions play an important role in the response of laminated structure. Herein, the amplitude-dependent natural frequencies for a [0/90/90/0] laminate under three different boundary conditions are studied. Figure 5.10a and 5.10b show the ratio of nonlinear fundamental frequency to linear frequency at different vibration amplitudes for a thin (S=100) and a thick (S=10) composite laminate, respectively. It is interesting to see that the thin laminate in a pinned-pinned boundary condition shows the most significant nonlinear effect. However, the least nonlinear effect is observed in the thick laminate at the same boundary condition. The reverse is true for the laminates in a clamped-clamped boundary condition.

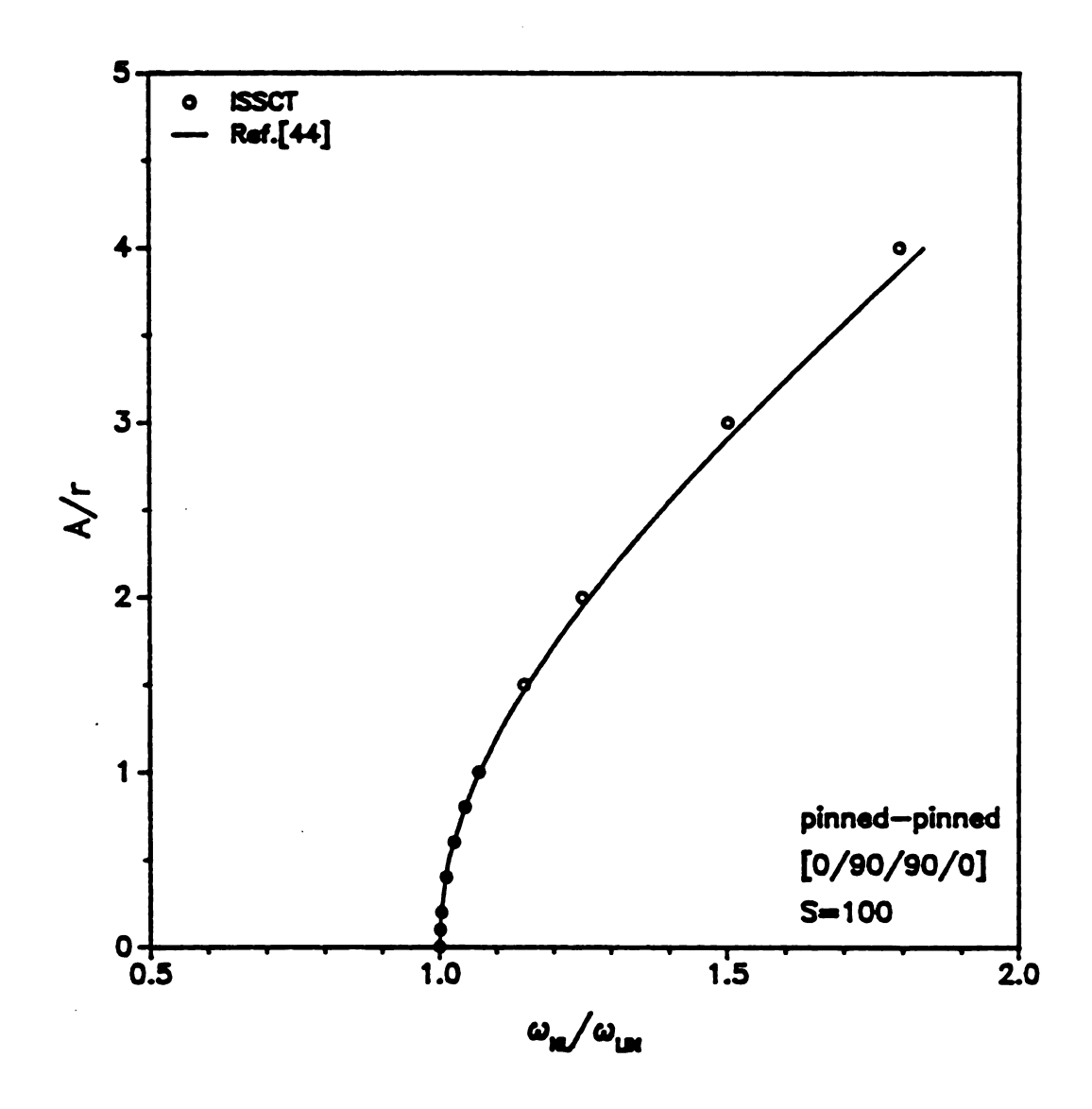


Figure 5.9 The amplitude-dependent fundamental frequency of a pinned-pinned [0/90/90/0] laminate with S=100 under cylindrical bending.

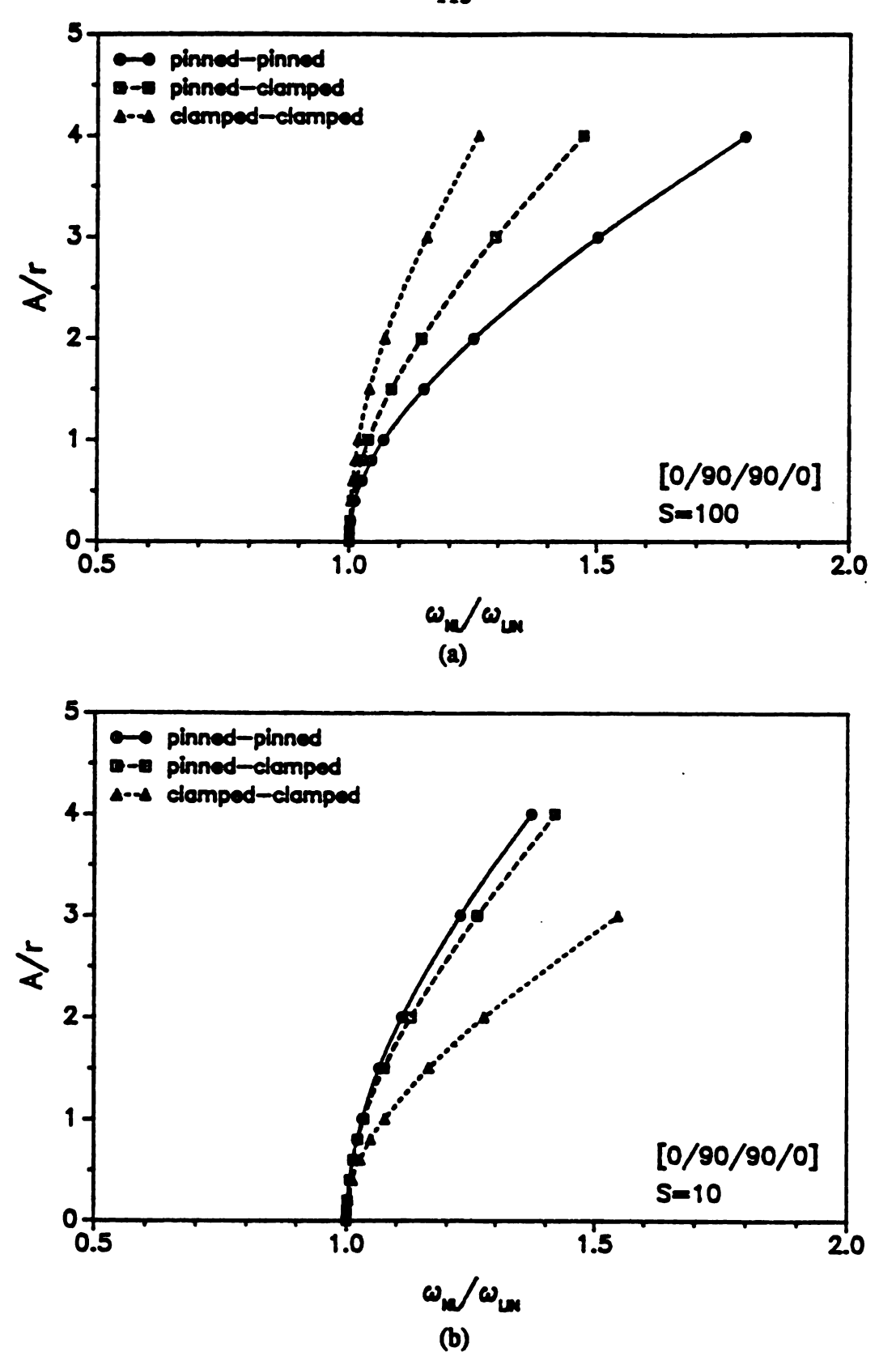


Figure 5.10 Normalized amplitude-dependent fundamental frequencies of [0/90/90/0] laminate in three different boundary conditions: (a) S=100; (b) S=10.

Due to this different behavior between thick and thin composite laminates, it is natural to investigate the effect of aspect ratio on the dynamic behavior of the structure. The result of frequency ratio for a [0/90/90/0] laminate with fixed amplitude ratio A/r = 2.0 is presented in Figure 5.11a. As can be seen from this diagram, the characteristics of the laminate undergoes a significant change as the aspect ratio of the laminate is smaller than 20. This result coincides with the finding of the transverse shear deformation effect on the composite laminate presented in Reference [6]. Therefore, there is a doubt if the transverse shear deformation plays an important role in the response of thick laminates. Beside the resonant frequencies, the information of mode shape is also crucial in structural analysis. In Figure 5.11b, a coherence factor between the linear and nonlinear mode shapes,  $\{\varphi_L\}$  and  $\{\varphi_{NL}\}$ , is intoduced in Reference [45], i.e.,

coherence = 
$$\frac{(\{\phi_{NL}\}^T \{\phi_L\})^2}{(\{\phi_{NL}\}^T \{\phi_{NL}\})(\{\phi_L\}^T \{\phi_L\})}$$

The coherence factor gives a value between zero and one. If two mode shapes are exactly the same, it gives a value of one. A zero coherence means that the two mode vectors are orthogonal. Figure 5.11b shows that as the aspect ratio of the laminate becomes less than 20, the coherence factor drops sharply for laminates of all kinds of boundary condition. This implies that the mode shapes obtained from nonlinear analysis deviates from those from linear analysis. This result may jeopardize the assumption of using linear mode shape for nonlinear structure analysis [46].

## 5.6 Free-Edge Stresses

The free-edge stress has long been recognized as a unique problem in laminated composites [47-49]. The purpose of this section is to assess the feasibility of using the interlaminar shear stress continuity theory presented for free-edge analysis. Since constant w through the thickness is assumed in ISSCT, i.e., the effect of  $\sigma$ , is ignored, a [45/45]s

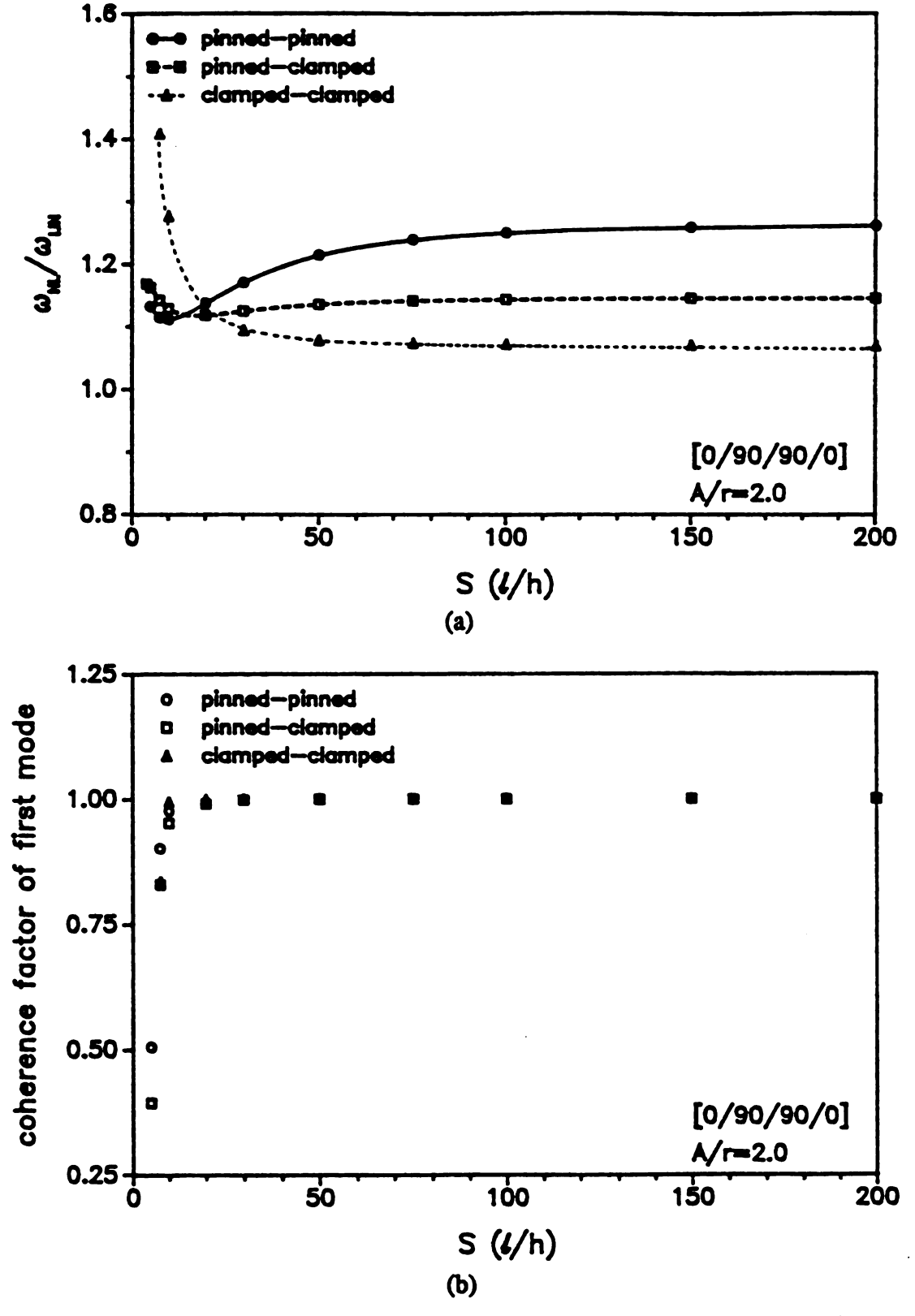


Figure 5.11 The change of nonlinear fundamental frequency and mode shape of a [0/90/90/0] laminate at the vibration amplitude A/r = 2.0: (a) fundamental frequency; (b) coherence factor.

laminate which does not generate transverse normal stress due to inplane loading is taken as an example. Figure 5.12 shows the mesh for finite element analysis. For convenience, it is possible to examine only one half of the specimen. In addition, specifying the uniform strain in the x-direction, as usually employed in the free-edge studies [49], is not a feasible technique in this analysis. Hence, a uniform tensile loading is applied at the laminate ends. However, the strain across the width is verified to be very close to uniform distribution.

Figures 5.13a and 5.13b present the normalized displacement u(0, y, h/2) and transverse shear stress  $\sigma_{xz}(0, y, h/4)$ , respectively. It is clear that the finite element analysis using ISSCT predicts excellent results as obtained in Reference [49]. With these results and the previous studies, it is believed that ISSCT can be used for general analysis for laminated composites.

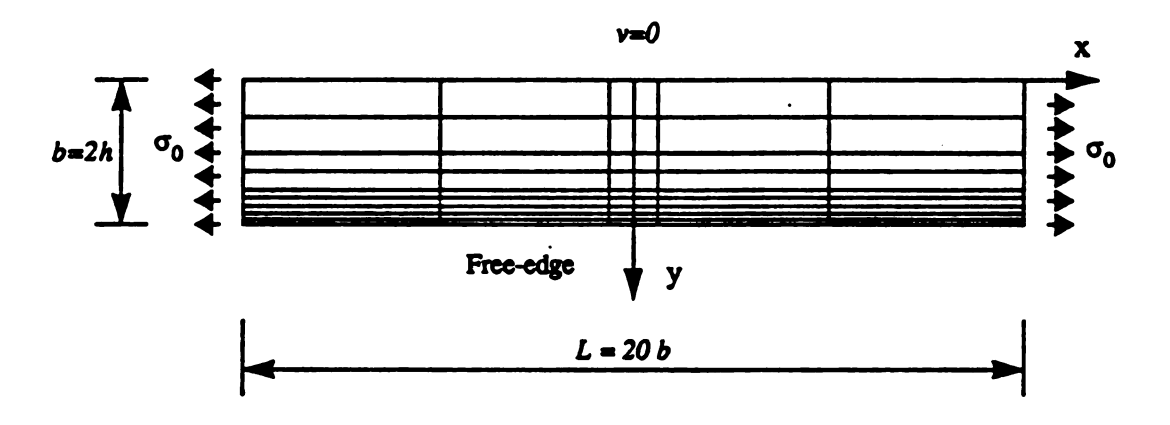


Figure 5.12 Mesh layout for [45/-45]s laminate in calculation of free-edge stress.

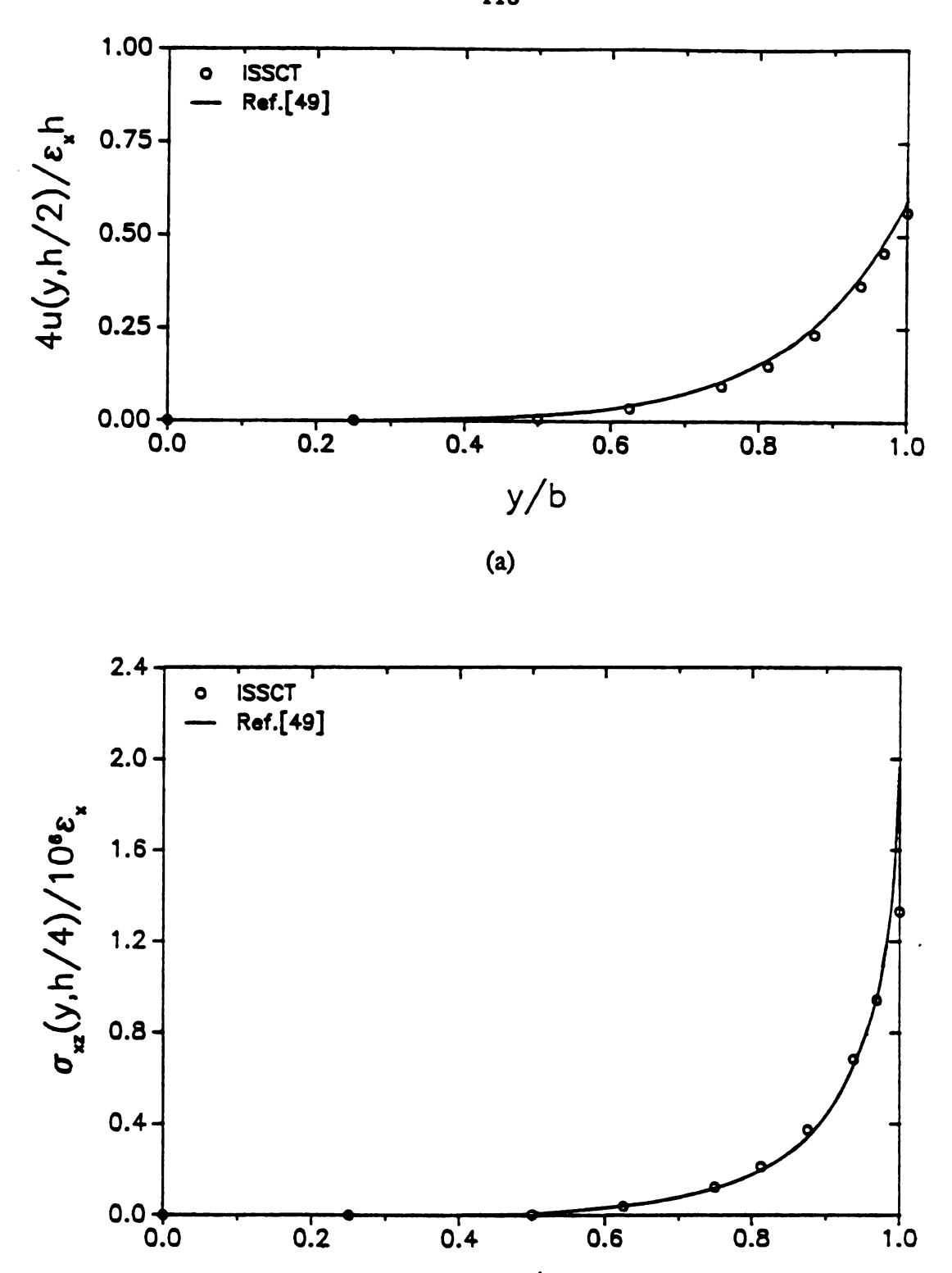


Figure 5.13 Normalized results of a [45/-45]s laminate subjected to uniform inplane loading: (a) through-the-width in-plane displacement u(0, y, h/2); (b) through-the-width interlaminar shear stress  $\sigma_{xz}(0, y, h/4)$ .

**(b)** .

y/b

0.4

0.6

8.0

1.0

0.2

# **CHAPTER 6**

# CONCLUSIONS AND RECOMMENDATIONS

#### 6.1 Conclusions

In this study, two laminate theories based on multiple-layer approach - ISCT and ISSCT - for the analysis of both thick and thin composite laminates are presented. The easiness of the direct stress calculation from constitutive equations and accuracy of the results from using stress continuity conditions are demonstrated by some numerical examples. Moreover, the expedience in computation for composite laminates with large number of layers is achieved by the layer reduction technique. A comprehensive investigation of using ISSCT in the vibration, buckling, nonlinear, and free-edge analysis of composite laminates also show a good potential of using the stress continuity theories for composite analysis. In summary, the following conclusions are drawn:

- 1. Two interlaminar stress continuity theories for laminated composites are developed. One considers the variation of transverse displacement through the composite thickness and the other assumes constant transverse displacement. The former is named the interlaminar stress continuity theory (ISCT) while the latter the interlaminar shear stress continuity theory (ISSCT). These theories enable a direct and accurate calculation of transverse stresses from consitutive equations for both thick and thin composite laminates.
- 2. A simple technique is developed for finding the closed-form solutions of some particular problems such as cylindrical bending and bidirectional bending. Since no approximation is included in this technique, the error from numerical analysis can be avoided.
- 3. With little modification, the multiple-layer laminate theory ISSCT can be reduced to single-layer theory, i.e., HSDT. This concludes that HSDT can be deemed as the sin-

gle-layer version of ISSCT.

- 4. From the numerical examples examined in this study, it is concluded that high-order shear deformation theory (HSDT) can be used for laminates with aspect ratios (S) greater than 10 while ISSCT S>5. Due to its three-dimensional approach in nature, ISCT has no limitation in aspect ratio.
- 5. A layer reduction technique for reducing the degree-of-freedom is developed by combining the interlaminar shear stress continuity theory (ISSCT) and high-order shear deformation theory (HSDT). This technique can give transverse stresses at desired interfaces without introducing too many degree-of-freedom.
- 6. The finite elements derived from ISCT have thickness the same as the composite laminates. Based on the numerical examples studied in this thesis, it is observed that as the aspect ratio of a finite element is close to one best result can be obtained. The finite element analysis using ISCT seems to suffer from the aspect ratio problem.
- 7. The applications of ISSCT for vibration, buckling, nonlinear bending, nonlinear vibration, and free-edge analyses of laminated composites show excellent results. All the investigations indicate that ISSCT is a very promising technique for composite analysis.

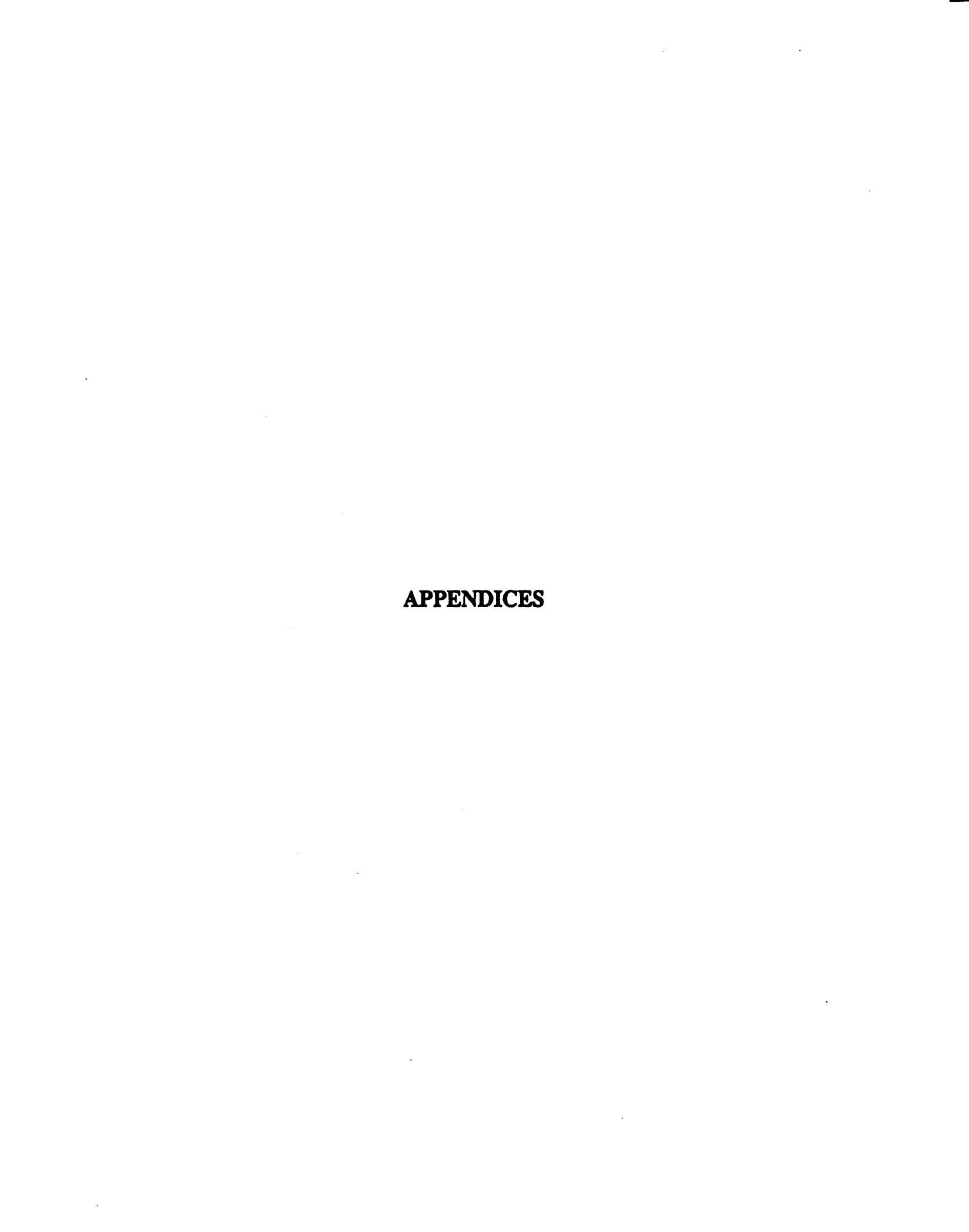
#### **6.2 Recommendations**

Based on the work performed in this thesis, the following studies are recommended for further investigation:

- 1. This thesis gives two accurate laminate theories for predicting both displacement and stress of laminated composites. The failure analysis can be performed with the help of these types of information. For example, the first-ply-failure or last-ply-failure analysis can be combined with the stress continuity theories while the delamination at the interface can be modeled with a soft and thin embedded layer or by a slip layer[50].
  - 2. The feasibility of using the stress continuity theories in analyzing both global

and local responses of composite laminates, as mentioned in Chapter 5, has recommended a potential application of these thoeries in assessing the performance of smart materials and intelligent system which are made of composite laminates and embedded sensors and actuators. The constitutive relations of piezo-electric crystal, shape memory alloy, electro-rheological fluid, and optical fiber can be incorporated into these stress continuity theories. In this way, the global response of the smart material and intelligent system can be simulated and the stress state around the embedded sensors can be examined.

3. The structures with viscoelastic damping materials in both constrained layer and extensional layer configurations can initially be analyzed with these stress continuity theories. Then, by using the specific damping capacity presented in Reference [51], the damping characteristics of the viscoelastic structures can be evaluated.



# APPENDIX A [E] AND {q} MATRICES

# A.1 Interlaminar Stress Continuity Theory

In ISCT, the constraint matrices  $[E_a]$  and  $[E_b]$  are defined as

1	г.	•	•	•	_	^	•	^	•	_											7
	1	0	0	0	0	0	0	0	0	_	•	•	•	•	•	•	•	•	•	•	•
		1	0	0	0	0	0	0	0	0	•	•	•	•	•	•	•	•	•	•	•
	0	0	1	1	0	0	0	Ī	•	-	•	•	•	•	•	•	•	•	•	•	٠,
	0		0		0		0	0	0	0	•	•	•	•	•	•	•	•	•	•	٠,
	0	0	0	0	1	0	0	0	0	-	•	•	•	•	•	•	•	•	•	•	
	0	0	0	0	0	1	0	0	0	_	•	•	•	•	•	•	•	•	•	•	•
	0	0	0	0	0	0	1	0	0	0	•	•	•	•	•	•	•	•	•	•	•
	0	0	0	0	0	0	0	1	0	0	•	•	•	•	•	•	•	•	•	•	•
	0	0	0	0	-	-1	0	0	0	0	•	•	•	•	•	•	•	•	•	•	•
	0	0	0	0	0	0	-1	0	0	0	•	•	•	•	•	•	•	•	•	:	٠.
	0	0	0	0	0	0	-1	0	0	v	•	•	•	•	•	•	•	•	•	•	٠.
	0	0	0	0	0	0	0	-1	0	0	•	•	•	•	•	•	•	•	•	•	•
	$Q_{13}^{(1)}$	Q(1)	$Q_{36}^{(1)}$	$Q_{23}^{(1)}$	0	0	0	0	0	0											
İ	$Q_{\mathbf{B}}^{(1)}$	$Q_{33}^{(1)}$	$Q_{33}^{(1)}$	$Q_{33}^{(1)}$	U	•	v	U	•	U	•	•	•	•	•	•	•	•	•	•	
$[E_a] =$	0	0	0	0	0	0	0	0	1	0											
	0	0	0	0	0	0	0	0	0	1					•		•				.
	•	•		•											•	•	•			•	
	•		•										1	0	0	0	0	0	0	0	0
		•	•	•									0	1	0	0	0	0	0	0	0
	•	•	•				•						0	0	1	0	0	0	0	0	0
	•	•	•	•	•			•					0	0	0	1	0	0	0	0	0
	•		•				•		•				0	0	0	0	1	0	0	0	0
•	•	•	•		•				•				0	0	0	0	0	1	0	0	0
	•	•	•		•							•	0	0	0	0	0	0	1	0	0
1	•	•	•				•						0	0	0	0	0	0	0	1	0
	•	•	•				•			•			0	0	0	0	0	0	0	0	1
	•	•	•		•		•			•		•	0	0	0	0	0	0	-1	0	0
	•		•	•									0	0	0	0	0	0	0	-1	0
	•	•			•		•			•			0	0	0	0	0	0	0	-1	0
	•	•	•	•	•		•		•			•	0	0	0	0	0	0	0	0	-1
														$Q_{\rm LS}^{\rm (A)}$	$Q_{36}^{(n)}$	$Q_{36}^{(a)}$	Q(a)	_	_	_	
													^	-6	~~			Λ	0	0	0
	•	•	•	•	•	•	•	•	•	•	•	•	0	$Q_{33}^{(a)}$	$Q_{33}^{(a)}$	$Q_{\mathbf{x}}^{(n)}$	$Q_{33}^{(a)}$	0	U	U	ויי

(13n+13)=(13n+3)

 $[E_s] =$ 

_																			_
1	0	0	0	0	0	0	0	0	0	0		•	•	•	•	•	•	•	
0	1	0	0	0	0	0	0	0	0	0		•	•	•	•	•	•	•	.
0	0	1	0	0	0	0	0	0	0	0		•	•	•	•	•	•	•	.
0	0	0	1	0	0	0	0	0	0	0		•	•	•	•	•	•	•	
0	0	0	0	1	0	0	0	0	0	0		•	•	•	•	•	•	•	.
0	0	0	0	0	1	0	0	0	0	0		•	•	•	•	•	•		.
0	0	0	0	0	0	1	0	0	0	0		•	•	•	•	•	•		
0	0	0	0	0	0	0	1	0	0	0		•	•	•	•	•	•	•	.
0	0	0	0	0	0	0	0	1	0	0		•	•	•	•	•	•	•	
0	0	0	0	0	0	0	0	0	1	0		•	•	٠.	•	•	•		
0	0	0	0	0	0	0	0	-1	0	0		•	•	•	•	•	•	•	
0	0	0	0	0	0	0	0	0	-1	0		•	•		•	•	•		.
0	$\frac{\mathcal{Q}_{13}^{(1)}}{\mathcal{Q}_{33}^{(1)}}$	$\frac{\mathcal{Q}_{\mathbf{x}}^{(1)}}{\mathcal{Q}_{\mathbf{x}}^{(1)}}$	0	0 -	$\frac{\mathcal{Q}_{36}^{(1)}}{\mathcal{Q}_{33}^{(1)}}$	$\frac{\mathcal{Q}_{\mathbf{B}}^{(1)}}{\mathcal{Q}_{\mathbf{B}}^{(1)}}$	0	0	0	0		•	•	•		•	•	•	
0	0	$\frac{Q_{13}^{(1)}}{Q_{23}^{(1)}}$	$\frac{\mathcal{Q}_{\mathbf{x}}^{(1)}}{\mathcal{Q}_{\mathbf{x}}^{(1)}}$	0	0	$-\frac{\mathcal{Q}_{36}^{(1)}}{\mathcal{Q}_{33}^{(1)}}$	$\frac{\mathcal{Q}_{\mathbf{B}}^{(1)}}{\mathcal{Q}_{\mathbf{B}}^{(1)}}$	0	0	0		•	•	•	•		•	•	
0	0	0	0	0	0	0	0	0	0	1		•	•			•			
.	•	•	•		•	•	•			•		•	•		•	•		•	.
1.	•	•	•	•	•	•	•	•	•	•		•	•	•	•	•	•	•	.
-	•	•	•	•	•	•	•	•	•	•	. 1	0	0	0	0	0	0	0	0
.	•	•	•		•	•	•	•	•	•	. 0	1	0	0	0	0	0	0	0
.	•	•	•	•	•	•	•		•		. 、0	0	1	0	0	0	0	0	0
1.	•	•	•	•	•	•	•	•	•	•	. 0	0	0	1	0	0	0	0	0
	•	•		•	•	•	•	•	•		. 0	0	0	0	1	0	0	0	0
.	. •	•	•		•	•	•	•	•	•	. 0	0	0	0	0	1	0	0	0
.	•	•	•	•	•	•	•	•	•	•	. 0	0	0	0	0	0	1	0	0
.	•	•	•		•	•	•	•			. 0	0	0	0	0	0	0	1	0
.	•	•	•	•		•	•		•		. 0	0	0	0	0	0	0	0	1
.	•	•		•		•	•		•		. 0	0	0	0	0	0	0	-1	0
.	•	•			•	•	•				. 0	0	0	0	0	0	0	0	-1
	•			•	. •		•	•	•	•	$\frac{\mathcal{Q}_{\mathfrak{B}}^{(a)}}{\mathcal{Q}_{\mathfrak{B}}^{(a)}}$	$-\frac{\mathcal{Q}_{36}^{(a)}}{\mathcal{Q}_{33}^{(a)}}$	0	0 -	$\frac{Q_{36}^{(n)}}{Q_{33}^{(n)}}$	$\frac{\mathcal{Q}_{23}^{(a)}}{\mathcal{Q}_{33}^{(a)}}$	0	0	0
	•			•	•	•	•	•	•	•	. 0	$\frac{Q_{13}^{(a)}}{Q_{33}^{(a)}}$	$\frac{\mathcal{Q}_{36}^{(a)}}{\mathcal{Q}_{33}^{(a)}}$	0	0	Q35 Q35	$\frac{Q_{23}^{(a)}}{Q_{33}^{(a)}}$	0	٥

(14n+14)x(14n+6)

$$\{q_n\} = \left[0, 0, 0, \dots, 0, 0, \frac{q}{Q_{33}^{(n)}}\right]^T$$

$$\{q_s\} = \left[0, 0, 0, \dots, 0, 0, \frac{1}{Q_{33}^{(n)}} \frac{\partial q}{\partial x} \frac{1}{Q_{33}^{(n)}} \frac{\partial q}{\partial y}\right]^T$$

$$(14n+14) \times 1$$

# A.2 Interlaminar Shear Stress Continuity Theory

In ISSCT, the following constraint matrices are used:

	ſı	0	0	0	0	0	0	0	0	0		0	0	0	0	0	0	0	0	0
	0	1	0	0	0	0	0	0	0	0		0	0	0	0	0	0	0	0	0
	0	0	1	0	0	0	0	0	0	0		0	0	0	0	0	0	0	0	0
	0	0	0	1	0	0	0	0	0	0		0	0	0	0	0	0	0	0	0
	0	0	0	0	0	0	0	0	0	0		0	0	0	0	0	0	-1	0	0
	0	0	0	0	0	0	0	0	0	0		0	0	0	0	0	0	0	-1	0
	0	0	0	0	0	0	0	0	0	0		0	0	0	0	0	0	0	-1	0
	0	0	0	0	0	0	0	0	0	0		0	0	0	0	0	0	0	0	-1
	0	0	0	0	1	0	0	0	0	0		0	0	0	0	0	0	0	0	0
	0	0	0	0	0	1	0	0	0	0		0	0	0	0	0	0	0	0	0
	0	0	0	0	0	0	1	0	0	0		0	0	0	0	0	0	0	0	0
	0	0	0	0	0	0	0	1	0	0		0	0	0	0	0	0	0	0	0
$[E_n] =$	0	0	0	0	0	0	0	0	1	0		0	0	0	0	0	0	0	0	0
~	0	0	0	0	0	0	0	0	0	1		0	0	0	0	0	0	0	0	0
	.																			
	١.																			•
	.																			
	0	0	0	0	0	0	0	0	0	0		1	0	0	0	0	0	0	0	0
	0	0	0	0	0	0	0	0	0	0		0	1	0	0	0	0	0	0	0
	0	0	0	0	0	0	0	0	0	0	•	0	0	1	0	0	0	0	0	0
	0	0	0	0	0	0	0	0	0	0		0	0	0	1	0	0	0	0	0
	0	0	0	0	0	0	0	0	0	0		0	0	0	0	1	0	0	0	0
	0	0	0	0	0	0	0	0	0	0		0	0	0	0	0	1	0	0	0
	0	0	0	0	0	0	0	0	0	0		0	0	0	0	0	0	-1	0	0
	0	0	0	0	0	0	0	0	0	0		0	0	0	0	0	0	0	-1	0
	0	Ö	0	0	0	0	0	0	0	0		0	0	0	0	0	0	0	-1	0
	0	0	0	0	0	0	0	0	0	0		0	0	0	0	0	0	0	0	-1
	0	0	0	0	0	0	0	0	0	0		0	0	0	0	0	0	1	0	0
	0	0	0	0	0	0	0	0	0	0		0	0	0	0	0	0	0	1	0
	0	0	0	0	0	0	0	0	0	0		0		0	0	0	0	0	0	1

## APPENDIX B

# THE EQUIVALENCE OF ISSCT AND HSDT FOR ONE-LAYER LAMINATE

For a single-layer laminate, the displacement field of ISSCT, Equation (2.27), can be simplified as

$$u = U_0 \phi_1 + \hat{T}_0 \phi_2 + U_1 \phi_3 + \hat{T}_1 \phi_4$$

$$v = V_0 \phi_1 + \hat{S}_0 \phi_2 + V_1 \phi_3 + \hat{S}_1 \phi_4$$

$$w = w_0$$
(B.1)

where

$$\phi_1 = 1 - \frac{3}{h^2} (z + \frac{h}{2})^2 + \frac{2}{h^3} (z + \frac{h}{2})^3$$

$$\phi_2 = -\frac{1}{h^2} (z + \frac{h}{2}) (z - \frac{h}{2})$$

$$\phi_3 = \frac{3}{h^2} (z + \frac{h}{2})^2 - \frac{2}{h^3} (z + \frac{h}{2})^3$$

$$\phi_4 = \frac{1}{h^2} (z + \frac{h}{2})^3 - \frac{2}{h} (z + \frac{h}{2})^2$$
(B.2)

Since there is only one layer, no interfacial shear stress continuity is enforced. However, the zero shear traction on top and bottom surfaces of the composite laminate should be satisfied, i.e., the shear strains at these locations must vanish,

$$2\varepsilon_{xz}\Big|_{z=-\frac{h}{2}} = \hat{T}_0 + \frac{\partial w_0}{\partial x} = 0 \quad ; \quad 2\varepsilon_{xz}\Big|_{z=\frac{h}{2}} = \hat{T}_1 + \frac{\partial w_0}{\partial x} = 0$$

Hence,

$$\dot{\tau}_0 = \dot{\tau}_1 = \frac{\partial w_0}{\partial x} \tag{B.3}$$

Similarly

$$\hat{S}_0 = \hat{S}_1 = \frac{\partial w_0}{\partial y} \tag{B.4}$$

Substituting these relationships into Equation (B.1), the displacement field becomes

$$u = U_0 \phi_1 + U_1 \phi_3 - (\phi_2 + \phi_4) \frac{\partial w_0}{\partial x}$$

$$v = V_0 \phi_1 + V_1 \phi_3 - (\phi_2 + \phi_4) \frac{\partial w_0}{\partial y}$$

$$w = w_0$$
(B.5)

By plugging the Hermite cubic interpolation functions (B.2) into the new displacement field and letting

$$u_0 = \frac{U_0 + U_1}{2} \tag{B.6a}$$

and

$$\Psi_x = \frac{1}{2} \frac{\partial w_0}{\partial x} - \frac{3}{2} \left( \frac{U_0 - U_1}{h} \right)$$
 (B.6b)

the new expression for displacement u in terms of new variables can be obtained

$$u = u_0 + z \left( \Psi_x - \frac{4}{3} \frac{z^2}{h^2} (\Psi_x + \frac{\partial w_0}{\partial x}) \right)$$
 (B.7a)

In the above expression,  $u_0$  is the midplane displacement in the x direction, while  $\psi_x$  relates to the rotation accounting for transverse shear deformation at the midplane. In a similar fashion, the new expression for  $\nu$  can also be derived as follows,

$$v = v_0 + z \left( \psi_y - \frac{4}{3} \frac{z^2}{h^2} (\psi_y + \frac{\partial w_0}{\partial y}) \right)$$
 (B.7b)

It then is clear that the displacement field for ISSCT can be reduced to a HSDT.



## LIST OF REFERENCES

- 1. Noor, A.K., and Burton, W.S., "Assessment of Shear Deformation Theories for Multi-layered Composite Plates," Applied Mechanics Review, Vol. 42, 1989, pp. 1-13.
- 2. Kapania, R.K., and Raciti, S., "Recent Advances in Analysis of Laminated Beams and Plates, Part I: Shear Effects and Buckling," AIAA Journal, Vol. 27, 1987, pp. 923-934.
- 3. Kapania, R.K., and Raciti, S., "Recent Advances in Analysis of Laminated Beams and Plates, Part II: Vibrations and Wave Propagation," *AIAA Journal*, Vol. 27, 1987. pp. 935-946.
- 4. Reddy, J.N., "A Review of Refined Theories of Laminated Composite Plates," Shock and Vibration Digest, Vol. 22, 1990, pp. 3-17.
- 5. Reddy, J.N., "A Generalization of Two-Dimensional Theories of Laminated Composite Plates," Communications in Applied Numerical Methods, Vol. 3, 1987, pp. 173-180.
- 6. Pagano, N.J., "Exact Solutions for Composite Laminates in Cylindrical Bending," *Journal of Composite Materials*, Vol. 3, 1969, pp. 98-411.
- 7. Yang, P.C., Norris, C.H., and Stavsky, Y., "Elastic Wave Propagation in Heterogeneous Plate," *International Journal of Solids and Structures*, Vol. 2, 1966, pp. 665-684.
- 8. Reissner, E., "On Transverse Bending of Plates Including the Effects of Transverse Shear Deformation," *International Journal of Solids and Structures*, Vol. 11, 1975, pp. 569-573.
- 9. Lo, K.H., Christensen, R.M., and Wu, E.M., "A High-Order Theory of Plate Deformation Part 1: Homogeneous Plates," *Journal of Applied Mechanics*, Vol. 44, 1977, pp. 663-668.
- 10. Lo, K.H., Christensen, R.M., and Wu, E.M., "A High-Order Theory of Plate Deformation Part 2: Laminated Plates," *Journal of Applied Mechanics*, Vol. 44, 1977, pp. 669-676.
- 11. Reddy, J.N., "A Simple Higher-Order Theory for Laminated Composite Plates," Journal of Applied Mechanics, Vol. 51, 1984, pp. 745-752.
- 12. Hong, S., "Central Delamination in Glass/Epoxy Laminates," Ph.D. Dissertation, Michigan State University, East Lansing, Michigan, 1990.
- 13. Ambartsumyan, S.A., *Theory of Anisotropic Plates*, translated from Russian by T. Cheron and edited by J.E. Ashton, Technomic Publishing Co., 1969.

- 14. Whitney, J.M., "The Effect of Transverse Shear Deformation on the Bending of Laminated Plates," *Journal of Composite Materials*, Vol. 3, 1969, pp. 534-547.
- 15. Pryor, C.W., Jr., and Barker, R.M., "A Finite-Element Analysis Including Transverse Shear Effects for Applications to Laminated Plates," AIAA Journal, Vol. 9, 1971, pp. 912-917.
- 16. Mau, S.T., Tong, P., and Pian, T.H.H., "Finite Element Solutions for Laminated Thick Plates," *Journal of Composite Materials*, Vol. 6, 1972, pp. 304-309.
- 17. Spilker, R.L., Chou, S.C., and Orringer, O., "Alternate Hybrid-Stress Elements for Analysis of Multilayer Composite Plates," *Journal of Composite Materials*, Vol. 11, 1977, pp. 51-70.
- 18. Murakami, H., "Laminated Composite Plate Theory with Improved In-plane Response," Journal of Applied Mechanics, Vol. 53, 1986, pp. 661-666.
- 19. Toledano, A., and Murakami, H., "A Composite Plate Theory for Arbitrary Laminate Configurations," *Journal of Applied Mechanics*, Vol. 54, 1987, pp. 181-189.
- 20. Reissner, E., "On A Certain Mixed Variational Theorem and A Proposed Application," International Journal for Numerical Methods in Engineering, Vol. 20, 1984, pp. 1366-1368.
- 21. Seide, P., "An Improved Approximate Theory for the Bending of Laminated Plates," *Mechanics Today*, Vol. 5, 1980, pp. 451-466.
- 22. Di Sciuva, M., "Development of An Anisotropic, Multilayered, Shear-Deformable Rectangular Plate Element," Computers & Structures, Vol. 21, 1985, pp. 789-796.
- 23. Di Sciuva, M., "Bending, Vibration and Buckling of Simply Supported Thick Multi-layered Orthotropic Plates: An Evaluation of A New Displacement Model," *Journal of Sound and Vibration*, Vol. 105, 1986, pp. 425-442.
- 24. Hinrichsen, R.L., and Palazotto, A.N., "Nonlinear Finite Element Analysis of Thick Composite Plates Using Cubic Spline Functions," AIAA Journal, Vol. 24, 1986, pp. 1836-1842.
- 25. Reddy, J.N., Barbero, E.J., and Teply, J.L., "A Plate Bending Element Based on a Generalized Laminate Plate Theory," *International Journal for Numerical Methods in Engineering*, Vol. 28, 1989, pp. 2275-2292.
- 26. Barbero, E.J., Reddy, J.N., and Teply, J.L., "An Accurate Determination of Stresses in Thick Laminates Using A Generalized Plate Theory," *International Journal for Numerical Methods in Engineering*, Vol. 29, 1990, pp. 1-14.
- 27. Pagano, N.J., and Hatfield, S.J., "Elastic Behavior of Multilayered Bidirectional Composites," AIAA Journal, Vol. 10, 1972, pp. 931-933.
- 28. Jones, A.T., "Exact Natural Frequencies for Cross-Ply Laminates," Journal of Composite Materials, Vol. 4, 1970, pp. 476-491.
- 29. Jones, A.T., "Exact Natural Frequencies and Modal Functions for A Thick Off-Axis Lamina," Journal of Composite Materials, Vol. 5, 1971, pp. 504-520.

- 30. Kulkarni, S.V., and Pagano, N.J., "Dynamic Characteristics of Composite Laminates," *Journal of Sound and Vibration*, Vol. 23, 1972, pp. 127-143.
- 31. Srinivas, S., Joga Rao, C.V., and Rao, A.K., "An Exact Analysis for Vibration of Simply-Supported Homogeneous and Laminated Thick Rectangular Plates," *Journal of Sound and Vibration*, Vol. 12, 1970, pp. 187-199.
- 32. Noor, A.K., "Free Vibrations of Multilayered Composite Plates," AIAA Journal, Vol. 11, 1973, pp. 1038-1039.
- 33. Noor, A.K., "Stability of Multilayered Composite Plates," Fibre Science Technology, Vol. 8, 1975, pp. 81-89.
- 34. Pagano, N.J., and Soni, S.R., "Models for Studying Free-Edge Effects," in *Interlaminar Response of Composite Materials*, edited by N.J. Pagano, Elsevier Science Publisher, 1989.
- 35. Vinson, J.R., and Sierakowski, R.L., *The Behavior of Structures Composed of Composite Materials*, Martinus Nijhoff Publishers, 1986.
- 36. Sun, C.T., and Chin, H., "Analysis of Asymmetric Composite Laminates," AIAA Journal, Vol. 26, 1988, pp. 714-718.
- 37. Whitney, J.M., Structural Analysis of Laminated Anisotropic Plates, Technomic Publishing Co., 1987.
- 38. Chia, C.Y., "Large Deflection of Rectangular Orthotropic Plates," Journal of the Engineering Mechanics Division, Proceedings of the A.S.C.E., Vol. 98, 1972, pp. 1285-1298.
- 39. Reddy, J.N., and Chao, W.C., "Large-Deflection and Large-Amplitude Free Vibrations of Laminated Composite-Material Plates," *Computers & Structures*, Vol. 13, 1981, pp. 341-347.
- 40. Barbero, E.J., and Reddy, J.N., "Nonlinear Analysis of Composite Laminates Using A Generalized Laminated Plate Theory," AIAA Journal, Vol. 28, 1990, pp. 1987-1994.
- 41. Wah, T., "The Normal Modes of Vibration of Certain Nonlinear Continuous Systems," *Journal of Applied Mechanics*, Vol. 31, 1964, pp. 139-140.
- 42. Singh, G., and Sadasiva Rao, Y.V.K., "Nonlinear Vibrations of Thick Composite Plates," *Journal of Sound and Vibration*, Vol. 115, 1987, pp. 367-371.
- 43. Meirovitch, L., Analytical Methods in Vibrations, The Macmillan Company, 1967.
- 44. Woinowsky-Krieger, S., "The Effect of an Axial Force on the Vibration of Hinged Bars," Journal of Applied Mechanics, Vol. 17, 1950, pp. 35-36.
- 45. Kuang, J.H., and Tsuei, Y.G., "A More General Method of Substructure Mode Synthesis for Dynamic Analysis," AIAA Journal, Vol. 23, 1985, pp. 618-623.
- 46. Kapania, R.K., and Raciti, S., "Nonlinear Vibrations of Unsymmetrically Laminated Beams," AIAA Journal, Vol. 27, 1989, pp. 201-210.

- 47. Pagano, N.J., and Pipes, R.B., "Some Observations on the Interlaminar Strength of Composite Laminates," *International Journal of Mechanical Science*, Vol. 15, 1973, pp. 679-688.
- 48. Pipes, R.B., and Pagano, N.J., "Interlaminar Stresses in Composite Laminate An Approximate Elasticity Solution," *Journal of Applied Mechanics*, Vol. 41, 1974, pp. 668-672.
- 49. Pagano, N.J., "Stress Fields in Composite Laminates," International Journal of Solids and Structures, Vol. 14, 1978, pp. 385-400.
- 50. Toledano, A., and Murakami, H., "Shear-Deformable Two-Layer Plate Theory with Interlayer Slip," Journal of Engineering Mechanics, Vol. 114, 1988, pp. 604-623.
- 51. Ungar, E.E., and Kerwin, E.M., Jr., "Loss Factors of Viscoelastic Systems in Terms of Energy Concepts," The Journal of The Accoustical Society of America, Vol. 34, 1962, pp. 954-957.